

**PETROGRAPHY, DIAGENESIS AND
RESERVOIR QUALITY OF
THE UPPER SPRABERRY FORMATION, TX**

by

Claudio J. Saleta

**Submitted in Partial Fulfillment of
the Requirements for the Degree of**

Masters of Science in Geology

**New Mexico Institute of Mining and Technology
Department of Earth and Environmental Science**

Socorro, New Mexico

August, 1999

ABSTRACT

The Spraberry Formation is part of the submarine fan and deep marine deposits of the Midland Basin. The unit consists of very fine-grained sandstones, siltstones, shales, and carbonate mudstones. These rocks show different degrees of lamination, bioturbation, convolute bedding, and a complex mineralogy.

The Spraberry reservoirs are naturally fractured, with very low matrix permeability that ranges from 0.1 to 1 md. Most of the reservoir fluid conductivity is due to the presence of a broad fracture system, wherein hydrocarbons stored in the pore space of the rock matrix flows at very low rates. The rock framework directly influences permeability, capillary pressure, and wettability characteristics of the reservoirs. For this reason the interaction between rock matrix, natural fractures and fluid flow must be well understood.

Small-scale lithofacies from thin-section and core-plug petrophysics were described for core intervals analyzed in the Upper Spraberry Formation. The analysis of these lithofacies included observation of their petrographic properties as well as results from fluid flow experiments for each lithofacies type. The Spraberry Formation contains two clean and porous sandstone lithofacies, one carbonate mudstone, one dolomitic-cemented siltstone, and two clay-rich lithofacies were also found using thin-section analysis. Among all lithofacies present, the clean and porous sandstones show good reservoir quality while other lithofacies exhibit poor or total lack of porosity and permeability. The main diagenetic processes affecting the unit are as follows: quartz cementation, clay precipitation, carbonate cementation, grain and cement dissolution, and fracture formation and mineralization.

Rock properties vary gradually from reservoir rocks to non-reservoir rocks following two main trends: 1) increasing organic and argillaceous content with decreasing porosity, 2) increasing carbonate sediments and cements with decreasing porosity. Both trends show a strong relationship to grain density, which in turn, suggests that lithological variability is an important control on reservoir properties. Water and oil saturation is also strongly controlled by lithofacies variability rather than a single water/oil contact controlled by gravity forces. The fluid distribution is probably mainly controlled by pore throat diameter, pore throat distribution, pore morphology, capillary pressures, and wetting behavior of the rock fluid system. In general it is observed that the very small sizes of pores and pore throats make capillary forces strong enough to hold fluids tightly to the pore system. Thus, gravity forces are less dominant in controlling the distribution of fluid saturation. Core plug fluid flow data suggest that fluid distribution is controlled by the wetting behavior of the different minerals that form each lithofacies along the stratigraphic sequence. Fine-grained lithofacies such as dolostones and argillaceous siltstones show high percentages of water saturation, whereas low water saturation is associated to clean very fine sandstones and siltstones richer in hydrocarbons.

ACKNOWLEDGMENTS

This investigation was sponsored by the Department of Energy (contract No. DE-FC22-95BC1494942) and Pioneer Natural Resources and in coordination with the New Mexico Petroleum Recovery Research Center (NMPRRC).

I am thankful to all my committee members for the assistance, patience, and encouragement during the progress of this research. I would like to express special gratitude to my research adviser, Dr. David S. Schechter, principal investigator of this project and head of the Integrated Naturally Fractured Reservoir Group at NMPRRC. Dr. David S. Schechter was confident on my ability to perform the geological characterization for this project and provided important guidance and criticisms at numerous stages of this study. I thank my academic advisor, Dr. Peter Mozley, for the helpful discussions, direction and insight during the research and editing stages of this investigation, and Drs. David Johnson and Larry Teufel for their valuable input. I would like to acknowledge my friend, Dr. Maqsood Ali for his assistance with the use of the minipermeameter, contributions on the integration of the different data sets and the overall reservoir characterization.

I am profoundly grateful to Martha Cather for her suggestions and assistance, and Liz Bustamante for editing the manuscript. Reservoirs Inc. laboratories from Houston provided the SEM photomicrographs and petrophysical data analyzed in this study.

Finally, special dedication of this work goes to Ines Gonzalez de Saleta, Claudio M. Saleta and Stephanie G. Monsterleet whose love and encouragement formed the basis of this effort.

TABLE OF CONTENTS

ABSTRACT	i
ACKNOWLEDGMENTS	iii
TABLE OF CONTENTS.....	iv
LIST OF TABLES	viii
LIST OF FIGURES	ix
NOMENCLATURE.....	xiv
CHAPTER 1 INTRODUCTION	1
1.1 Geological Background.....	8
1.1.1 Midland Basin Paleogeography and Major Geological Units Related to the Spraberry Formation	8
1.1.2 Tectonic History.....	10
1.2 Depositional Systems and Reservoir Quality: Previous Studies.....	11
CHAPTER 2 METHODS	15
2.1 Techniques to Examine Rock Character	15
2.1.1 Core Description and Sedimentological Analysis	15
2.1.2 Petrographic Analysis	16
2.1.3 X-Ray Powder Diffraction Analysis (XRD).....	18
2.1.4 Scanning Electron Microscopy – SEM (Reservoirs Inc.).....	19
2.2 Log Analysis Techniques.....	19
2.2.1 Gamma Ray Log	19
2.3 Petrophysical Analysis Techniques.....	20
2.3.1 Computer-Controlled Scanning Air Minipermeameter (CCSAM).....	20
2.3.2 Flow-Through Rock for Nitrogen Permeability and Helium Porosity Determination	22
2.3.3 Mercury Injection Techniques: Capillary pressure, Pore Distribution, Pore Throat Size and Connectivity	24
2.3.4 Dean Stark Methodology for Determination of Water and Oil Saturation.....	25

CHAPTER 3	CORE INTERPRETATION AND	
	SEDIMENTOLOGICAL ANALYSIS	27
3.1	Core Description – Large Scale Lithofacies	27
	3.1.1 Mudrock Lithofacies	31
	3.1.2 Sandstone Lithofacies	37
3.2	Lithofacies Interpretation	38
	3.2.1 Deep Marine Sediment Deposition in the Midland Basin	40
	3.2.2 Depositional Setting for Mudrock Lithofacies.....	42
	3.2.3 Depositional Setting for Sandstones Lithofacies Non-Cyclical Deposit.....	44
CHAPTER 4	PETROGRAPHY AND DIAGENESIS	46
4.1	General Textures and Mineralogy.....	46
4.2	Pore Morphology, Distribution and Pore Throat Radii.....	62
4.3	Categories of Small Scale Lithofacies	66
	4.3.1 Relation Between Large Scale Lithofacies (Chapter 3) and Small Scale Lithofacies (Chapter 4).....	66
	4.3.2 SSL-A.....	79
	4.3.3 SSL-B.....	80
	4.3.4 SSL-C.....	81
	4.3.5 SSL-D.....	82
	4.3.6 SSL-E.....	82
	4.3.7 SSL-F	83
4.4	Diagenetic Interpretation.....	84
	4.4.1 Arkosic Sandstones, Quartz Overgrowths and Pressure Solution of Quartz Grains	85
	4.4.2 Clay Diagenesis.....	91
	4.4.3 Hydrocarbon Emplacement and Relation to Clay Diagenesis	100
	4.4.4 Pyrite Cement.....	102
	4.4.5 Carbonate Diagenesis.....	102

4.4.6	Origin and Mineralization of Spraberry Fractures	104
4.4.7	Paragenesis	112
CHAPTER 5 PETROPHYSICS		
	Rock and Fluid Flow Analysis Assessing Reservoir Quality	119
5.1	Description of Petrophysical Properties.....	120
5.1.1	Gamma Ray Log Resolution.....	120
5.1.2	Computer-Controlled Scanning Air-Minipermeameter	123
5.1.3	Permeability, Porosity, Water Saturation, Grain Density and Capillary Pressure from Flow-Through Rock Analysis and Dean Stark	123
5.1.4	Analyzed Cores	124
5.2	Discussion of Petrophysical Properties.....	126
5.2.1	Permeability, Porosity and Water Saturation Relationships	126
5.2.2	Grain Density and Porosity Relationships	135
5.2.3	Pore Throat Relationships Based on Mercury Capillary Pressure	138
CHAPTER 6 CONTROLS ON RESERVOIR QUALITY		
	IN THE UPPER SPRABERRY FORMATION	142
6.1	Factors Controlling Porosity, Permeability and Other Petrophysical Parameters	142
6.1.1	Primary Controls	144
6.1.2	Secondary Controls (diagenetic).....	146
6.1.3	Secondary Porosity Processes	149
6.1.4	Preservation of Rock Fabric Porosity and Formation of Fracture Porosity Due to Overpressuring.....	152
6.2	Use of Small-Scale Lithofacies to Describe Reservoir Quality Variability	153
6.2.1	Petrophysical Description of Small-Scale Lithofacies – SSL.....	154
6.2.2	Interpretation of Petrophysical Properties of Small-Scale Lithofacies	158
6.3	Significance of the Small-Scale Lithofacies Analysis	161

CHAPTER 7 CONCLUSIONS AND RECOMMENDATIONS 164

7.1 Lithofacies Interpretation of Cores and Sedimentological Analysis 165

7.2 Petrography and Diagenesis..... 165

7.3 Petrophysical Data Integration with Thin Section Controls 167

7.4 General Conclusions 168

7.5 Recommendations..... 170

REFERENCES..... 172

Appendix 180

LIST OF TABLES

Table 1.1: Techniques and number of samples examined for each core from the 1U and 5U units in the Upper Spraberry Formation	3
Table 1.2: Stratigraphic column for the Permian Basin and shelves (Midland Map Company, 1993).	5
Table 1.3: Stratigraphic units in the Spraberry formation, Midland Basin, west Texas.....	6
Table 3.1: Summary of large-scale lithofacies (LSL) obtained from core description showing sedimentary structures, occurrence of fossils and environment of deposition for each lithofacies	30
Table 4.1: Mineralogical averages for point counts of thin sections for six categories of small-scale lithofacies in three cored wells	47
Table 4.2: X-ray diffraction (XRD) clay mineralogy	60
Table 5.1: This table summarizes grain density data in relation to the major lithofacies. Patchy dolomitic siltstone (SSL-D) is a lithofacies that falls between SSL-B and SSL-F	137
Table 5.2: This table summarizes helium, nitrogen and mercury injection data for plugs of different lithofacies that occur in the Spraberry Formation	140

LIST OF FIGURES

Fig. 1.1:	Map showing location of Spraberry trend area in west Texas. Also included are well locations for the three cored wells used in this study.....	2
Fig. 1.2:	Permian paleogeographic map (left) showing the location of the Midland Basin and the Spraberry Trend in relation to surrounding shelves, channels, platforms and neighboring basins	9
Fig. 1.3:	Depositional model developed by C. R. Handford (1981)	12
Fig. 2.1:	Schematic illustration of the computer controlled scanning minipermeameter equipment developed by Heller (1992)	21
Fig. 3.1:	Correlation of gamma ray log with core description for the E.T. O'Daniel 37 core	28
Fig. 3.2:	Correlation of gamma Ray log with core description for the Shackelford 138A core	29
Fig. 3.3:	Large Scale Lithofacies (LSL) from Core Description: Mudrock Lithofacies.....	32
Fig. 3.4:	Large Scale Lithofacies (LSL) from Core Description: Sandstone and Laminated Lithofacies	34
Fig. 4.1:	Ternary diagrams for three samples from three cored wells in the Upper Spraberry Formation	49
Fig. 4.2:	Photomicrographs showing general petrographic characteristics from thin sections.....	50

Fig. 4.3:	Photomicrographs showing quartz overgrowths and pressure solution.....	53
Fig. 4.4:	Photomicrographs showing dissolution textures in the Upper Spraberry Formation	55
Fig. 4.5:	SEM photomicrographs showing different types of illite accumulation, dolomite cement and pyrite in the Upper Spraberry formation.....	58
Fig. 4.6:	Two X-ray diffractograms showing clay composition	61
Fig. 4.7:	Photomicrographs showing carbonate cement replacement.....	63
Fig. 4.8:	Very fine sandstone and coarse siltstone, with moderate porosity – SSL-A	67
Fig. 4.9:	Photomicrographs of siltstone and very fine sandstones, slightly patchy cemented and laminated – SSL-B	69
Fig. 4.10:	Photomicrographs of silty dolomite mudstone “Dolostone” – SSL-C.....	71
Fig. 4.11:	Photomicrographs of patchy dolomitic siltstone – SSL-D	73
Fig. 4.12:	Photomicrographs of shale and silty shale – SSL-E	75
Fig. 4.13:	Photomicrographs of very argillaceous laminated siltstones – SSL-F	77
Fig. 4.14:	Model developed by Thomson (1959) for the effect of clay intercalation near quartz dissolution and precipitation	89

Fig. 4.15: The Hower model (1981) for illitization has a number of Similarities with the diagenetic characteristic observed in the Spraberry formation	95
Fig. 4.16: The effective stress at depth is the sum of the external stresses minus The pore pressure. See fracture plane parallel to σ_1 and σ_2	106
Fig. 4.17: Three possible models for regional fracturing. (A) An increase in the maximum stress enlarges the stress circles to where it touches the yield envelope. (B) A decrease in the minimum stress also enlarges the stress circle reaching the point of failure. (C) An increase in pore pressure shifts the position of the stress circle to where it may touch the yield envelope (compiled from Lorenz, Teufel, and Warpinski, 1991)...	107
Fig. 4.18: Two photomicrographs showing barite mineralization on fracture surface ..	109
Fig. 4.19: Generalized paragenetic sequence for the Upper Spraberry Formation	113
Fig. 4.20: Photomicrographs showing diagenetic sequence for dolomite cement, quartz overgrowths and clays.....	116
Fig. 5.1: Core E.T. O'Daniel 37. Integration of petrographic and petrophysical data	121
Fig. 5.2: Core Shackelford 138A. Integration of petrographic and petrophysical data	122
Fig. 5.3: Porosity-permeability from core-plug measurements. Colored dots represent different core plugs lithofacies in correlation with thin section information.....	125

Fig. 5.4: Cross plots showing differences in porosity-permeability correlation for samples above and below 7195-ft depth for E.T. O’Daniel 37 core127

Fig. 5.5: Core plug data (Sw and porosity) for Shackelford 138A - Relatively similar sandy units do not show obvious evidence of major heterogeneity in core samples. Petrophysical properties measured in the lab show important variations between fluorescing pay zones and non-pay zones richer in clay129

Fig. 5.6: Core plug data (permeability and porosity) for Shackelford 138 – 1U unit, Upper Spraberry Formation. Non fluorescent zones are commonly lower quality reservoirs and non-reservoir rocks strongly affected by pore lining and pore bridging clays.....129

Fig. 5.7: Core plug data (Sw and porosity) for cores Shackelford 138A and E.T. O’Daniel. Colored dots represent thin section control for small-scale lithofacies. There is a general increase in water saturation with a gradual decrease of porosity130

Fig. 5.8: This graph shows several curves for Sw and capillary pressure from Imbibition experiments done with core plugs from various depths in the Spraberry sandstones.....134

Fig. 5.9: This is a chart of porosity vs. grain density data from core plugs from Shackelford 138A and E.T. O’Daniel 37136

Fig. 5.10: These three cross-plots of mercury injection data (porosity-permeability and pore throat radius) from cored wells Shackelford 138A and E.T. O'Daniel 37. Cross-plots suggest that rock-fluid behavior is tied to lithological variability for the six small-scale lithofacies (SSL) under study.....	139
Fig. 6.1: Point Count data for porosity vs. matrix summation by small-scale lithofacies.....	143
Fig. 6.2: Point Count data for porosity and cement summation by small-scale lithofacies.....	147
Fig. 6.3: This series of cross-plots shows pore throat distribution for the six lithofacies cited before.....	155

NOMENCLATURE

K	=	air permeability (darcy)
μ	=	viscosity of fluid (air in the case of the minipermeameter, centipoise)
A	=	syringe area (centimeter squared)
Δx	=	distance traveled by the plunger from x_1 to x_2 (centimeters)
a	=	inner radius of tip (centimeters)
G	=	geometrical factor
Γ	=	pressure correction factor
P_g	=	gauge pressure inside syringe ($P - P_a$) (Fractions of a standard atmosphere)
P	=	absolute value of the applied pressure
P_a	=	atmospheric pressure
T	=	time interval for syringe plunger to sink from x_1 to x_2 (seconds)
t_{kt}	=	time interval in which the syringe plunger will move downwards by the distance Δx in the absence of flow into the rock (seconds)
Kb	=	core plug permeability (md)
ϕ	=	porosity (fraction)
q	=	liquid flow rate (ml/h)
L	=	length of core plug (cm)
A	=	Transversal area of core plug (cm^2)
ΔP	=	drop in flow pressure (psi)
P	=	helium pressure (psi)
$V1$	=	volume helium chamber (cm^3)
$V2$	=	volume of system including helium chamber and matrix cup (cm^3)

PV_t	=	total pore volume for core plug (cm^3)
V_b	=	core plug bulk volume (cm^3)
GD	=	grain density (g/cc)
GV	=	grain volume (cm^3)
W_{dry}	=	amount of weight of core or grain material (g)
S_w	=	water saturation (fraction)
S_{wi}	=	irreducible or non-movable water saturation (fraction)
I_w	=	Amott wettability index to water (fraction)
LSL	=	large-scale lithofacies
SSL	=	small-scale lithofacies
IRF	=	igneous rock fragment
MRF	=	metamorphic rock fragment
SRF	=	sedimentary rock fragment
SEM	=	scanning electron microscopy
XRD	=	x-ray diffraction
I/S	=	illite/smectite interlayer
σ_1	=	major principal stress (vertical; psi)
σ_2	=	intermediate principal stress (horizontal; psi)
σ_3	=	minimum principal stress (horizontal; psi)
σ'	=	effective stress (psi)
σ	=	total stress (psi)
p	=	pore pressure (psi)

CHAPTER 1

INTRODUCTION

The Spraberry reservoirs (Fig. 1.1) are traditionally considered marginal producers. They were discovered in 1949 and have been producing oil since then. The objective of this project is to develop a detailed geological and petrophysical characterization of the reservoir and non-reservoir rocks of the upper Spraberry Formation in west Texas. The upper Spraberry sandstones are under investigation to develop CO₂ injection techniques for enhanced oil recovery (Schechter et al., 1998). Understanding rock/fluid interaction is key to the assessment of optimum recovery using CO₂ injection. For this reason, a combined characterization of rock and fluid flow behavior is performed in this thesis using petrographic and petrophysical properties. This knowledge in relation to the post-depositional rock forming processes (diagenesis), is also of major importance in understanding the present quality of the reservoirs and to allow extrapolations for infill drilling, perforations, workover-jobs and horizontal well programs. In this investigation, the Spraberry Formation has been evaluated by various analytical techniques to define relationships between facies variability and fluid conductivity (Table 1.1).

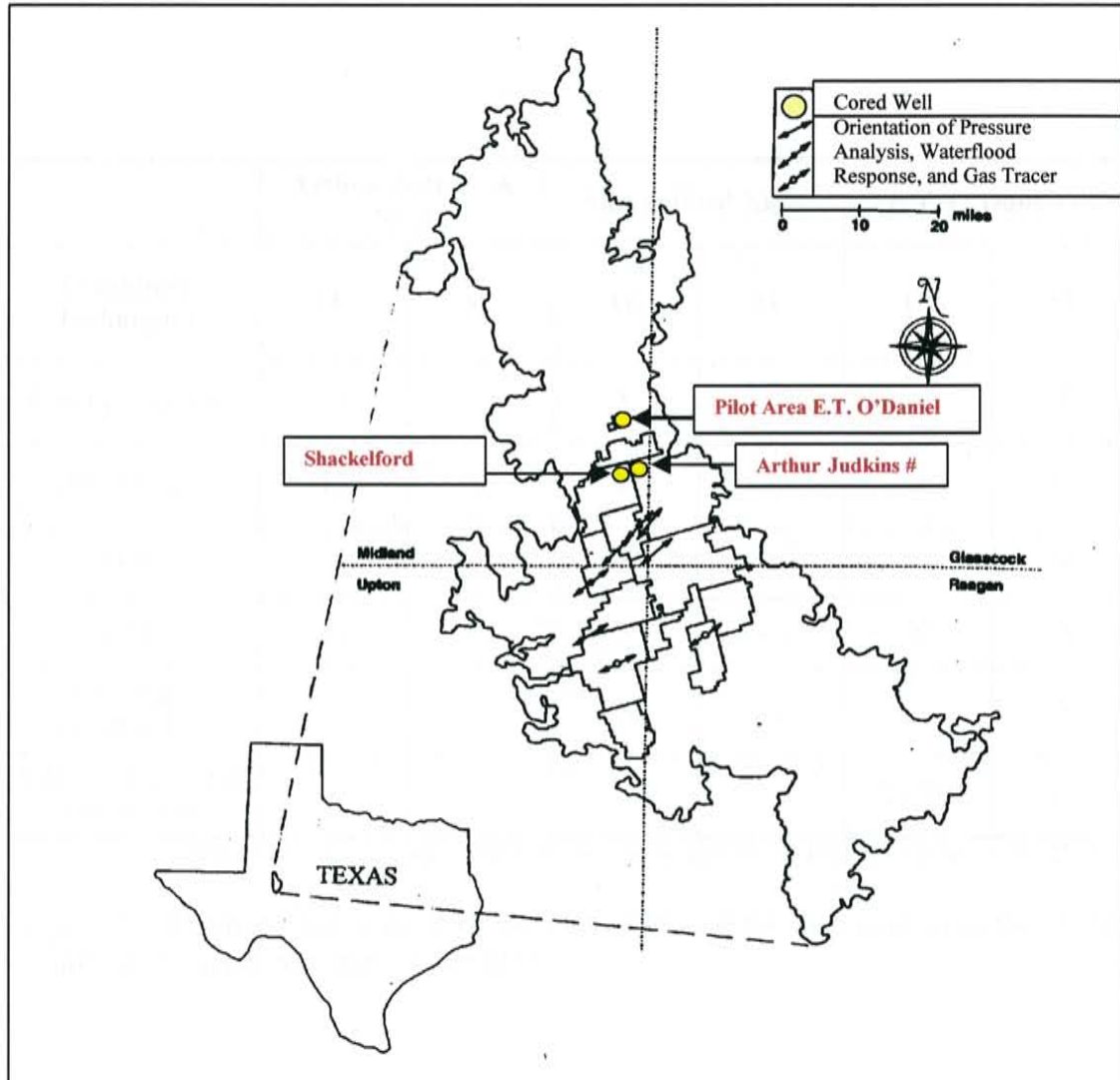


Figure 1.1 - Map showing location of Spraberry trend area in west Texas. Also included are well locations for the three cored wells used in this study.

Combined Techniques	Arthur Judkins A No.5		Shackelford 138A		E.T. O'Daniel 37	
	1U	5U	1U	5U	1U	5U
Core Descriptions	---	---	X	---	---	X
Thin Sections	13	9	34	---	5	19
XRD	---	---	8	---	---	---
SEM	---	---	X	---	X	X
Core Plug Petrophysics	---	---	X	---	---	X
Side Wall Core Plugs Petrophysics	---	---	---	---	X (2U)*	---

*Side-wall core plugs were initially thought to come from 1U although these belong to the 2U unit.

Table 1.1: Techniques and number of samples examined for each core from the 1U and 5U units in the upper Spraberry Formation.

These clastic reservoirs consist of low permeability, fine-grained sandstones and siltstones interbedded with shaly non-reservoir rocks. The Spraberry Formation occurs in Leonardian age rocks (Silver and Todd, 1969; Table 1.2) from the Permian period and its occurrence is restricted to the subsurface of the Midland Basin. Although the formation is composed of three members — upper, middle, and lower — the upper member is the main focus of this study (Table 1.3). The “operational units” in the upper Spraberry comprise two crude, coarsening-upward intervals designated as the Floyd Submarine Fan (operational units 1U-4U) and the Driver Submarine Fan (operational units 5U-6U), respectively.

The regional geological setting of the Spraberry Trend area is discussed in this and subsequent chapters. This is based on the investigation of all previous literature written on the Permian Basin and Spraberry Formation.

I have also described two cores, the Shackelford 138A and E.T. O’Daniel 37, in order to create a sedimentological analysis (Chapter 3). This analysis includes valuable input from previous work on the sedimentology of the area. A total of seven large-scale lithofacies (LSL) from core description were defined. These lithofacies are based on distinguishable sedimentary structures, textures, grain size, mineralogy, and depositional behavior observed in core samples. Depositional environments have been interpreted with reference to previous investigations.

Petrographic analysis and diagenesis are presented in Chapter 4. A third core is included as a source of samples for the thin section analysis (well cored: *A. Judkins 5*). Each of the three wells examined are covered to a different extent depending on the quality of the data and the samples. In Chapter 4 six petrographic categories are introduced based on thin section observation, point count analysis, scanning electron

SYSTEM	SERIES	GROUP	FORMATION
Permian	Ochoa		Dewey Lake
			Rustler
			Salado
			Castile
	Guadalupe	Whitehorse	Tansill
			Yates
			Seven Rivers
			Queen
			Grayburg
		Word	San Andres
			San Angelo
			Clear Fork
		Leonard	
		Leonardian	Wichita
	Middle Spraberry		
	Lower Spraberry		
	Dean		
	Wolfcamp		Wolfcamp

Table 1.2 – Stratigraphic column for the Midland Basin and shelves (modified from the Midland Map Company, 1993).

SYSTEM	FORMATION	OPERATIONAL UNIT	DEPOSITIONAL UNIT		
LOWER PERMIAN	U. SPRABERRY	1U	FLOYD SUBMARINE FAN		
		2U			
		3U			
		4U			
		5U	DRIVER SUBMARINE FAN		
		6U			
	MIDDLE SPRABERRY		1M		
			2M		
			3M		
			4M		
			5M		
			6M		
			1L		JO MILL SUBMARINE FAN
		L. SPRABERRY	2L		
			3L		

Table 1.3 – Stratigraphic units in the Spraberry Formation, Midland Basin, west Texas. Note the 1U and 5U units (under investigation) within the upper Spraberry Formation (Modified from Tyler et al., 1988).

microscopy, and X-ray diffraction analysis. To differentiate them from the lithologic categories obtained from core description, the thin-section categories are called “Small Scale Lithofacies” (SSL). Pore space and cement characteristics were studied in order to assess reservoir quality. Based on the results obtained from the thin sections, scanning electron microscopy (SEM), and X-ray diffraction (XRD), rock-forming processes during burial (diagenesis) were analyzed to better understand the manner and extent to which the reservoir quality has been enhanced or damaged.

The analysis presented in Chapter 5 includes the integrated results of the previous petrographic analysis with petrophysical measurements (e.g., porosity, permeability, and log response) in order to define combined rock and fluid flow characteristics. Previous studies of the Spraberry attempted to define reservoir targets based on the strength and shape of the gamma ray (GR) deflection as criteria for determination of net pay. Isopach maps were developed based on this type of delineation of the pay zones. The present investigation attempts to develop a more precise definition of Spraberry rock quality. In order to reach this objective, it is necessary to integrate very accurate mineralogical and diagenetic data concerning the heterogeneous character of the formation with knowledge of fluid distribution, saturation, porosity, conductivity, and how tight capillary pressures are holding the fluids to the rock-pore system.

It was the initial intention to include log analysis of all wells in relation to the rock and fluid flow model. However, the scope of this type of investigation prevents us from including further analysis. Geophysical well log response should be understood in relation to the rock, pore, and fluid model in order to perform correct and efficient log estimations of uncored wells. Sound petrophysical results and log interpretation in the Spraberry

Formation are used in definition of pay zones, exploration of new horizons, determination of targets in horizontal drilling, isopach mapping, reserve estimations and input data used in simulation. In these areas this type of study is of extreme importance in managing reservoir production of the Spraberry trend; therefore, this is the subject of current and future investigations.

1.1 GEOLOGICAL BACKGROUND

1.1.1 Midland Basin Paleogeography and Major Geological Units Related to the Spraberry Formation

Within the Midland Basin, the surrounding shelves (Fig. 1.2) have the following names: Matador arch to the north, Northwestern shelf on the northwest boundary, the Central Basin Platform to the west, and the Southern shelf in the south. The shelf boundary situated to the east of the Midland Basin is correspondingly named the Eastern shelf. The Hobbs and the Sheffield channels connected the Midland Basin to the open ocean and also to the Delaware Basin.

Correlation of the shelf to the deep basin facies has been very difficult. Jeary (1978) and Handford (1981) have shown that the Spraberry Formation is coeval with the upper Clear Fork and Glorieta Formations. The Dean and the Spraberry Formations are divisible into four genetic sequences, referred to as the Dean, Lower Spraberry, Middle Spraberry and upper Spraberry sequences (Table 1.3). Each of these units include a coarsening upward sequence of shales, carbonates, very fine-grained sandstones, and siltstones.

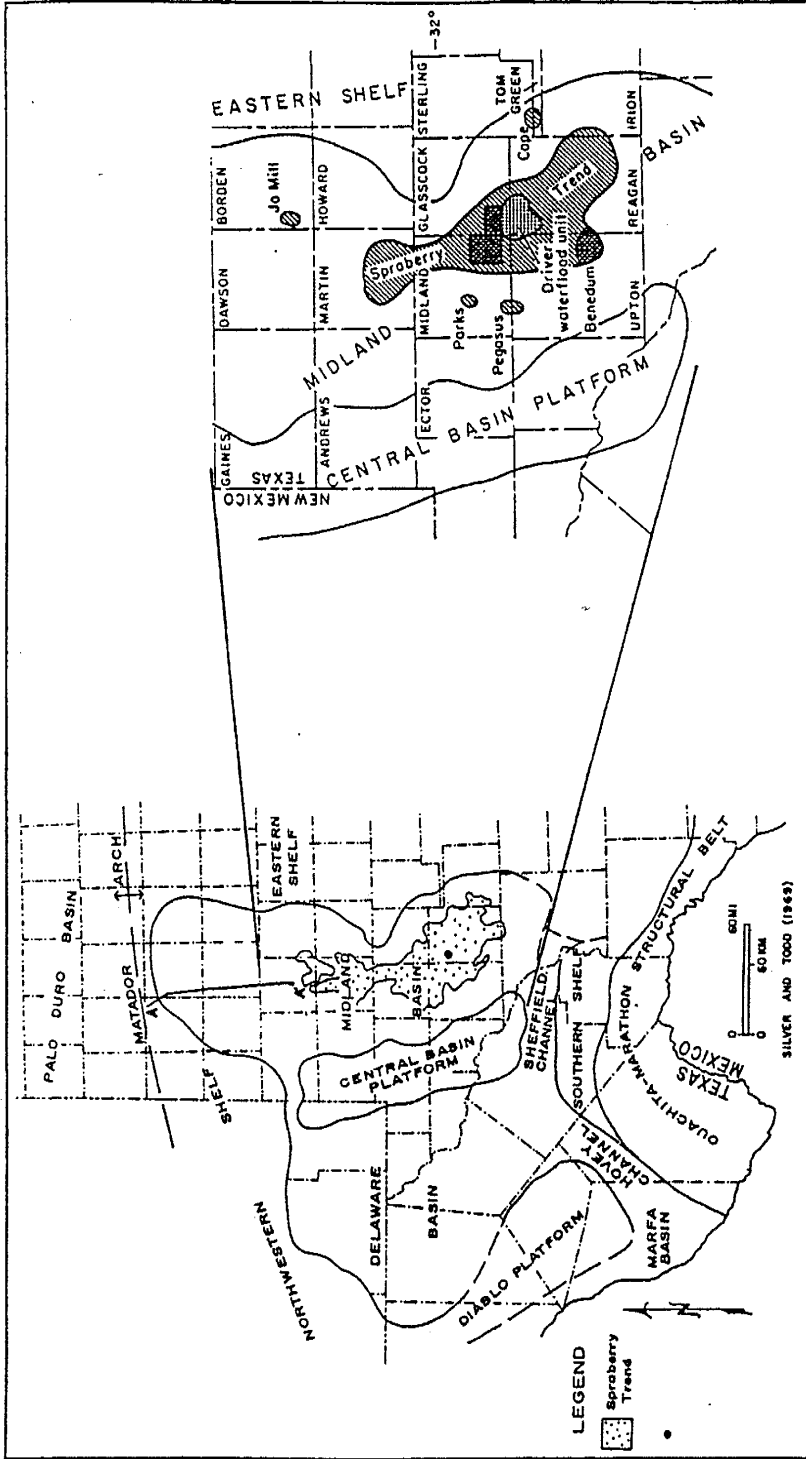


Fig 1.2 - Permian paleogeographic map (left) showing the location of the Midland Basin and the Spraberry Trend in relation to surrounding shelves, channels, platforms and neighboring basins. To the right, an enlarged map exhibits more details of the Spraberry Trend area, the Midland Basin, the Eastern Shelf and the Central Basin Platform.

1.1.2 Tectonic History

A series of tectonic events have shaped the Midland Basin throughout its history. Episodes of subsidence affected the basin from Ordovician to early Pennsylvanian time (Houde, 1979; Horak, 1985). Before the early Pennsylvanian, the area was occupied by the Tobosa Basin (Adams, 1965) then reshaped to form the proto-Permian basin. The Ouachita Fold Belt affected the shelves surrounding the basin and the Midland Basin itself during different orogenic events (late Mississippian to early Pennsylvanian time and also early Permian; Harrington, 1963). As a result of late Pennsylvanian uplift the Eastern Shelf slope was reversed to a westerly direction (Cheney et al., 1952). Harrington (1963) shows how the Central Basin Platform started forming at the same time that the Ouachita-Marathon Fold Belt was undergoing deformation. A series of thrust-faulted anticlines during late Mississippian to early Pennsylvanian time formed the Central Basin Platform. At this time the Tobosa Basin started to become two separate basins: the Midland and Delaware Basins. The Matador Arch or Archipelago (to the north) was formed as a series of basement uplifts, trending in an east-west direction. Arkosic sediments and carbonates were spread in all directions, especially to the south where the depositional slope was more pronounced (Horak, 1985).

Horak (1985) explained that all parts of the Permian Basin were merged acting as an integrated unit throughout most of the Mesozoic. Then during early to middle Cretaceous weak subsidence permitted the Cordilleran and Gulf of Mexico seaways to connect. Horak (1985) describes the Laramide, a very important tectonic event that probably intervened in the formation of natural regional fracture patterns in the Spraberry Formation of the Permian Basin. He described this event as an epeirogenic

uplift and weak orogenic (compressive) overprinting that affected the Permian Basin east of the Laramide front. The Laramide phase elevated the western portion, which affected the whole region in a weak compressional regime. A weak extensional event then followed the Laramide orogeny. The effect of the Laramide orogeny is presently regarded as the only important compressive tectonic event that could have produced the necessary stress to form regional natural fractures with a roughly northeast orientation in the Spraberry Formation. This will be evaluated in the discussion about fractures in Chapter 4.

1.2 DEPOSITIONAL SYSTEMS AND RESERVOIR QUALITY

Depositional patterns within the Spraberry Formation were partially controlled by the paleogeographic setting of the Permian Basin and shelf (Fig. 1.2). The deep marine deposits of the Midland Basin are surrounded by shallow-marine carbonate shelves and are considered to be of Leonardian age (Silver and Todd, 1969). Handford (1981) presented an important regional sedimentological work on the deep-water, fine-grained clastic and carbonate facies of the Dean and Spraberry Formations (Fig. 1.3). He also provided cross-sections, lithofacies descriptions, maps and interpretations that have been useful in exploration and production strategies.

Other studies that cover cores, well logs and isopach mapping on a regional scale have been performed recently by the Texas Bureau of Economic Geology (BEG; Guevara, 1988; Tyler and Gholston, 1988). The BEG studies demonstrated that sediments in the Spraberry Formation show highly variable stratification with a laterally complex character.

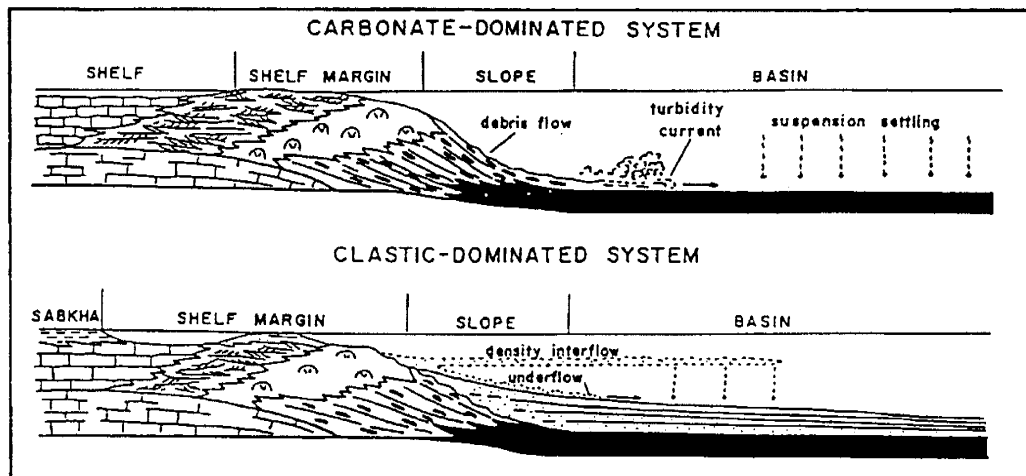
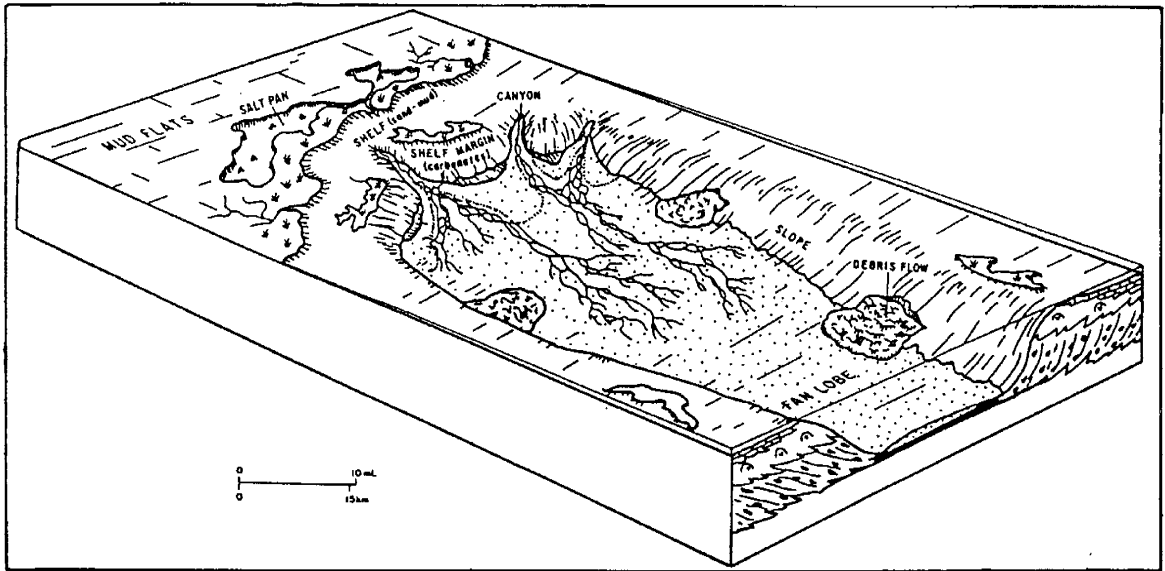


Fig. 1.3 – Depositional model developed by C. R. Handford (1981). Upper illustration shows a north-south sketch of the Midland Basin with a marine fan and channel system eroding shelf materials and deposition along the basin plane. Lower illustration shows the carbonate-dominated and clastic-dominated systems of Handford.

They proposed that submarine fan channels stacked vertically and inter-stratified with interaxial shaly laminated siltstones and massive shales produce strong variability in reservoir quality. Tyler and Gholston (1988) also found that lateral variation in fluid saturation is pronounced and is strongly tied to depositional facies.

To uncover the lithological and fluid flow relationships related to the complexities described above form an important objective of investigation in this study. Until now, detailed studies concerning petrography, diagenesis and petrophysics have not been performed to an appropriate extent.

Reservoir Quality: Warn and Sidwell (1953) found that pressure solution and interstitial clay were the main factors that led to the low porosity and permeability values observed. The quality of Spraberry reservoirs is also strongly related to their fractured nature. Hubbert and Wills (1955) noted that the Spraberry Formation is a classic example of a naturally fractured reservoir, and explained how a tight and impermeable reservoir can become an economic prospect due to such fractures. This has been a major reason for the investigation of the extremely low permeability Spraberry reservoirs throughout the exploitation history. Another issue is the compartmentalization of Spraberry reservoirs. Guevara (1988) suggested that mud finely interstratified with sandstone reservoirs produced compartmentalization. His analysis shows that each compartment has an oil-water contact controlled by gravity forces. In Chapter five of this thesis, alternative explanations for the fluid distribution in the Spraberry Formation are discussed.

Schmitt (1954) stated that petroleum in the Spraberry originated from the organic matter deposited along with the mudrocks. Initially, anoxic bottom seawaters promoted

organic matter preservation. Later generation of hydrocarbons was fostered by overburden and temperature increase during burial (Cordell, 1977).

CHAPTER 2

METHODS

This chapter describes the techniques used to analyze the rock and fluid flow characteristics of the upper Spraberry Formation. These techniques are grouped in three categories: 1) examination of rock character using core description and microscopic analysis of rocks, 2) geophysical log analysis, and 3) study of fluid flow behavior, fluid saturation, porosity and pore throat distribution (petrophysics).

2.1 TECHNIQUES TO EXAMINE ROCK CHARACTER

A variety of sample types were examined, including: slabbed conventional cores, core plugs, side-wall core-plugs, thin sections, and broken pieces of rock from conventional cores.

2.1.1 Core Description and Sedimentological Analysis

The stratigraphic and sedimentological analysis is based on observations made from two conventional cores obtained from the upper part of the Spraberry Formation: operational units 1U and 5U. Sedimentary structures, facies classification, depositional environments, and other important information were determined. This core description

summarizes the sedimentological and stratigraphic setting of this investigation. Cored wells, from which samples were taken in order to develop a database for this project, are described as follows:

- Shackelford 138-A: The cored interval in this well covers the 1U operational unit and has been used in core description, sedimentological and depositional environment analysis, petrographic and diagenetic study and petrophysics.
- E.T. O'Daniel 37: This core covers the 1U and the 5U operational units. Samples from this core were used in analysis of the sedimentology and environment of deposition, petrographic and diagenetic analysis, and petrophysics.
- Arthur Judkins "A" 5: A description of this old core is not presented due to its poor condition (lack of multiple core portions and some material is not in proper depth sequence). This core covers the 1U and 5U operational units. We have used samples from this core for thin section analysis of diagenesis (thin sections from Mobil Oil).

2.1.2 Petrographic Analysis

Petrographic techniques were used to quantify mineral abundance, distribution, and types (grains and cements), to measure porosity, to document diagenetic textures (especially dissolution, cements, compaction, and discrete authigenic clays) and to identify depositional features. The data obtained are presented in photomicrographs, and cross-plots, and correlated in vertical log profiles with data from petrophysical measurements.

All thin sections were impregnated with blue-dyed epoxy to differentiate true porosity from that formed by plucking of grains during thin-section preparation. To aid in determining carbonate mineralogy (calcite, dolomite and ferroan dolomite), staining techniques such as alizarin red-s, and potassium ferrocyanide were used for some of the thin sections. Difficulties in impregnating the low permeability Spraberry rocks with blue epoxy makes recognition of porosity in some thin sections very difficult. In thin sections made later in the study, tight rock impregnation was used, which improved the quality of the porosity observations.

Out of approximately 100 thin sections analyzed, 80 were point-counted (Tables 1, 2, and 3 of Appendix). Modal composition is based on 300-points counted for each sample. By counting 300-points, a maximum of 0.06 error is expected for mineral phases that are as abundant as 50%. This error is obtained from a chart constructed by Van der Plas and Tobi (1965), which plots the standard deviation for a given component as a function of the number of total counts and area percent for that component. The “counting error” obtained from that chart for components less abundant than 50% is even smaller than 0.06. Thus, samples used in this investigation with point counts below 50% percent for most of the thin sections are considered representative of the mineralogical composition of the formation. The detailed point-count analysis was conducted to determine the percentage of detrital and authigenic minerals, the amount and type of pore filling constituents, and the percentage of visible pore space. Components that were not detected during the point count, but were observed in thin section, are recorded as “trace” amounts. Textural comparitors were used to determine mean grain size, degree of sorting and angularity of grains. A complete diagenetic analysis of the upper Spraberry

Formation has been performed based on observations of these thin sections, XRD clay mineralogy analysis, and SEM photomicrographs.

2.1.3 X-Ray Powder Diffraction Analysis (XRD)

Samples from the Shackelford 138-A core were prepared for clay mineralogy analysis, following procedures recommended by Dr. George Austin of the New Mexico Bureau of Mines and Mineral Resources. Samples were ground and dispersed in deionized distilled water, standing for 10 min in order to separate the floating finer part (<2.0 μm) by using a pipette to withdraw sufficient material to cover a glass slide. By using this procedure, samples strongly oriented to the slide surface with intense basal X-ray reflection are produced. Sodium hexamethaphosphate (Calgon) was used when persistent flocculation occurred. Sandy and cleaner samples that contain higher porosity and hydrocarbons showed an air-surfactant effect, with air bubbles floating part of the sediment to the surface, thus avoiding proper sedimentation. To correct this, the samples were placed under vacuum in distilled water before proceeding further.

X-ray powder diffraction (XRD) was used in the analysis of clay composition in the upper Spraberry Formation. The use of XRD provides qualitative and semiquantitative data on clay mineral abundance (units in parts in 10 are recommended by Dr. G. Austin to be acceptable estimates of mineral composition). A Rigaku 3064 diffractometer with Cu-radiation and a curve crystal were used to examine all samples. Three routine X-ray patterns 1) air-dried, 2) ethylene glycolated, and 2) heated to 350°C were recorded for each slide. An unoriented slide of cements coating a fracture in the Shackelford 138-A core was also examined by the X-ray diffractometer.

2.1.4 Scanning Electron Microscopy - SEM (Reservoirs Inc.)

Reservoirs Inc., a core laboratory based in Houston, provided photomicrographs from scanning electron microscopy. Sample trims from core plugs were mounted on aluminum stubs and sputter-coated with gold. SEM photomicrographs were used to examine rock fabric, porosity development, clay presence and distribution, and pore and mineral morphology. Specific clay mineralogy was seldom determined, due to the very fine nature and high compaction of the Spraberry sediments. In some areas flakes of illite were observed using SEM.

2.2 LOG ANALYSIS TECHNIQUES

2.2.1 Gamma Ray Logs

Conventionally, gamma ray log (GR) response is thought to be an adequate tool for determining pay and non-pay zones. Gamma ray logs can be used with a fair amount of certainty to differentiate between clay-rich and sandy units in the Spraberry Formation. However, log analysis accuracy should be improved in order to perform good estimations of carbonate rich zones and porosity determination. In this study I compare GR response with a large amount of data from different analytical techniques, petrophysical examination, and simple core observations in order to uncover relationships that lead to a more accurate interpretation of gamma ray and other geophysical well logs.

2.3 PETROPHYSICAL ANALYSIS TECHNIQUES

2.3.1 Computer-Controlled Scanning Air Minipermeameter (CCSAM)

A computer-controlled scanning air minipermeameter (Fig. 2.1) from the New Mexico Petroleum Recovery Research Center was used in this study. This equipment was developed by Dr. John P. Heller at the NMPRRC and has been extensively tested in numerous experiments by Heller (1992) and Ali (1993, 1996). The minipermeameter is particularly useful for obtaining a large number of small-scale permeability measurements.

A syringe provides a constant pressure supply, air flow is measured by a network of computer-controlled sensors and actuators, and a tight seal is formed when a silicon rubber probe tip is pressed against the surface of a rock specimen. The combined probe, syringe, and necessary electronics are mounted on a computer-controlled movable carriage, which can scan the length and width of a given core sample. Right-angle movement permits the implementation of a x-y grid pattern. Two parallel lines of measured points were used separated one to one and a half inches along the lines, and one or less inches between points in perpendicular direction to the pair of lines. The force of gravity acting on a weight resting on the plunger supplies constant air pressure inside the syringe. Lower permeabilities are reported after longer periods of time, whereas high permeability readings are obtained at a faster pace. A modified Darcy law determines permeability readings:

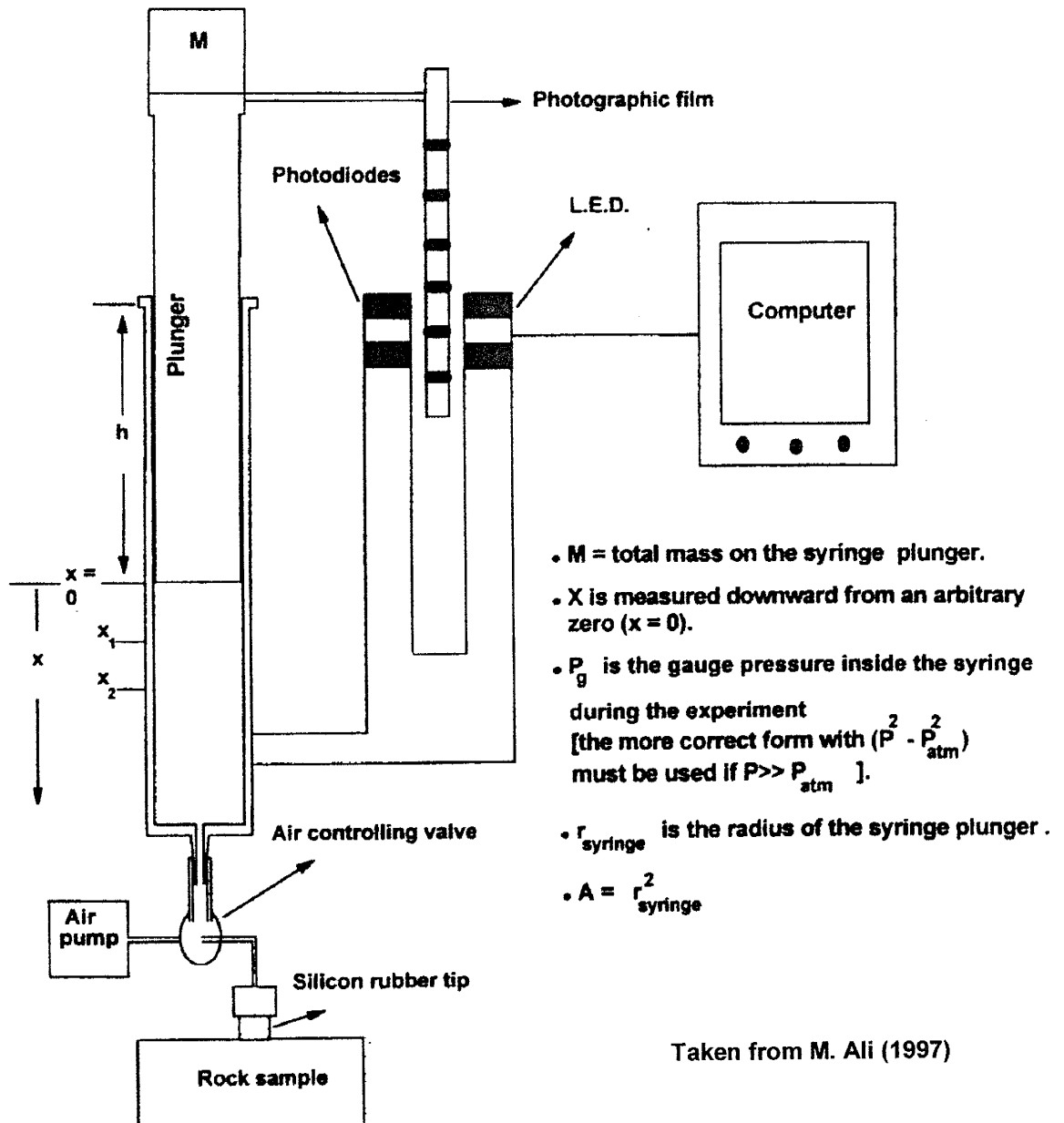


Fig. 2.1 – Schematic illustration of the computer controlled scanning minipermeameter equipment developed by Heller (1992) and extensively used by Ali (1997).

$$K = \frac{\mu A \Delta X}{a G \Gamma P_g} \left[\frac{1}{T} - \frac{1}{t_{ikt}} \right] \quad (2.1)$$

K = air permeability (darcy)

μ = viscosity of air (centipoise)

A = syringe area (square centimeter)

Δx = distance traveled by the plunger from x_1 to x_2 (centimeters)

a = inner radius of tip (centimeters)

G = geometrical factor

Γ = pressure correction factor

P_g = gauge pressure inside syringe ($P - P_a$) (fractions of a standard atmosphere)

P = absolute value of the applied pressure, and P_a = atmospheric pressure

T = time interval for syringe plunger to sink from x_1 to x_2 (seconds)

t_{ikt} = time interval in which the syringe plunger will move downwards by the distance Δx in the absence of flow into the rock (seconds)

2.3.2 Flow-Through Rock for Nitrogen Permeability and Helium Porosity Determination

Core plug samples of 1 and 1.5 inch diameter were used to measure petrophysical properties of the different lithofacies for two cores from the upper Spraberry Formation. Data gathered include porosity (ϕ), permeability (K), and grain density (from Reservoirs Inc., 1996). Formulas for the calculation of permeability, porosity and water saturation are given below. The data required to calculate permeability was obtained by injecting nitrogen gas into the samples at a constant pressure until a constant flow rate of gas

through the sample was attained (steady-state conditions). A core holder (Hassler-type) with a specific confining pressure (300 psia) was used. Permeability is a function of flow rate (q), viscosity of the fluid (μ), length of the core plug (L), transversal area of core plug (A), and drop in flow pressure (ΔP):

$$Kb = \frac{q \times \mu \times L}{A \times \Delta P} \quad (\text{Darcy Equation}) \quad (2.2)$$

Boyle's law was used to calculate porosity for each core plug sample:

$$P1 \times V1 = P2 \times V2 \quad (2.3)$$

Helium was used as the gas phase. Two chambers of known volumes were connected, one containing helium at a given pressure ($P1$) and another (matrix cup) with a core plug. The helium expanded into the matrix cup and an equilibrium pressure ($P2$) was recorded. The initial volume ($V1$) of the sole helium chamber was known; thus the volume of the new system -helium chamber and matrix cup ($V2$) was determined using Boyle's Law. By subtracting $V1$ from $V2$ the total pore volume (PVt) for the given core plug was obtained. Then, porosity (ϕ) is simply the fraction between the total pore volume (PVt) obtained and core plug bulk volume (Vb) determined from mercury immersion (*Archimedes principle*) and corroborated by measuring core plug dimensions.

$$\phi = \frac{PVt}{Vb} \quad (2.4)$$

Grain density (GD) for each core plug is a function of the grain volume and weight of the clean and dry core material. Grain volume (GV) is the result of subtracting the total pore volume (PV_t) from the bulk volume (V_b) for each plug sample:

$$GV = V_b - PV_t \quad (2.5)$$

GD is thus the amount of weight of grain or core material (W_{dry}) per volume of grain (GV) in the given sample:

$$GD = \frac{W_{dry}}{GV} \quad (2.6)$$

These sets of data are analyzed using cross-plots correlating pairs of data to define relationships and controls on reservoir quality. Implications regarding variability and lithological controls on rock-fluid behavior are discussed in the last chapter.

2.3.3 Mercury Injection Techniques: Capillary Pressure, Pore Distribution, Pore Throat Size and Connectivity

Mercury injection (data compiled from Reservoirs Inc., 1996) into core plugs was used to determine capillary pressures, pore throat sizes, connectivity, relative quality of different rocks and Leverett's "J" function. This procedure uses a vacuumed injection chamber to hold a core plug. A specific distance between the injection of mercury and the core plug is maintained to avoid unwanted change of pressure. Mercury starts intruding into the core pore system as a response to applied pressure (threshold

pressure). This determined amount of applied pressure was maintained until mercury intrusion ceased. At this point the pressure and the amount of mercury injected is recorded. The pressure then is increased incrementally and the same procedure is repeated. In this case the range of pressures selected was essentially 0-2000 psia and 0-60,000 psia for high-pressure measurements. The test results were used to calculate pore throat radii and Leverett's "J" function.

2.3.4 Dean Stark Methodology for Determination of Water and Oil Saturation

Saturation of fluids is commonly obtained from core plugs extracted from representative intervals from the reservoir and non-reservoir rocks. These are remnants of the original fluids contained in the rocks. In order to obtain representative and accurate results, preventive procedures and treatment of each sample before installing them in the Dean Stark apparatus should be performed. Prompt application of these procedures minimizes the loss of fluids and the level of error. In the case of the Spraberry Formation, the cores retrieved were preserved to avoid fluid lost due to the decrease in pressure. In the same way, after cutting the samples the excess fluid on the plug surface was wiped off taking care not to pull fluid out or push it into the interior of the sample. Weight of the plug samples was obtained on an analytical balance. After this, the samples were quickly placed in the apparatus or stored in a container to prevent evaporation. The distillation/extraction process lasted a minimum of 48 hours and it was stopped only when the water recovery was stabilized for 24 hours. Specific time duration would depend on the size of samples and their permeability. Then the oil extraction procedure is followed. Volumes of water and oil recovered were recorded. These data

were analyzed as percentages in the petrophysics chapter (Chapter 5) in combination with the rest of the petrophysical and petrographic data.

CHAPTER 3

CORE INTERPRETATION AND SEDIMENTOLOGICAL ANALYSIS

3.1 CORE DESCRIPTION – LARGE SCALE LITHOFACIES

In this investigation, I have developed a detailed core description that classifies lithofacies in two cores. Figures 3.1 and 3.2 show core descriptions for the E.T. O'Daniel No. 37 and Shackelford 138A wells. A total of seven lithologic categories (Table 3.1) were described in this study. These are called large-scale lithofacies (LSL) in order to differentiate them from the ones found using thin section analysis in the next chapter. These lithofacies are based on distinguishable sedimentary structures, textures, grain size and main mineralogy type observed macroscopically in cores. Depositional environments were interpreted based on core descriptions in order to find support for and further improve previous interpretations. The purpose of this core and sedimentological analysis is to serve as a framework for the subsequent petrographic and petrophysical analyses. The following list shows the different lithofacies defined by this core analysis.

**E.T. O'Daniel 37
Core Description
and
Gamma Ray Log
(API units)**

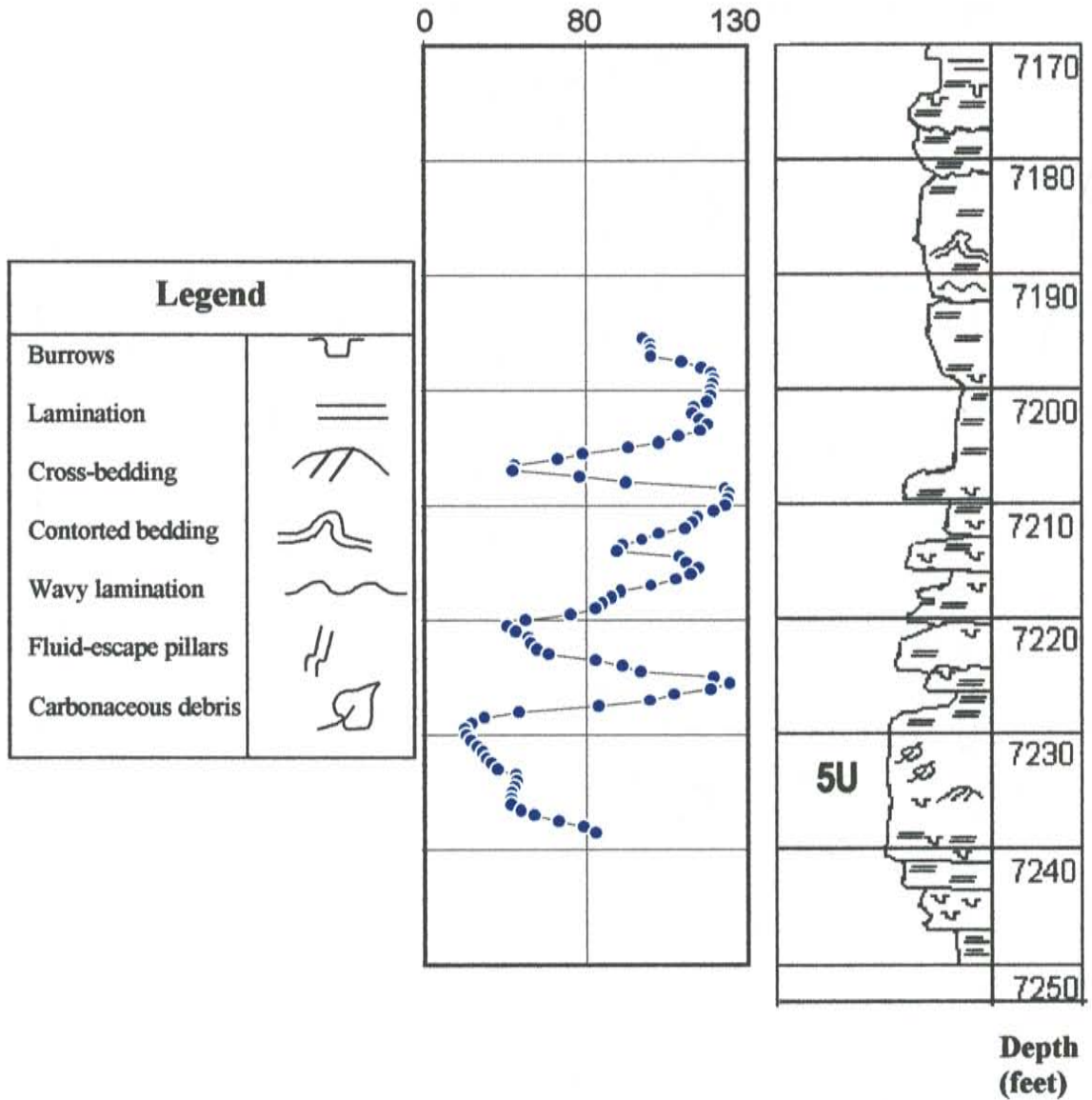


Fig. 3.1 – Correlation of gamma ray log with core description for the E.T. O'Daniel 37 core.

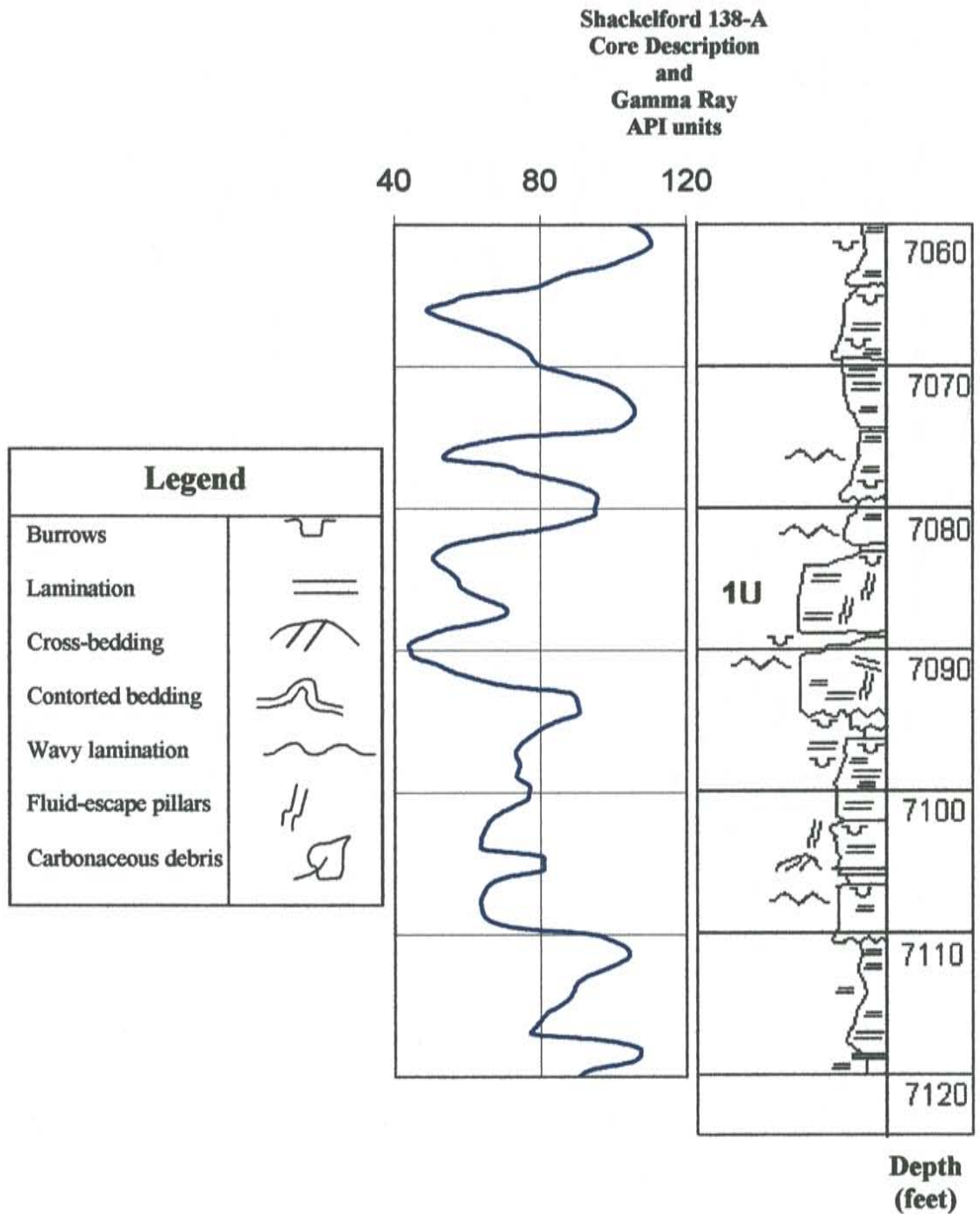


Fig. 3.2 – Correlation of gamma Ray log with core description for the Shackelford 138A core.

LSL NUMBER	LITHOLOGY	SEDIMENTARY STRUCTURES	BIOTURBATION	DEPOSITIONAL ENVIRONMENT
1	Silty dolomitic mudstones/ dolomite cemented siltstones	Massive to Laminated		Basinal, slump debris, turbidity currents, suspension settling, from shelf edge
2	Shale and laminated siltstone rich in clay/organic matrix	Structureless or finely parallel laminated	Rare-Absent	Basinal, High sea level stand: gray shale = weakly oxygenated bottom waters, black shale = deoxygenated bottom waters
3	Bioturbated, convoluted, clay and organic rich coarse siltstone	Intensely bioturbated Convolute bedding (<0.1 feet)	Nereites Zoophycos and/or Cruziana	Basinal, suspension settling from interflows, and tail of interflows Oxygenated bottom waters supporting Burrowing infauna
4	Coarse siltstone	Parallel finely laminated ("varved")	Rare-Absent	Basinal, suspension settling from interflows, poorly oxygenated, deoxygenated bottom waters
5	Very fine sand/ Coarse siltstone	Thick bedded Massive sandstone/siltstone, some fluid escape structures	Absent	Traction current deposits, Submarine channel fill
6	Very fine sand/ Coarse siltstone	Thin bedded massive sandstone/ siltstone, lamination, planar bedding, lenticular lamination	Absent	Upper channel fill and non-channelized middle fan
7	Very fine sand/ Coarse siltstone	Thin bedded, graded, Cross-laminated/ very fine sandstone and siltstone	Absent	Distal turbidities, low density turbulent flows, outer part of middle fan

Table 3.1 - Summary of large-scale lithofacies (LSL) obtained from core description showing sedimentary structures, occurrence of fossils and environment of deposition for each lithofacies. Bioturbation (LSL-3), feeder organisms have been suggested by Handford (1981).

Mudrock Lithofacies:

LSL 1: Silty dolomitic mudstone and dolomite cemented siltstones.

LSL 2: Shales and very argillaceous laminated siltstones.

LSL 3: Bioturbated argillaceous siltstones with lenticular or convolute laminations

LSL 4: Parallel finely laminated siltstone.

Sandstone Lithofacies:

LSL 5: Thick bedded, massive very fine sandstones and siltstones.

LSL 6: Thin bedded, massive very fine sandstones and siltstone.

LSL 7: Thin bedded, graded cross-laminated very fine sandstones and siltstones.

3.1.1 Mudrock Lithofacies

Low energy deposits consist of siltstones, shaly laminated siltstones, thin layers of black shale, and silty dolostones (Figs. 3.3-a, b, c, d and 3.4-c, d). Volumetrically these are the most abundant lithofacies in the upper Spraberry Formation. The following lithofacies are observed in cores:

LSL 1: Silty dolomitic mudstone and dolomite cemented siltstones - These are dark gray to black, massive, very well indurated, silty dolomite mudstones and siltstones, which display massive or faint planar horizontal bedding (Fig. 3.3-d). Ripple laminae and contorted bedding are rare. Beds range from 1 to 3 feet thick and have sharp or scoured basal contacts or grade into underlying sandstones. These carbonate-cemented rocks are not very common in the analyzed cores.

LSL 2: Shales and very argillaceous laminated siltstones – Shales are typically dark gray to black massive to faintly laminated rocks composed mainly of clays and organic

Figure 3.3: Large Scale Lithofacies (LSL) from Core Description: Mudrock Lithofacies.

This plate shows different sedimentary structures and textures observed in core samples. They represent the large-scale lithofacies that occur within the Spraberry Formation (Scale units are inches).

Photos A, B, and C:

Light gray, bioturbated argillaceous coarse-grained siltstone with lenticular or convoluted laminations (LSL-3). Burrowing and/or soft sediment-deformation destroyed primary bedding features in these dark gray siltstones.

Photo A, depth: 7226.4-7227.0 ft; E.T. O'Daniel 37 well

Photo B, depth: 7117.6-7118.0 ft; E.T. O'Daniel 37 well

Photo C, depth: 7092.0-7092.4 ft; E.T. O'Daniel 37 well

Photo D:

Light gray, dolomitic siltstone, cross-stratified (LSL-1) sharply overlies a dark gray to black, massive silty shale (LSL-2). Characteristic sharp basal contact of many siltstone beds in the cored intervals.

Depth: 7208.8-7209.2 ft; E.T. O'Daniel 37 well



Figure 3.4: Large Scale Lithofacies (LSL) from Core Description: Sandstone and Laminated Lithofacies.

This plate shows different sedimentary structures and textures observed in core samples. They represent the large-scale lithofacies that occur within the Spraberry Formation.

Photo A:

Thick-bedded, faintly laminated fine sandstone and siltstone (LSL-5). Fluid escape pillars obliterated planar horizontal stratification. Depth: 7084.0-7084.5 ft; Shackelford No. 138 well.

Photo B:

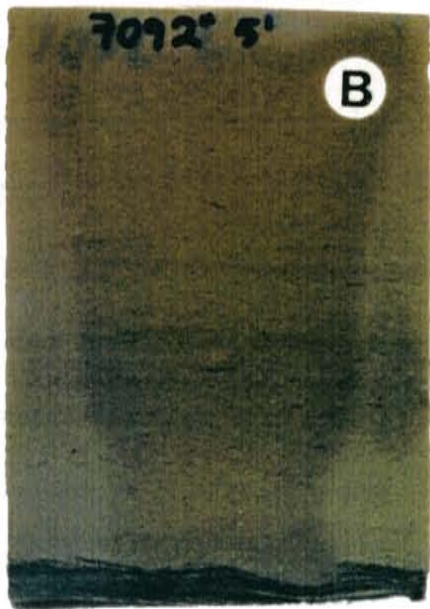
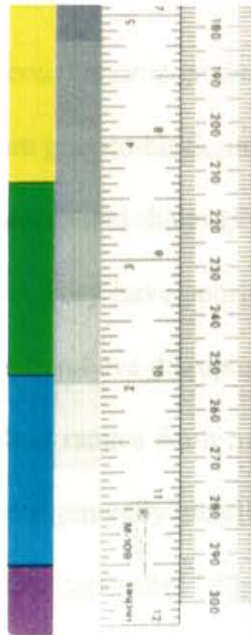
Thick-bedded, massive, fine sandstone and siltstone (LSL-5). Note the scoured basal contact. Depth: 7092.5-7092.9 ft; Shackelford No. 138 well.

Photo C:

Parallel-finely laminated (“varved”) siltstone (LSL-4). Note organic and clay rich, planar laminae increase slightly near the top of the sample. Depth: 7099.3-7099.8ft; Shackelford No. 138 well.

Photo D:

Dark gray to black, very finely laminated silty shale (LSL-2). Depth: 7122.3-7122.8ft; E.T. O’Daniel 37 well.



matter and lesser amounts of silt sized detrital grains. Shale beds are typically less than 2 feet thick and also grade into underlying siltstones (Figs. 3.3-d and 3.4-d). The shales are structureless or faintly laminated and are locally disrupted by small horizontal burrows. Thin, isolated lenses of silt occur infrequently; the black color of these shales is a function of their high organic carbon content. Organics occur in association with locally abundant pyrite; phosphatic nodules are also common. Shales and very argillaceous laminated siltstones are relatively abundant.

LSL 3: Bioturbated argillaceous coarse-grained siltstone with lenticular or convoluted laminations - These rocks are gray-to-black, argillaceous siltstones consisting of thin (<0.5 feet) interbedded coarse siltstones and shales (Figs. 3.3-a, b and c). The siltstones contain variable amounts of clay matrix. They have poorly preserved lenticular lamination. Bioturbation and soft-sediment deformation have disrupted most of the original bedding in these rocks. The intensity of bioturbation ranges from moderate to extreme. Burrows are browsing or feeding forms with traces generally parallel to bedding. This trace fossil assemblage is indicative of deposition in deep-water (slope to basin) settings (Basan et al., 1978).

LSL 4: Parallel finely laminated siltstone - This is a coarse-grained siltstone, finely laminated lithofacies (Fig. 3.4-c). This lithofacies is characterized by alternations of light and dark fine laminae, each a few millimeters (generally <5mm) in thickness. Light colored laminae are quartz-rich, coarse siltstone. Dark colored laminae consist of some silt-sized detrital grains mixed with organic detritus and argillaceous material. Commonly, laminae have sharp/erosional bases. Normally graded bedding is common. Lamination is generally parallel. A few tops of finely laminated sequences are ripple laminated.

3.1.2 Sandstone Lithofacies

The mudrocks described above are widespread along the Spraberry Trend (Handford, 1981). They form a depositional continuum and encase the more localized very fine-grained "clean" sandstones and coarse siltstones (Figs. 3.4-a and b). These sandstones are very fine grained and moderately-well to well-sorted. The following sandstone lithofacies are observed in the cores:

LSL 5: Thick-bedded, massive very fine sandstones and siltstones – This lithofacies consists of light gray to light brown, fine grained, well-sorted sandstones and coarse-grained siltstones (Figs. 3.4-a and b). These sandstones occur as individual beds, 1 to 3 feet, that stack vertically to form much thicker composite units. Sand beds have scoured basal contacts (Fig. 3.4-b), often marked by a thin layer of intraformational mud clasts (matrix supported). Beds are internally massive or faintly bedded and often exhibit fluid escape structures (vertical pillars). There is no evidence of bioturbation.

LSL 6: Thin bedded, massive, very fine sandstones and coarse siltstones – These are light gray to light brown, very fine grained, moderately-well to well-sorted, very fine sandstones and coarse-grained siltstones. Individual sandstone beds are less than 1.5 feet thick. Beds are composites consisting of basal intervals of massive sandstones, which may grade vertically into parallel laminated or cross-laminated siltstones. The tops of some beds display evidence of fluid escape such as dish and pillar structures (Fig. 3.4-a). Individual beds have scoured bases often marked by thin layers of intraformational mudclast conglomerate (matrix supported). Composite beds are often difficult to identify due to a relatively uniform grain size.

LSL 7: Thin bedded, graded, cross-laminated very fine sandstones and siltstones –

This lithofacies consists of thin bedded (<1 foot) very fine grained, light gray to brown, moderately-well to well-sorted very fine sandstones interbedded with dark gray shales. Individual sand beds have sharp, erosive bases and are normally graded. A thin layer of shale rip-up clasts often overlies basal surfaces. Normally graded sandstone beds are characterized by vertical sequences of sedimentary structures indicative of deposition from waning flow (i.e. so-called Bouma sequences). Such sequences consist of a basal section of parallel laminated sandstones. Sand beds grade vertically into overlying beds of dark gray shale or lenticular laminated silty shale.

3.2 LITHOFACIES INTERPRETATION

The total sedimentary package described above is interpreted as a marine basinal deposit, based on the following combination of factors. These factors taken as a whole eliminate environments of deposition other than deep marine basin.

- 1) A marine environment is suggested by the considerably high salinity (130,000 mg/L; Yanfidra, 1998) of brines contained in rocks from the area.
- 2) Several sedimentological studies have been performed that present cross-sections and maps with correlation of shelf facies and fine grained facies based on information obtained from wells (Schmitt, 1954; Silver and Todd, 1969; Handford, 1981).
- 3) A prominent feature in cores is evidence of browsing organisms in shaly siltstone intervals of less than one-foot with intensive bioturbation (Handford, 1981). This assemblage (Nereites, Zoophycos, and Cruziana sediment feeders) is typical of deep

marine basin deposits and oxygenated to poorly oxygenated bottom waters (Basan, 1978).

- 4) Preservation of delicate, fine grained, parallel argillaceous lamination within non-burrowed sections, which is suggestive of anoxic conditions in very calm waters of a restricted environment (Fig 3.4-c and b) and distal location during deposition. Common evidences cited for poor water circulation, little or no oxygen, and toxic conditions are the occurrence of pyrite and organic-rich dark gray to black shales and dense, dark gray to black dolomite (Schmitt, 1954; Handford, 1981). Dark coloration of sediments is related to decay of sinking organic matter, which in turn caused depletion of oxygen in bottom waters. Restricted water circulation is due in part to the fact that shelves closely surround the basin, which in periods of low sea level does not allow considerable shelf-to-basin circulation or access to the open sea.
- 5) Local presence of abundant preserved organics, probably marine kerogens, suggestive of very slow rates of deposition in poorly oxygenated or deoxygenated bottom waters.

Sandstone beds display evidence of deposition from waning traction currents including:

- 1) Erosional, scoured bases (often sole marked, with rip-up clasts; Fig. 3.4-b) and gradational bed tops, which denote tractional currents with a subsequent decrease in velocity.
- 2) Normal graded bedding typical of turbidite currents (individual beds fine upward; Fig 3.4-c).
- 3) Occasional cross bedding indicative of transport by high energy traction currents.

- 4) Some fluid escape, load, or flame structures indicative of rapid deposition and subsequent dewatering (Fig. 3.4-a) associated with turbidites (Boggs, 1995).
- 5) Vertical sequence of sedimentary structures recording gradation from high to low flow regime conditions (“Bouma” sequences).
- 6) A general lack of bioturbation within sandstones is probably due to rapid traction deposition which did not allow browsing organisms to develop (Handford, 1981). Spraberry sandstone sediments are expected to have formed in oxygen-rich areas since these are associated with turbidity currents and other random mechanisms of deposition that commonly carry oxygen bearing waters from the shelves. Nevertheless, because Spraberry sandstone lacks evidence of browsing organisms, the absence of bioturbation is related to rapid deposition from traction currents.

3.2.1 Deep Marine Sediment Deposition in the Midland Basin

Silver and Todd (1969) developed a model for sediment transport and deposition from the shelves to the basin. Their model is based on information from multiple wells that cover the northern part of the Midland and Delaware Basins. Detailed stratigraphic correlation sections were performed based on well information. A falling sea level and its control of sedimentary patterns was attributed to major fluctuations of sea level and contemporaneous subsidence. Silver and Todd (1969) described a series of four stages for sea level changes. They show that during stages three and four sea level was low, allowing continental and near-shore clastics to prograde seaward. The reefs and/or banks ceased to develop and were replaced by an extensive stable land surface dissected by canyons and tidal channels.

Fine-grained sand, silt, and mud were the main types of sediments deposited in the Midland Basin during the late Paleozoic, whereas the surrounding shallow shelves experienced carbonate deposition. The so-called Abo Reef (Wright, 1962) is the result of a carbonate bank buildup that formed at the outer edge of the shelf. Calcareous algae, siliceous sponge spicules, bryozoans, fusulinids, and probably some coral were the biota that formed the carbonate banks. Deposition of carbonates on the shelves and clays in the basin are inferred to have occurred during transgressive events and high sea level. Periods of regression and low sea level gave way to progradation of fluvial-deltaic systems toward the marine shelves. Later eroding channel cuts developed throughout the shelf edge and served as feeding conduits with clastic sediments transported toward the basin (Bloomer, 1977). The movement of carbonate sediments downslope into the basin was mainly due to slumps, debris flows, and turbidity currents (Handford, 1981).

Handford (1981) presented net clastic isopach maps with widespread genetic patterns for the Spraberry and Dean Formations. Based on a consistent north-to-south thinning of clastics, sediments are interpreted as originally dispersed across the northern shelf margin and transported longitudinally down the axis of the basin to form elongate fans (Fig. 1.3). A northward coarsening pattern and also log patterns that are thicker near the shelf margins are both evidence of a north-south transition (Schmitt, 1954). Feeder channels or submarine canyons and submarine fan systems are considered the conduits for transportation of terrigenous clastics carried by saline density currents, turbidity currents, and suspension settling into the deep basin (Fig. 1.3).

3.2.2 Depositional Setting for Mudrock Lithofacies

The finely parallel-laminated siltstones (LSL-4) were probably formed by suspension settling of silt and very fine sand-sized particles from submarine density currents (Handford, 1981). Handford proposed that such deposits result from density stratification of the water column when shelf-derived density currents periodically move out over the basin as an interflow (Fig. 1.3) suspended above the basin floor. Suspension settling of thin layers of silt and very fine-grained sand resulted from eventual mixing of waters near the end of such flows.

Burrowed siltstone (LSL-3) alternates with the parallel, finely laminated siltstone (LSL-4) and with thin shale beds (LSL-2). A possible explanation for the oxygen source for such bioturbated zones is the mixing of oxygen-rich surface waters from storms and shelf water with stagnant basin water (Bozabich, 1979). The lithological transition from laminated to burrowed intervals or, less frequently, into shales, is interpreted as recording periodic changes in bottom water chemistry due primarily to changes in bottom water oxygen content. Such changes may have occurred in response to fluctuations in eustatic sea level through time, the upwelling of cold, nutrient-rich bottom waters along the shelf edge promoting plankton growth, and the migration of the dysaerobic zone. Migration of the dysaerobic zone probably resulted from sea level fluctuations (Silver and Todd, 1969) and migration of the thermocline/pycnocline along the bottom slope. Also decay of sinking organic matter resulted in depletion of oxygen in bottom waters. The lack of variety in organisms is probably the result of the small amount of oxygen.

The presence of pyrite, dark organic-rich laminae, phosphatic nodules and the lack of bioturbation suggest that anoxic and reducing conditions prevailed in the bottom waters

of the Midland Basin (Schmitt, 1954; Krumbein and Garrels, 1952; Handford, 1981). Conditions that favored the formation of phosphate nodules, which are present in the Spraberry Formation, are as follows: abundant organic matter, low concentration of dissolved oxygen, low rate of clastic sedimentation, and presence of trace amounts of calcium carbonate in the sediment (Manheim et al., 1975). Also, pH should be greater than 7.0 and concentration of $(\text{PO}^{-3})_4$ should be 0.1 ppm or greater (Ames, 1959).

Narrow channels with access to the open ocean make the Midland Basin more susceptible to the formation of anoxic bottom waters. Cordell (1977) suggested that the water, which had become more saline and dense due to evaporation on the Central Basin Platform, would sink into the basin and aid in the formation of density-stratification. Houde (1978) suggested that high levels of evaporation under arid conditions prevailed during deposition in the Midland Basin. He described the climate conditions in the region during the Permian as arid and tropically warm, and gave an approximate position of 25 to 30 degrees south of the Permian paleo-equator during the time.

A different scenario for deposition of parallel-interbedded siltstones and shale laminae is proposed by Folk (1989). He shows mathematical procedures strongly suggesting that random in-time processes do not produce the Spraberry laminae. Folk (1989) cited periodic annual events as probable mechanisms for deposition of the thinly laminated silts uniformly interbedded with clay-organic laminae (LSL-2 and LSL-4). Events cited by Folk (1989) for annual cycles of deposition of clay/organic laminae are organic pelagic seasons and spring floods by clay-laden streams. Sandy laminae are probably due to eolian deposition caused by annual dust storms and bottom currents that flow in a specific direction during a specific time of the year. Folk concluded that laminations of 0.5-2mm

thickness, with most particles finer than 80 μm , and scarce clays in the Spraberry sandy facies, are consistent with eolian sand grain size, and are probably the result of annual cycles. Interbedded organic-clay laminae are the result of low-energy settling of suspended loads after the dusty season.

3.2.3 Depositional Setting for Sandstones Lithofacies – Non-Cyclical Deposition

Facies that contain very fine sandstones and siltstones (LSL 5), and are featureless (massive), with relatively high porosity, occur with a random distribution in the stratigraphic sequence. Thus these are not considered as the result of cyclical events. These facies differ from the laminated facies in thickness, texture and porosity. These relatively thick sandstones show a lack of lamination. Gradation with fining upward sequences is common, presenting sharp erosional basal contacts. From well correlation and isopach mapping, Handford (1981) shows a southward thinning of submarine fans, which is attributed to deposition of sand and silt by density currents. He also found that dip-oriented isopach patterns suggest that some sediments were deposited in channels. Locally thick clastics have been identified along the shelf margin and these were probably conduits (feeder channel systems or submarine canyons) for tractionally deposited sand and silt into the basin.

Thick sandy Spraberry sediments are related to temporally random events such as turbidity currents, hurricanes and earthquakes. Based on the association of traction current structures with the coarser grained rocks, evidence presented above for basinal deposits, isopach patterns (Handford, 1981; Guevara, 1988; Tyler and Gholston, 1988), facies sequences and sedimentary structures indicate that sandstones were deposited from turbidity currents and saline density underflow. The sandstones represent deposition in submarine

channels and fans (Walker, 1978). The Spraberry sandstones are interpreted as deposits of waning traction currents that were responsible for the filling of erosional channel cuts on the higher energy, inner/middle portions of submarine fans.

Lithofacies LSL-5 and LSL-6 were formed in the channelized portions of the inner fan to the non-channelized middle submarine fan. Thinly bedded, graded, cross-laminated, very fine sandstones and siltstones (LSL-7) are classical turbidite deposits. These deposits occur within the upper portions of channel fills and within non-channelized portions of the middle fan. Very fine sandstones and siltstones commonly form the coarser bottom part of fining upward sequences having sharp erosional contacts with underlying shales and muddy burrowed tops. Suspension settling, saline density currents, and turbidities are the main mechanisms of sediment transport and deposition for very fine sandstone (Handford, 1981; Guevara, 1988; Tyler and Gholston, 1988).

CHAPTER 4

PETROGRAPHY AND DIAGENESIS

This chapter emphasizes the relationships among mineralogical framework and mechanisms affecting distribution of pore space. This approach is based on small-scale observations from a comprehensive petrographic analysis that utilizes various analytical techniques. In addition to differentiating the various petrographic assemblages and the influence of diagenetic processes upon them, this investigation serves as the background for the determination of different categories of reservoir and non-reservoir rocks within the Spraberry Formation (Chapter 5).

4.1 GENERAL TEXTURES AND MINERALOGY

Six different small-scale lithofacies (SSL) representative of the major lithological groups in the upper Spraberry Formation have been identified based on thin section analysis (Table 4.1). A variety of sedimentary rocks are seen including porous fine sandstones and siltstones, dolomite cemented and laminated siltstones, and shales. Spraberry reservoir rocks are typically low porosity, coarse siltstones to very fine

PETROGRAPHIC POINT COUNT SUMMARY BY ROCK TYPE																													
TEXTURE		GRAIN COMPOSITION										MATRIX			CEMENT COMPOSITION					POROSITY									
SMALL SCALE LITHOFACIES		GRAIN SIZE (µm)		MONOCRYSTALLINE QTZ.	POLYCRYSTALLINE QTZ.	TOTAL QUARTZ	CHERT	MUSCOVITE	PLAGIOCLASE	K-FELDSPAR	IRF	MRF	SRF	CARBONATE FRAGMENTS	ACCESSORY MINERALS	LAMINAR	DISPERSED	ORGANICS	DEPOSITIONAL CARBONATE	TOTAL MATRIX	UNDIFFERENTIATED CLAY	QUARTZ OVERGROWTHS	CALCITE	DOLOMITE	PYRITE	PRIMARY	SECONDARY	MICRO	TOTAL POROSITY
	MAXIMUM	66.0	44.7	6.0	47.0	1.7	2.7	16.7	14.7	2.0	4.0	2.7	3.0	3.0	4.3	4.3	2.3	7.7	12.3	8.3	7.0	0.3	7.3	2.0	13.3	7.7	1.3	18.7	
	MINIMUM	45.0	36.0	1.0	39.0	0.3	0.3	6.3	3.7	0.7			0.3					0.7	1.7	1.0	3.3	0.3	2.7	0.7	7.3	2.7		10.3	
	AVERAGE	60.0	40.2	2.7	42.8	1.0	1.4	11.8	6.8	1.2	0.5	0.2	1.6			1.5	1.2	1.6	3.7	6.6	3.6	5.2	0.3	4.9	1.1	9.8	4.4	0.2	14.3
	MAXIMUM	66.0	47.0	5.7	52.0	1.3	4.7	17.3	11.7	1.7	1.7	2.7	1.0	4.3	13.0	3.0	5.3	7.7	25.0	12.7	7.0			8.7	4.0	8.7	4.7	1.7	13.0
	MINIMUM	40.0	29.0	0.7	30.0	0.7	0.3	6.3	3.3	0.7	0.3	0.7	1.0	0.7	0.7	1.3	0.7	1.3	5.0	0.7	2.7			1.0	0.7	0.3	1.0	0.7	1.0
	AVERAGE	57.3	40.2	2.5	42.5	1.0	1.9	11.5	6.3	1.0	1.1	1.3	0.8	2.1	5.2	1.7	2.5	4.0	11.6	5.1	4.5			4.4	2.0	4.9	2.9	1.1	7.5
	MAXIMUM	60.0	23.7		23.7	0.3	2.0	5.7	2.7	0.7	0.7		7.7		2.7	2.7	8.7	38.3	41.0	4.3			3.3	31.3	3.7				
	MINIMUM	50.0	19.7		19.7	0.3	0.3	3.3	1.0	0.3	0.3		3.7		1.3	2.7	0.3	25.0	33.0	4.3			1.7	21.3	0.7				
	AVERAGE	54.8	22.3		22.3	0.3	1.2	4.1	1.8	0.5	0.5		5.7		2.0	2.7	4.2	30.7	36.1	4.3			2.5	26.4	2.1				
	MAXIMUM	60.0	39.3	4.7	42.0		2.3	8.0	3.7	0.3	0.7	0.3	2.0		4.3	2.3	2.7	25.7	35.0	3.0	4.7	3.0	18.3	3.0	4.3	4.0			7.3
	MINIMUM	56.0	27.3	1.0	27.3		1.0	5.0	2.0	0.3	0.3	0.3	0.7		1.7	1.3	1.3	9.3	14.0	1.0	2.3	1.7	13.7	3.0	2.0	1.3			3.3
	AVERAGE	58.3	34.9	2.3	36.8		1.8	6.3	3.1	0.3	0.4	0.3	1.1		2.3	1.6	1.9	17.6	22.2	2.4	3.7	2.5	16.1	3.0	3.1	2.5			5.6
	MAXIMUM	62.0	44.3	3.3	44.3	0.3	7.7	9.3	5.3	0.7	1.0	0.3	2.3	3.7	44.0	3.3	9.7	4.7	56.7	20.7	1.3	2.3	2.0	6.7				1.0	1.0
	MINIMUM	25.0	21.0	3.3	21.0	0.3	1.0	1.3	0.7	0.3	0.3	0.3	2.0	0.3	25.0	0.7	4.3	1.3	34.0	4.3	1.3	2.3	0.7	0.3				0.3	0.3
	AVERAGE	39.2	29.0	3.3	29.3	0.3	5.5	4.9	2.9	0.5	0.7	0.3	2.2	1.7	30.7	2.1	7.1	2.2	41.1	13.3	1.3	2.3	1.3	3.0				0.7	0.7
	MAXIMUM	58.0	42.7	4.0	46.7		5.3	16.3	11.7	0.7	1.7	0.7	0.7	2.0	19.3	8.0	5.3	8.7	33.3	14.0	4.7	1.0	4.3	5.0	4.7	2.3	0.7	7.0	
	MINIMUM	40.0	34.0	1.0	35.0		1.3	7.3	1.3	0.3	0.3	0.7	0.7	0.7	3.3	1.0	0.7	2.0	7.3	1.0	2.0	1.0	1.7	2.3	1.0	0.7	0.7	1.0	
	AVERAGE	52.6	38.8	2.0	40.0		3.0	11.7	5.6	0.5	0.7	0.7	1.1	1.1	13.4	4.2	3.0	3.4	22.8	6.1	3.0	1.0	3.1	3.5	2.4	1.2	0.7	2.9	

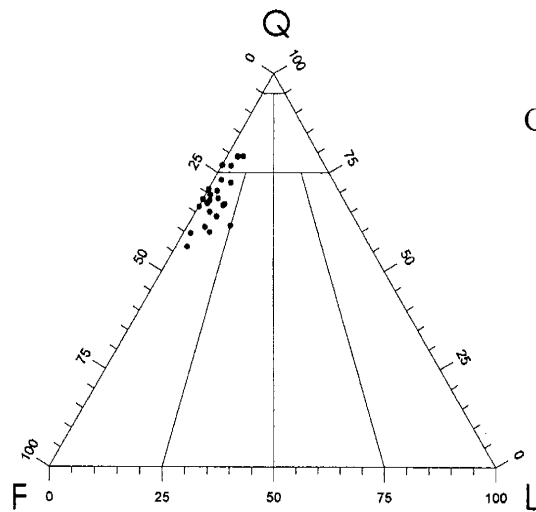
Table 4.1 - Mineralogical averages for point counts of thin sections for six categories of small scale lithofacies in three cored wells.

sandstones that are intercalated with clay/organic rich non-reservoir rocks. Most of the carbonate muds and argillaceous facies are matrix-supported, whereas sandstones and siltstones display grain-supported fabric. Mineralogical composition varies from arkosic to subarkosic (Fig. 4.1). Spraberry sandstones and coarse siltstones (SSL-A) have an average grain size of 60 μm ranging from 45 to 66 μm (Table 4.1). Sorting varies from moderately well sorted, clayey coarse siltstones to very well sorted, clean sandstones. Roundness ranges from subrounded to angular.

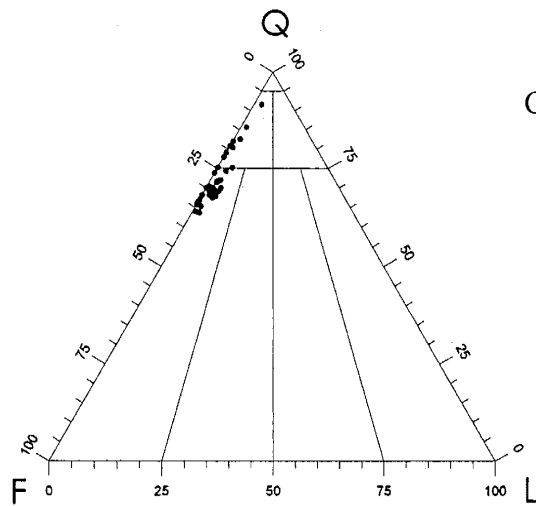
The rock fabric displays two main forms: massive and laminated (Fig. 4.2). Other sedimentary structures such as burrows, water escape structures, convolute bedding and cross stratification were noted in hand specimens (Chapter 3). Mottled sedimentary fabric is common and is associated with burrowing and/or dewatering. Burrowing produced patches of coarser grain size that look cleaner and sandier than surrounding shaly sediments (Fig. 4.2). Cross stratification is fairly common in the very fine sandstones.

Monocrystalline quartz is the dominant type of detrital grain. Other abundant detrital grains are Na-plagioclase and lesser amounts of K-feldspar and muscovite. Rock fragments, heavy minerals, and carbonate fragments are present in minor amounts. Some quartz with rutile is present. Detrital clay matrix (laminar clays, dispersed clays, and organics) averages 20% in argillaceous laminated siltstones (SSL-F) and 40% in shales (SSL-E) (Table 4.1). Clays, organic debris, carbonate mud, and considerable amounts of mica and pyrite typically form laminae. Massive, very fine sandstones and siltstones contain only minor amounts of clay matrix.

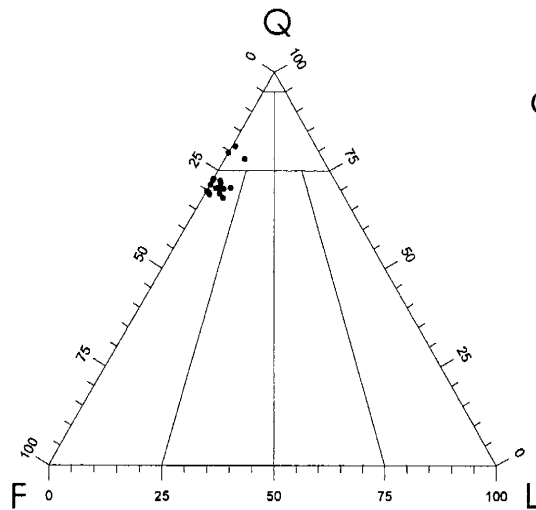
Authigenic minerals observed in variable amounts depending on the small-scale lithofacies include quartz, dolomite and ferroan dolomite, calcite, and pyrite. Barite is



CORE: E.T. O'Daniel 37



CORE: Shackelford 138A



CORE: A. Judkins 5

Fig. 4.1 – Sandstone classification for samples from three cored wells in the Upper Spraberry Formation (using Folk's classification, 1974). Samples studied are arkosic to subarkosic in composition.

Fig. 4.2 -- Photomicrographs showing general petrographic characteristics from thin sections:

A: This photomicrograph shows a clean, massive siltstone with relatively well-interconnected pore system consisting predominantly of reduced intergranular pores enhanced by oversized, grain dissolution pores. Framework grains are subangular to angular and are predominantly monocrystalline quartz, potassium feldspar and plagioclase.

E. T. O'Daniel 37 cored well

Depth, ft:	7228.45	Sample No.:	ET12-H2
Grain Size:	52 μm	Sorting:	Well Sorted
Porosity:	10.3 %	SSL:	A

B: This is a well-sorted, very fine-grained sandstone, laminated and arkosic composition. The rock framework consists predominantly of monocrystalline quartz, plagioclase and K-feldspar. Note intercalation of porous clean sand with very fine clay laminae.

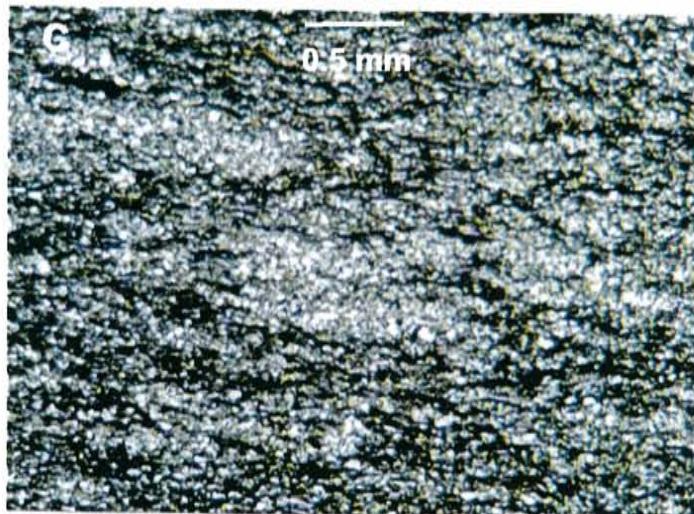
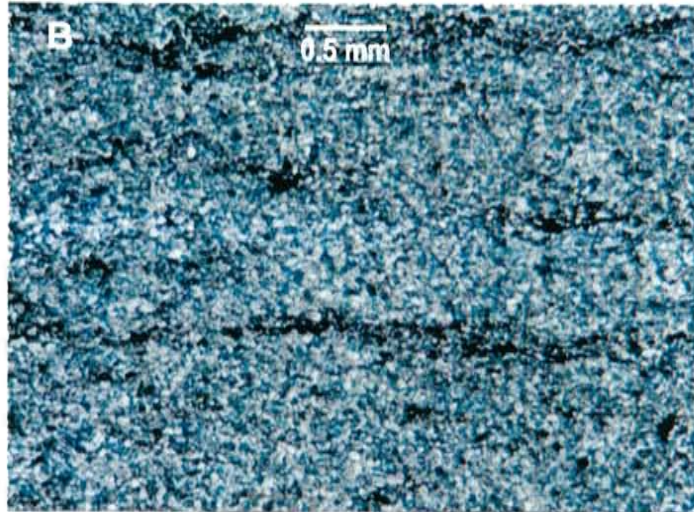
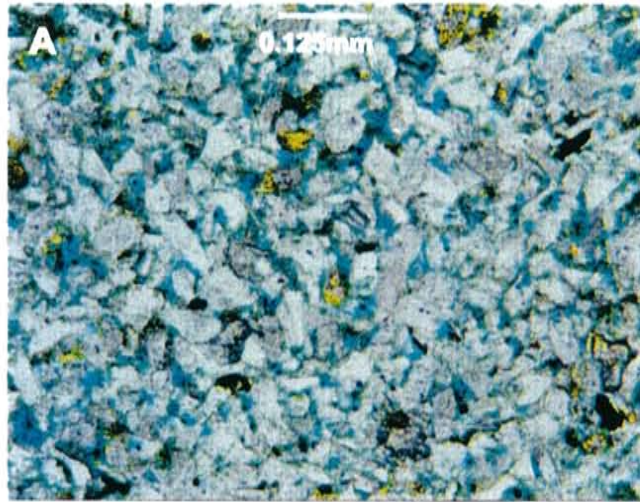
Shackelford 138A cored well

Depth, ft:	7099.8	Sample No.:	SPX17
Grain Size:	60 μm	Sorting:	Well Sorted
Porosity:	11.1 %	SSL:	B

C: This is a laminated, burrowed, very clay siltstone, moderately well to well sorted, and rich in organics. Note abundant clay matrix.

Shackelford 138A cored well

Depth, ft:	7088.0	Sample No.:	SPX10
Grain Size:	32 μm	Sorting:	MWS to WS
Porosity:	Trace	SSL:	F



also abundant as a fracture-filling cement. Amounts of primary and secondary porosity also show variable quantities for the different lithofacies (Table 4.1). Very fine sandstones and siltstones (SSL-A) are the most affected by dissolution of feldspar, dolomite and dolomite cement, and probably some dissolution of quartz cement.

Quartz overgrowths: Quartz overgrowths are noted as euhedral grain boundaries or by the presence of vacuoles or dust rims that separate grain from cement (Fig. 4.3). Quartz cement is most abundant in SSL-A and SSL-B rocks, with an average of 5.2% for SSL-A and 4.5% for SSL-B rocks. SSL-A and SSL-B are the cleaner, sandier and more porous lithofacies. In general, median values of quartz overgrowth percentages (from point count) vary from one petrographic category to another (Table 4.1).

Authigenic feldspar: Authigenic feldspar is a minor cementing agent occurring in quantities of 1% or less. Alteration and dissolution of less stable feldspars are found repeatedly in the Spraberry Formation (Fig. 4.4). The exact amount of feldspar alteration in each lithofacies is difficult to determine. For instance feldspar dissolution in argillaceous lithofacies (SSL-E and SSL-F) appears to be large; however, the complex mixtures of very fine minerals and organics make observations difficult.

Pressure solution: Overpressuring during compaction, in conjunction with several other factors, can cause pressure solution. The effect of compaction is clearly observed within the matrix-free, sandy lithofacies (SSL-A and SSL-B). Flat and concavo-convex grain suturing contacts are common in these lithofacies, denoting the high-pressure effect between quartz grains (Fig. 4.3).

Clays: The Spraberry Formation contains abundant clay in a number of forms. It is not an easy task to differentiate between depositional and authigenic clays. Certainly an

Fig. 4.3 – Photomicrographs showing quartz overgrowths and pressure solution

A: This photomicrograph shows concavo-convex contacts between quartz grains. Interlocking grain walls are commonly evidence of pressure solution effects.

Arthur Judkins 5 cored well

Depth, ft:	7199.0	Sample No.:	J38
Grain Size:	66 μm	Sorting:	Well Sorted
Porosity:	10 %	SSL:	A

B: This sample is another example of the effect of quartz overgrowths and pressure solution in reduction of porosity. Reams of fluid inclusions partially or totally surrounding grains suggest the presence of quartz overgrowths.

Arthur Judkins 5 cored well

Depth, ft:	7195.0	Sample No.:	J36
Grain Size:	66 μm	Sorting:	Well Sorted
Porosity:	17 %	SSL:	A

C: Quartz overgrowths surround almost all grains in this area.

Shackelford 138A cored well

Depth, ft:	7088.0	Sample No.:	SPX11
Grain Size:		Sorting:	
Porosity:	%	SSL:	

D and E: Total porosity is drastically reduced by microcrystalline quartz cement (Qc). Very poor interconnection of intergranular pores (P).

E.T. O'Daniel 37 cored well

Depth, ft:	7113.0
Porosity:	4.0 % (from helium injection)
SSL:	C

F: Quartz overgrowths (Qo) occlude porosity in this sample.

E.T. O'Daniel 37 cored well

Depth, ft:	7058.0
Porosity:	8.9 % (from helium injection)
SSL:	B

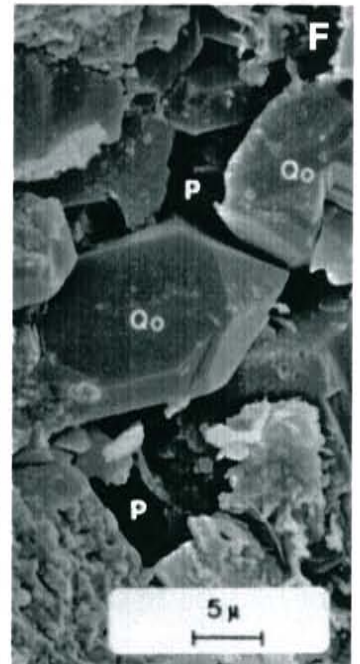
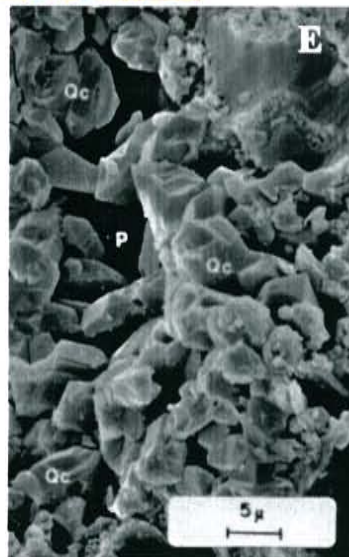
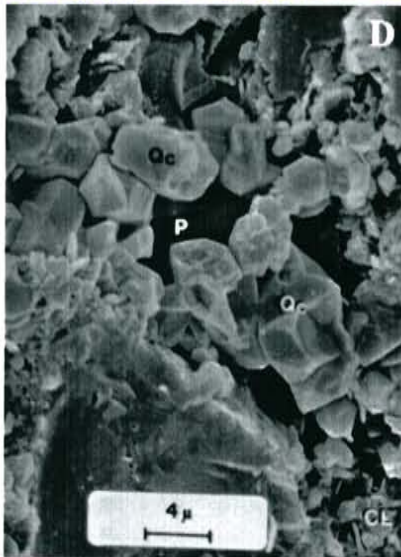
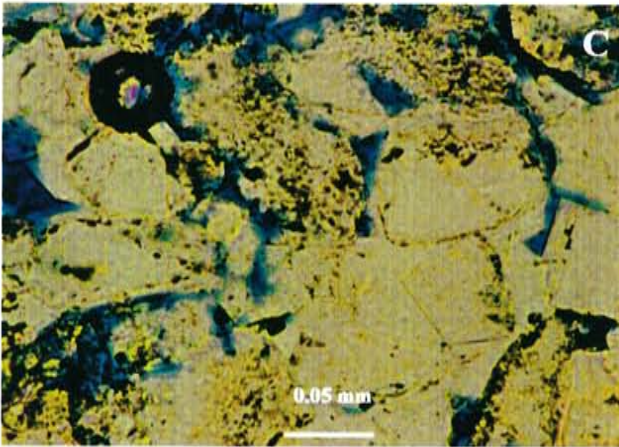
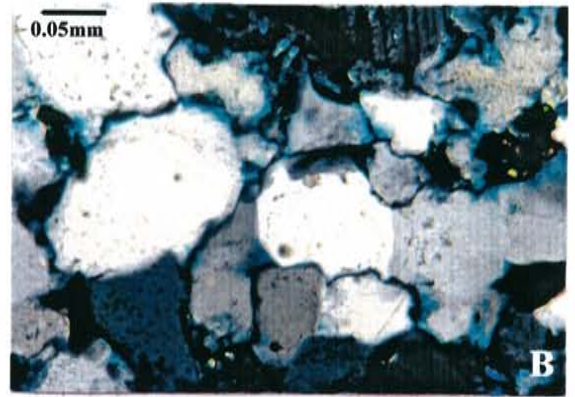
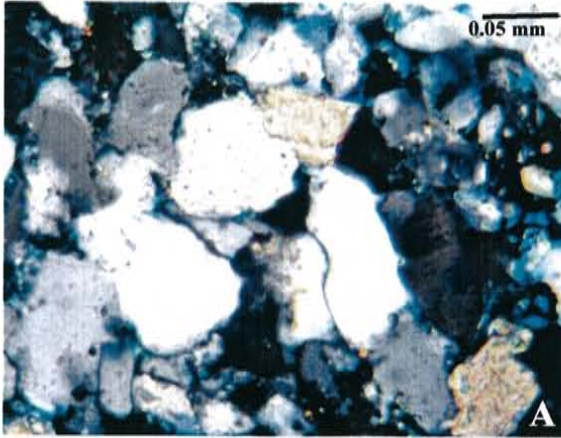


Fig. 4.4 – Photomicrographs showing dissolution textures in the Upper Spraberry Formation

A: This is a coarse grained, massive, well-sorted, arkosic siltstone. Framework grains are subangular to angular and are predominantly monocrystalline quartz, potassium feldspar and plagioclase. Secondary oversized pores (DP) from partially and totally dissolved cements and framework grains, and reduced intergranular pores predominantly form the pore system.

E.T. O'Daniel 37 cored well

Depth, ft:	7230.3	Sample No.:	ET12-1
Grain Size:	55 μm	Sorting:	Well Sorted
Porosity:	12 %	SSL:	A

B: SEM photomicrograph showing selective partial dissolution of a feldspar grain (LG).

Shackelford 138A cored well

Depth, ft:	7091.5
Porosity:	10.3 % (from helium injection)
SSL:	A

C: This is a very fine-grained, well-sorted, arkosic, sandstone to coarse-grained siltstone. Angular to subangular grains. Secondary pores (LG) were created by the partial to complete dissolution of unstable feldspar grains, considerably enhancing total porosity and reservoir quality.

E.T. O'Daniel 37 cored well

Depth, ft:	7232.17	Sample No.:	ET14-H5
Grain Size:	57 μm	Sorting:	Well Sorted
Porosity:	13.2 %	SSL:	A

D: Secondary pores associated with leached feldspar grains (LG) contribute to total porosity.

E.T. O'Daniel 37 cored well

Depth, ft:	7228.3
Porosity:	11.5 % (from helium injection)
SSL:	A

E: Micropores (MP) are the result of intergranular pore partitioning by pore-filling clay (CL). Porosity is also reduced by quartz overgrowths (Qo) and dolomite cement (D).

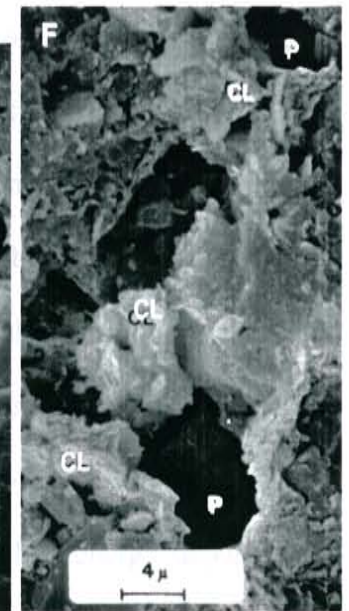
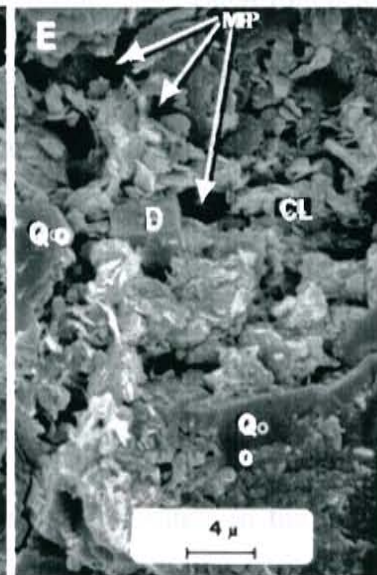
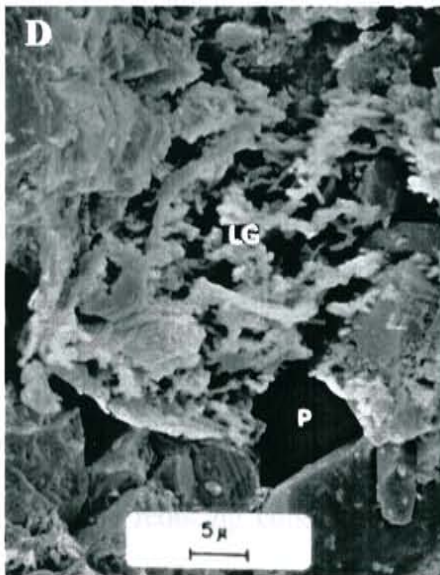
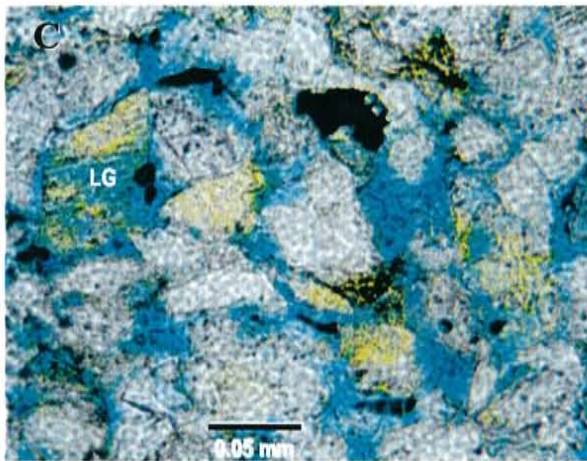
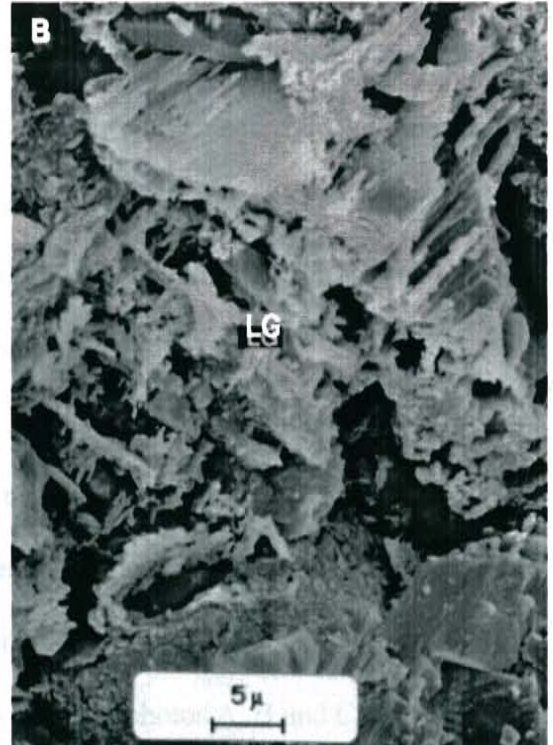
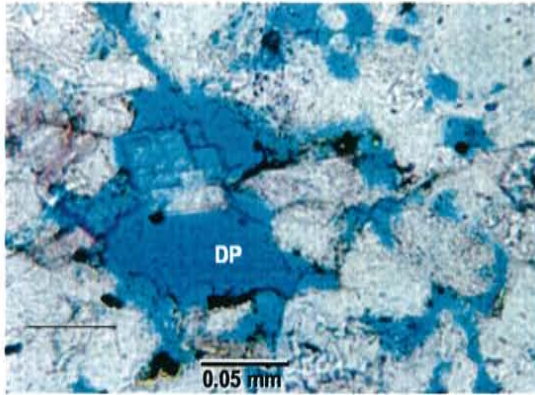
E.T. O'Daniel 37 cored well

Depth, ft:	7093.5
Porosity:	9.6 % (from helium injection)
SSL:	B

F: This photomicrograph shows intergranular porosity (P) and partial pore obstruction by pore-filling clays (CL).

E.T. O'Daniel 37 cored well

Depth, ft:	7066.0
Porosity:	12.0 % (from helium injection)
SSL:	A



obvious difference exists between the argillaceous and organic rich clays of shales and laminated siltstones lithofacies (SSL-E and SSL-F) and the much less abundant clays in the clean and porous sandy lithofacies (SSL-A and SSL-B). SSL-E and SSL-F present a thick mixture of clays, organics, carbonate muds, and common associated pyrite framboids and mica sheets that appear very well compacted (Fig. 4.2). The other type of clay composition is organic-free and more coarsely crystalline, exhibiting hair-like illite in association with the porous, very fine sandstones and coarse siltstones (Fig. 4.5).

For this thesis, XRD diffractograms were recorded for samples along 60 feet of core (Shackelford 138A) in order to define clay mineralogy within the various types of lithologies and determine the effect of clays on reservoir quality. The dominant clay is illite, followed by chlorite, and in lesser amount kaolinite and I/S mixed-layer (Table 4.2). Illite has been identified using SEM photomicrographs (Fig. 4.5 photos A, B and C).

X-ray diffraction analysis of Spraberry clay samples also revealed different clay diffractogram patterns between a clean and porous, very fine sandstone at 7087-ft, and the argillaceous sample from 7104-ft depth (Fig. 4.6). The difference of peak intensity between these two lithofacies is probably due to different levels of crystallinity.

Pyrite: Authigenic pyrite occurs in small quantities in all lithologies and is especially abundant in organic rich shales and shale-laminated siltstones in the upper Spraberry (Fig. 4.5). Nodules of pyrite, 1 to 0.5cm, flattened due to compactional pressure, are visible in hand specimens. Microscopic framboidal pyrite (Fig. 4.5) is also present. Pyrite tends to be more abundant with an increase in clay and organic content (SSL-E and SSL-F), probably due to the reducing conditions of anoxic seawaters in the very low energy depositional environments.

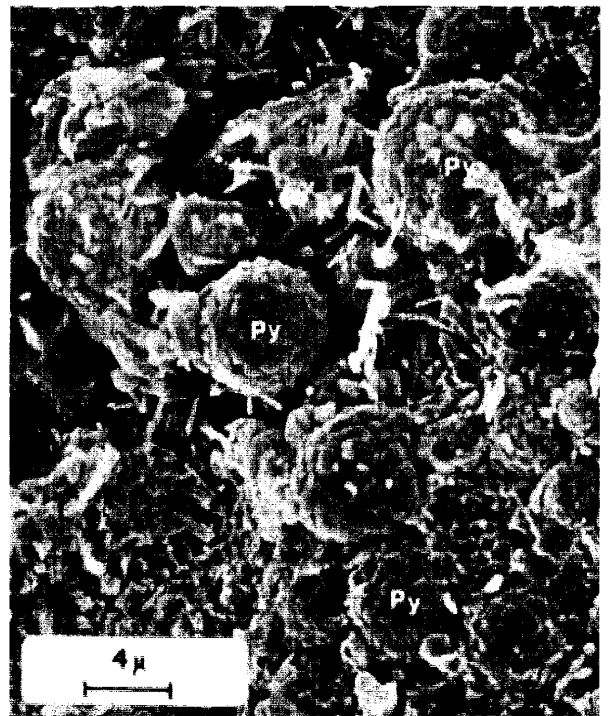
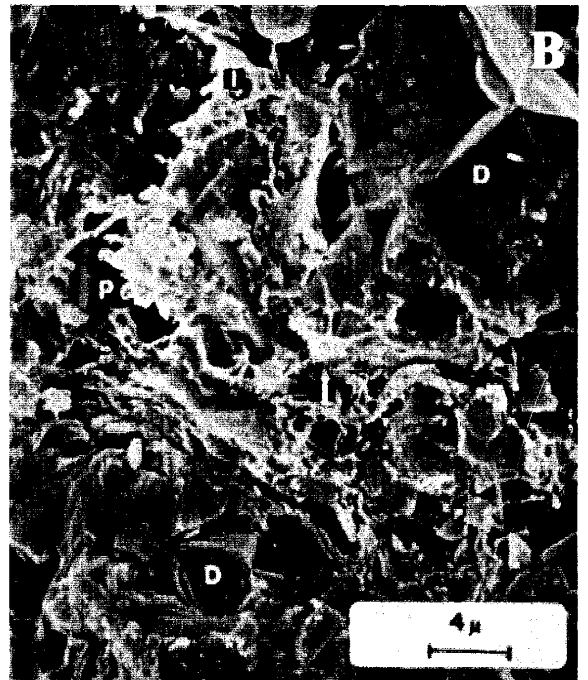
Fig. 4.5: SEM photomicrographs showing different types of illite accumulation, dolomite cement, and pyrite in the Upper Spraberry Formation.

A: Tightly compacted siltstone (7050 ft, E.T. O'Daniel 37) showing fibrous authigenic illite (i) that obstructs intergranular pores. Also note the very small, rhombic dolomite crystals (D) intermixed with the illitic clays.

B: Intergranular pores (P) are rare in this dolomitic siltstone. Dolomite cement (D) and fibrous authigenic illite (i) have occluded a great amount of the original porosity. Illite appears to have precipitated after dolomite cementation. Depth 7040.0 ft. Core: E.T. O'Daniel 37.

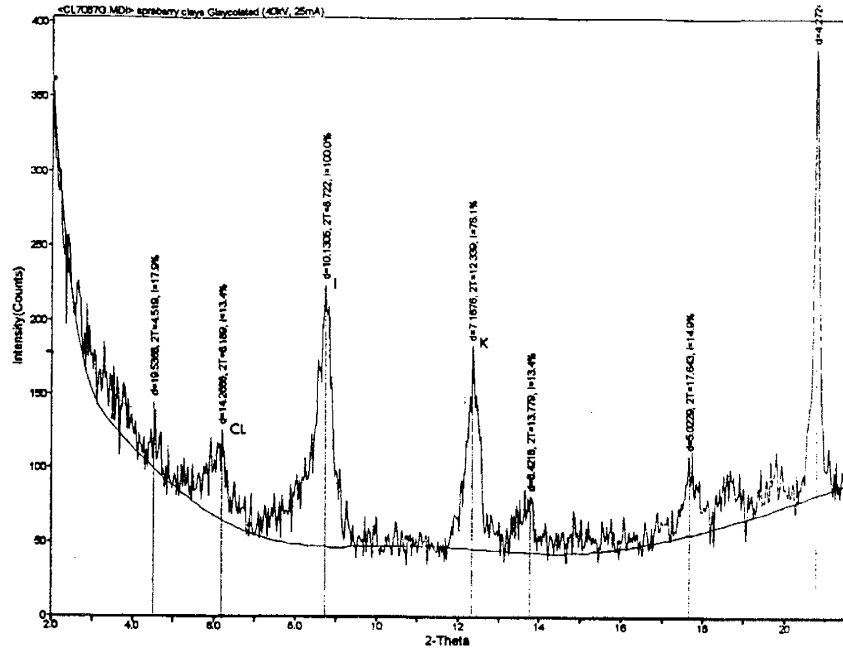
C: This laminated siltstone sample from 7117.5 ft in the Shackelford 138A well core, exhibits total occlusion of intergranular pores by pore-filling clays (CL). Clays were affected by compaction and probably suffered some re-crystallization. Micropores exist among the individual clay crystals and probably account for most of the measured core porosity.

D: Pyrite framboids (Py) are commonly found in thin sections and SEM samples of the Spraberry argillaceous rocks. Pyrite exists as discrete, pore filling crystals and as large, grain-replacing aggregates. Depth: 7117.5 ft. Core: Shackelford 138A.



CLAY COMPOSITION FROM XRD ANALYSIS (parts in 10)				
Sample Depth (feet)	Illite	Chlorite	Kaolinite	I/S
7069	4	4	1	1
7076	10	--	--	--
7081	6	2	1	1
7082	6	2	1	1
7083	5	3	2	1
7085	7	2	1	--
7087	4	4	1	1
7290	6	3	1	--
7092	6	3	1	--

Table 4.2 – X-ray diffraction (XRD) clay mineralogy (parts in ten). Illite is the dominant clay mineral present.



Clay Mineralogy on XRD Pattern Shackelford 1-38A (7104 Ft)

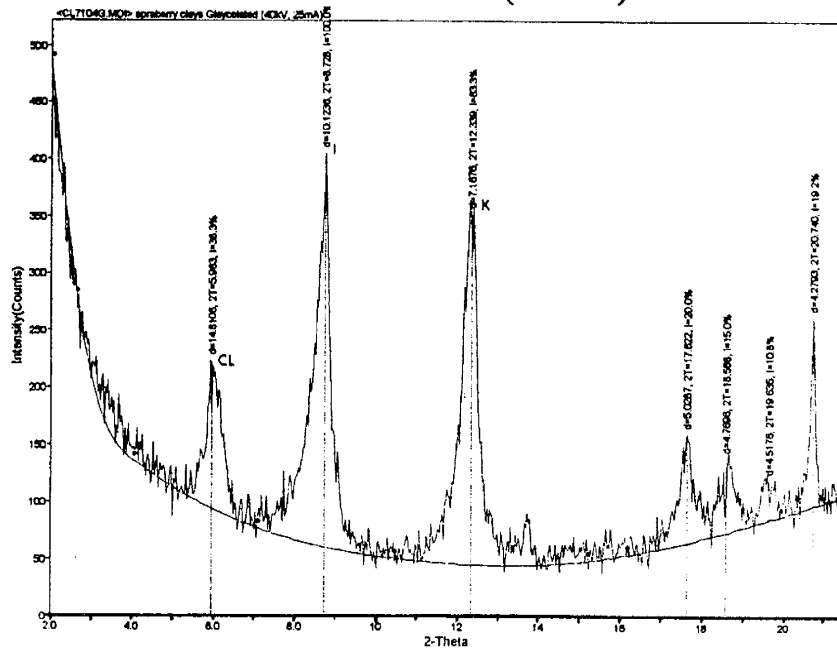


Fig. 4.6 – Two X-ray diffractograms showing clay composition. The top diffractogram for Shackelford 138A (7104-ft) presents sharper and longer peaks, suggesting greater abundance or probably better crystallinity of clay minerals than the bottom diffractogram at 7087 ft. (I) illite, (K) kaolinite and (CL) chlorite.

Carbonate: Authigenic carbonates are relatively abundant cementing agents in the Spraberry Formation. Utilization of proper staining along with observations in scanning electron microscopy helped us identify dolomite cementation and replacement of microorganisms and detrital grains (Fig. 4.7). The authigenic character of the dolomite is quite clear when observed as large patches of poikilotopic cement and replacement of detrital grains. At least three stages of dolomite and ferroan dolomite cement have been found (Fig. 4.7). Dolomite cements are most abundant in lithofacies “C” (silty dolomite mudstone) and “D” (patchy cemented dolomitic siltstone). Dolomite cement is less abundant in SSL-A and SSL-B and form part of a complex mixture of fine-grained sediments and cements in SSL-E and SSL-F.

4.2 PORE MORPHOLOGY, DISTRIBUTION AND PORE THROAT RADII

Based on thin section and scanning electron microscopy observations, I have detected two major categories of pore types and a total of five subcategories depending on pore size, pore shape, origin, and general pore morphology.

Primary Pore Types: These are original framework pores that have often been reduced by compaction and cement precipitation.

Pore Type 1 – Large primary intergranular macropores. Pores are relatively large (30-40 μm diameter) and well interconnected, irregularly shaped. Pore throat mean radius ranges from 0.5-1 μm .

Fig. 4.7 – Photomicrographs showing carbonate cement and replacement

A: This is a coarse-grained siltstone to very fine sandstone. This thin section has been stained for recognition of ferroan dolomite (stained dark blue). Note that ferroan dolomite cement (4.0%) usually surrounding a nuclei of dolomite is more abundant than the non-ferroan dolomite cement (0.6%). Recrystallization of dolomite cement to ferroan composition is believed to have occurred.

E. T. O'Daniel 37 cored well

Depth, ft:	7233	Sample No.:	ET18-H9
Grain Size:	58 μm	Sorting:	Well Sorted
Porosity:	11.3 %	SSL:	A

B: This photomicrograph shows a very shaly, burrowed, very fine-grained sandstone to coarse siltstone. Lenses of clean siltstone are probably the result of burrowing. These are well cemented by calcite (stained red) or dolomite.

E. T. O'Daniel 37 cored well

Depth, ft:	7213.5	Sample No.:	ET7
Grain Size:	62 μm	Sorting:	MWS to WS
Porosity:	Traces	SSL:	E OR F

C: This is sparry dolomite cement replacing indistinct microfossil (probably shell). Abundant matrix formed by sparry and micritic dolomite cement.

Shackelford 138A

Depth, ft:	7076.0
Porosity:	Trace
SSL:	C

D: Calcareous carbonate debris and/or fossil fragments (stained red) form part of the framework components.

E. T. O'Daniel 37 cored well

Depth, ft:	7195.4	Sample No.:	ET5
Grain Size:	52 μm	Sorting:	Well Sorted
Porosity:	Trace	SSL:	E or F

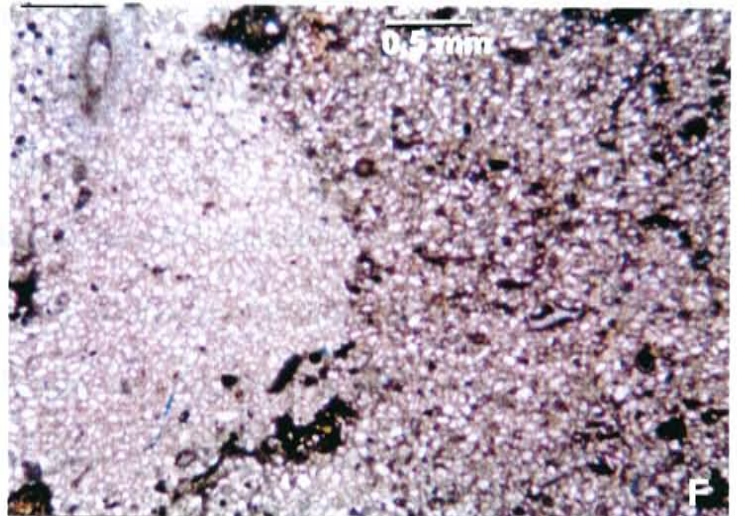
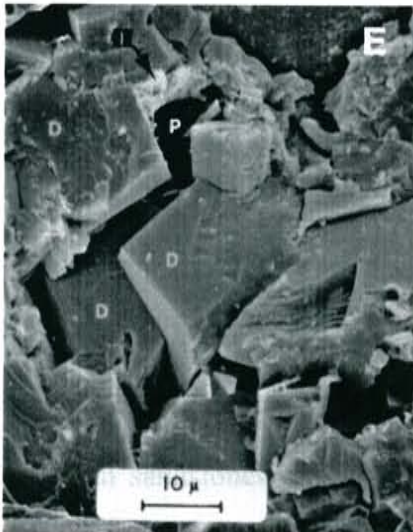
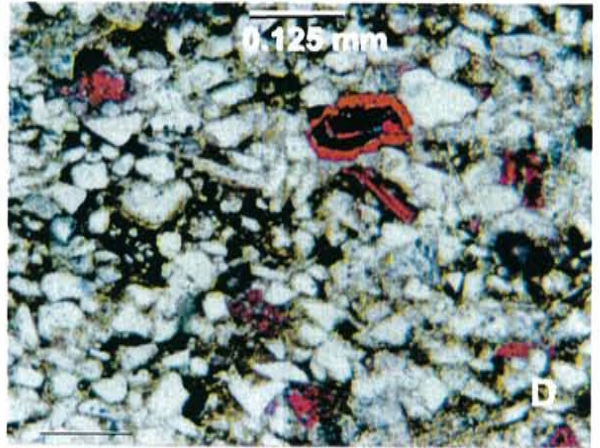
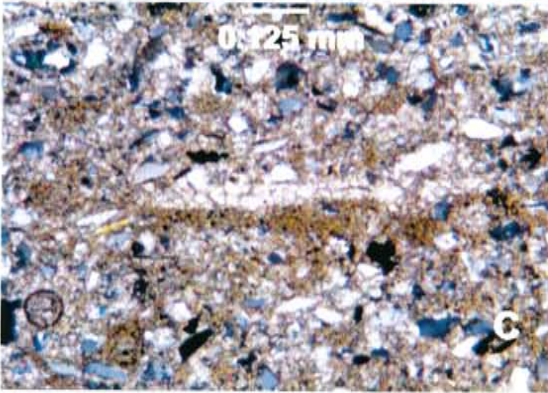
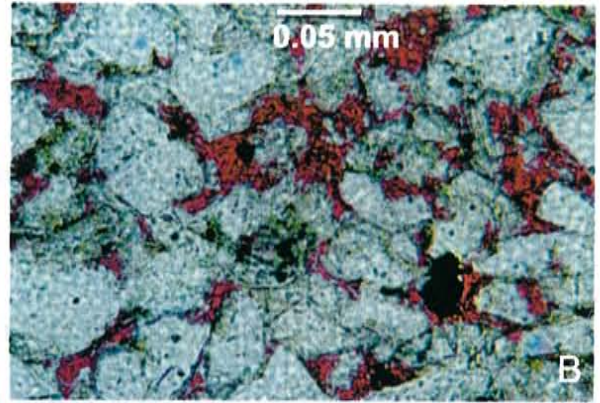
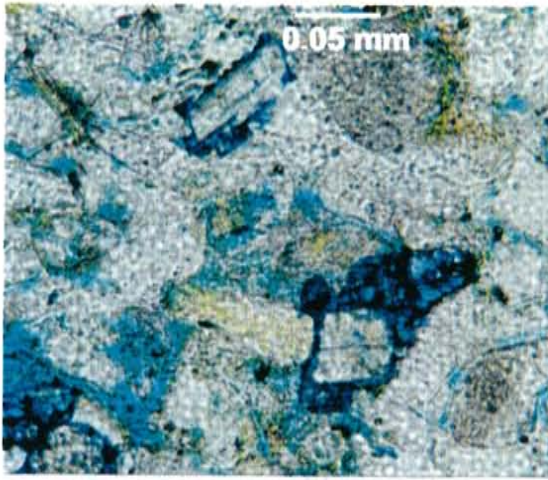
E: Dolomite cement is the major pore-filling constituent in this sample. Extremely low porosity is exhibited.

E.T. O'Daniel 37 cored well.

Depth, ft:	7040.0
Porosity:	0.7 % (from helium injection)
SSL:	C

F: This is a highly dolomitic cemented siltstone or dolostone. Note the difference in texture for cement in the burrowed area (left) and the dolomitic matrix (right).

Arthur Judkins 5 cored well.	Sample No.: J5
Depth, ft:	7018.0
Porosity:	Trace
SSL:	C



Pore Type 2 – Small primary intergranular macropores, 15-30 μm in diameter. Pores are irregular in shape and are moderately interconnected through pore throats 0.4-0.8 μm in radius.

Pore Type 3 – Primary intergranular mesopores, generally 5-15 μm in diameter. Pore shapes are polyhedral and are poorly interconnected through pore throats <0.4 μm in radius.

Pore Type 4 – Micropores. Pores are much less than 5 μm in diameter (generally $<1\mu\text{m}$ diameter). They are developed within authigenic clay rims on framework grains, between fibrous illite growths (often bridging pore throat openings), within partially dissolved grains, and within shale laminae.

Secondary dissolution pores: These are pores that are the product of the chemical dissolution of grains, cements and matrix promoted by the action of brines and/or gases that cause corrosion when their system is altered by considerable increase in temperature and pressure.

Pore Type 5 – Pores are usually oversized to 50 μm in diameter or more, and usually show polygonal shapes as remnants of preexisting grains. Pores of this type are common in upper Spraberry sandstones.

The most common recognizable secondary porosity feature is the partial or total dissolution of feldspar grains (Fig. 4.4). Remnants of partially dissolved grains within a pore space with typical polyhedral shape are often found in thin sections from the very fine clean sandstones and siltstones (SSL-A). Relict features of cleavage with typical extinction patterns of plagioclase (probably Ca-rich) are also commonly found. Dissolution is also observed in unstable carbonate grains and cements. One type of

secondary pore is an oversized pore formed by dissolution of framework grains, patches of matrix, or cements. This type of pore has a greater diameter than the average detrital grain size. Moldic pores are also seen in thin sections from the Spraberry Formation, and are recognized by geometrical shapes of the precursor grains. Another very common secondary pore is the intra-constituent pore, which occurs mainly within framework grains, but also in cement and matrix. Secondary intergranular pores are difficult to differentiate from primary intergranular pores due to their similar habit.

4.3 CATEGORIES OF SMALL-SCALE LITHOFACIES

4.3.1 Relation Between Large-Scale Lithofacies (Chapter 3) and Small-Scale Lithofacies (Chapter 4)

In chapter 3 (*Core Interpretation and Sedimentological Analysis*) I described seven different large-scale lithofacies (LSL), based on observations of hand specimens from core samples. The objective was to define the depositional factors that affect the character of Spraberry Formation. Observations were based on sedimentary textures, sedimentary structures, and depositional characteristics of the different lithofacies and the interaction between them.

From detailed thin section analysis, petrographic characteristics such as grain size, clay mineralogy and content, bedding type, degree of cementation, carbonates species and amounts, and pore type were used to define six different small-scale lithofacies (SSL) in thin section samples (Figs. 4.8 to 4.13). Any one of the six petrographic categories described below could comprise one or more of the different lithofacies from the core-

Fig. 4.8 - Very Fine Sandstones and Coarse Siltstone, with Moderate Porosity – SSL-A:

A, B and C: Coarse grained, well-sorted arkosic siltstone. The sample is massive with no distinct laminations. Subangular to angular framework grains are predominantly monocrystalline quartz, potassium feldspar and plagioclase. Grains are cemented by quartz overgrowths, patchy dolomite, and undifferentiated clays. SEM photomicrograph showing intergranular pore (P) partially occluded by quartz overgrowths. Despite compaction and cementation effects, the rock retains sufficient porosity and permeability to contribute to fluid production. This massive siltstone has good interconnection of pores with somewhat reduced intergranular primary macropores and oversized secondary pores.

E.T. O'Daniel 37 cored well	Sample No.:	ET12-1
Depth, ft:	Sorting:	Well Sorted
Grain Size:	SSL:	A
Porosity:		

7230.3
55 μm
12 %

D: Clean, massive siltstone with a relatively well-developed pore system consisting predominantly of reduced intergranular pores somewhat enhanced by oversized, secondary pores. Siltstone, coarse grained, well-sorted, of arkosic composition. Framework grains are subangular to angular and are predominantly monocrystalline quartz, potassium feldspar and plagioclase. Framework grains are cemented by quartz overgrowths, patchy dolomite, and undifferentiated clays.

Shackelford 138A cored well	Sample No.:	SPX14
Depth, ft:	Sorting:	VWS
Grain Size:	SSL:	A
Porosity:		

7092.65
65 μm
18.8 %

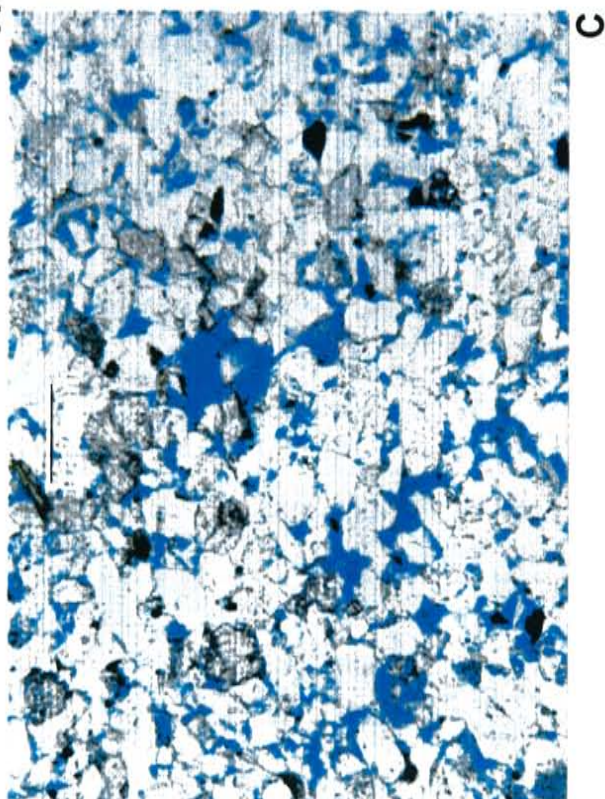
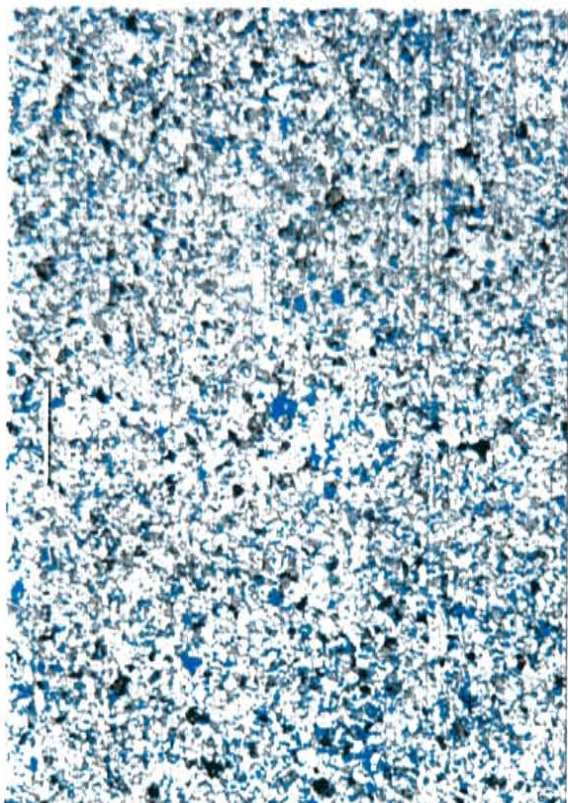
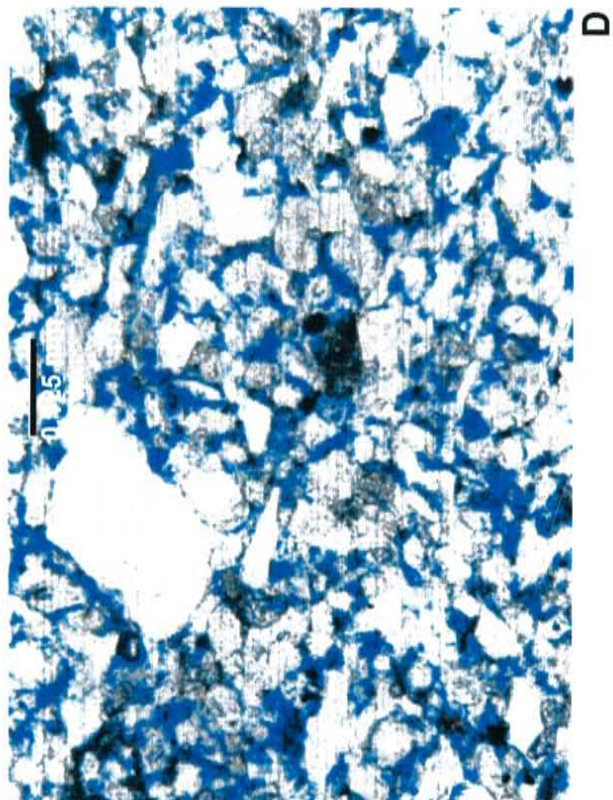
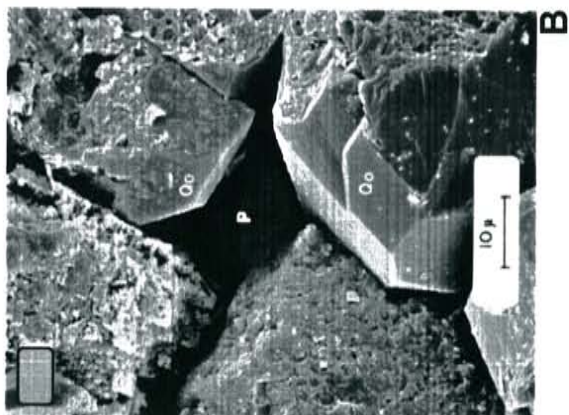


Fig. 4.9 – Photomicrographs of Siltstone and Very Fine Sandstones, Slightly Patchy Cemented and Laminated – SSL-B:

A and B: Survey view of the 7099.8-foot interval. Well-sorted, very fine-grained sandstone, laminated and roughly of arkosic composition. The rock framework consists predominantly of monocrystalline quartz, plagioclase and K-feldspar. The rock displays an intercalation of porous clean sand with very fine shaly laminae. It appears possible that strong dissolution of framework grains and cements have influenced the clean sandy laminae.

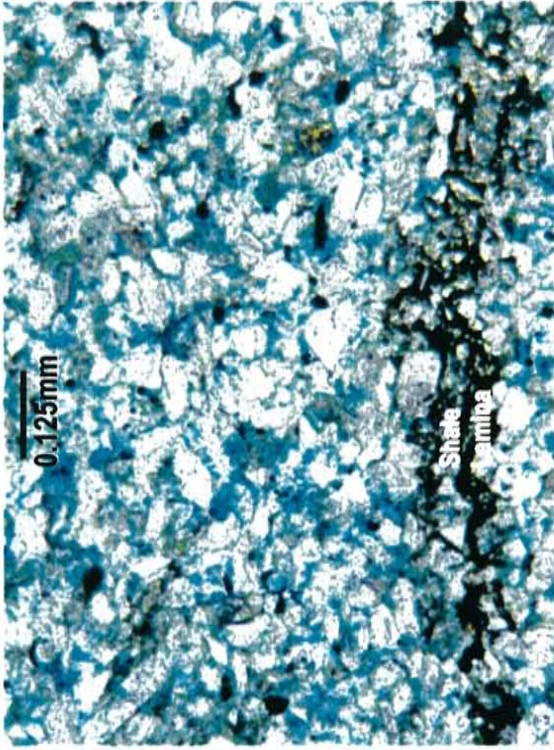
Shackelford 138A cored well		Sample No.:	SPX17
Depth, ft:	7099.8	Sorting:	Well Sorted
Grain Size:	60 μm	SSL:	B
Porosity:	11.1 %		

C: Very fine grained, well-sorted burrowed arkosic sandstone to coarse siltstone. Notice porous lens to the center of the photo associated with burrowing. The rock is slightly shaly consisting predominantly of monocrystalline quartz grains, and less abundant potassium feldspar and plagioclase. Quartz overgrowths, dolomite cement, and slight clayey moderately occlude pore spaces.

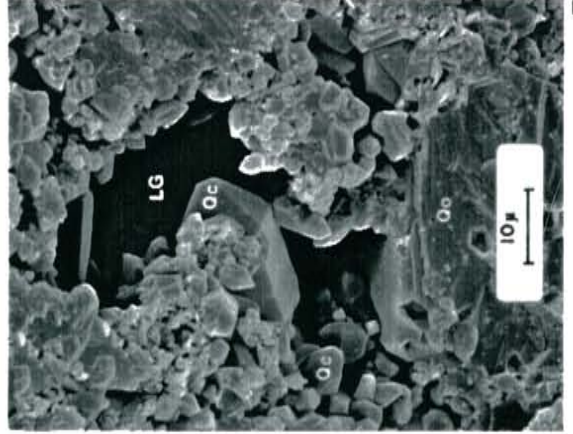
E.T. O'Danile 37 cored well		Sample No.:	ET15-H6
Depth, ft:	7232.25	Sorting:	Well Sorted
Grain Size:	58 μm	SSL:	B
Porosity:	9 %		

D: SEM photomicrograph showing microcrystalline quartz cement (Qc) occluding pore space.

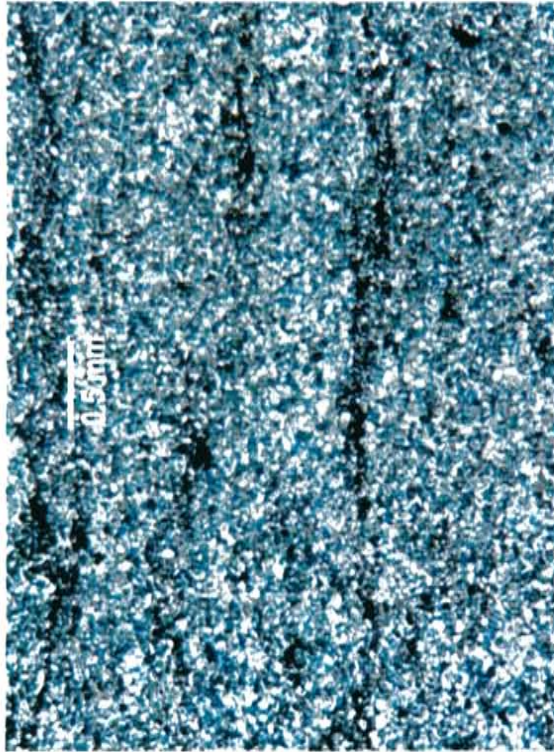
E.T. O'Danile 37 cored well	
Depth, ft:	7131.8
Porosity:	9.6 %
SSL:	B



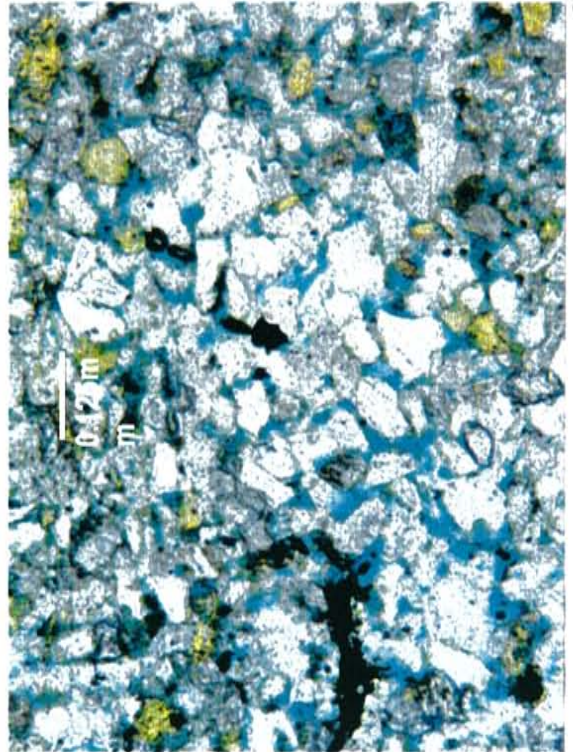
B



D



A



C

Fig. 4.10 – Photomicrographs of Silty Dolomite Mudstone “Dolostone” – SSL-C:

A and B: Moderately well to well sorted, arkosic, coarse grained siltstone to very fine grained sandstone, with a micritic dolomite matrix. Framework grains include monocrystalline quartz, K-feldspar, calcareous debris (foraminifera and calcareous carbonate grains-stained red).

E.T. O’Daniel 37 cored well

Depth, ft: 7206.9
 Grain Size: 60 μm
 Porosity: 1.2 %

Sample No.: ET6
 Sorting: MWS to WS
 SSL: C

C: Burrowed, coarse silty dolostone shows micritized indistinct microfossil. Note the difference in distribution between sparry dolomite cement (sparse) and the more localized micritic matrix associated with precursor organisms (Bu), probably burrows.

Arthur Judkins 5 cored well

Depth, ft: 7018
 Grain Size: 57 μm
 Porosity: Traces

Sample No.: J5b
 SSL: C

D: Slightly fossiliferous, silty micritic dolostone. Sedimentary fabric is massive, lamination and other sedimentary structures are probably destroyed due to diagenetic processes such as burrowing and dolomitization.

Shackelford 138A

Depth, ft: 7076
 Porosity: Traces

Sample No.: SPX3
 SSL: C

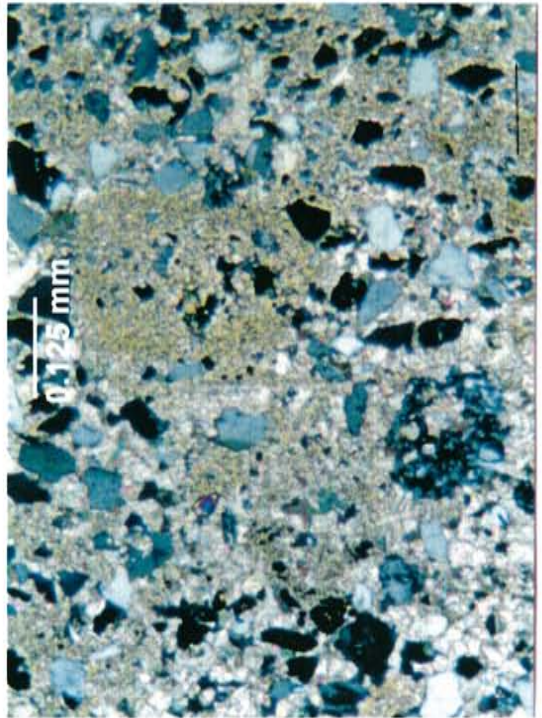
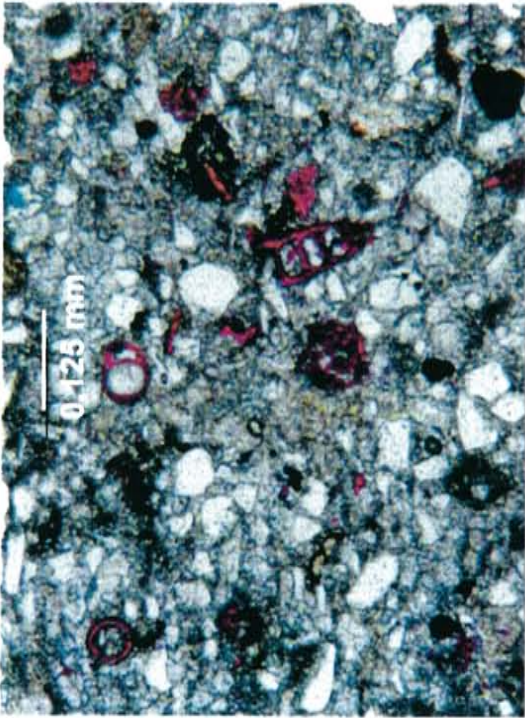
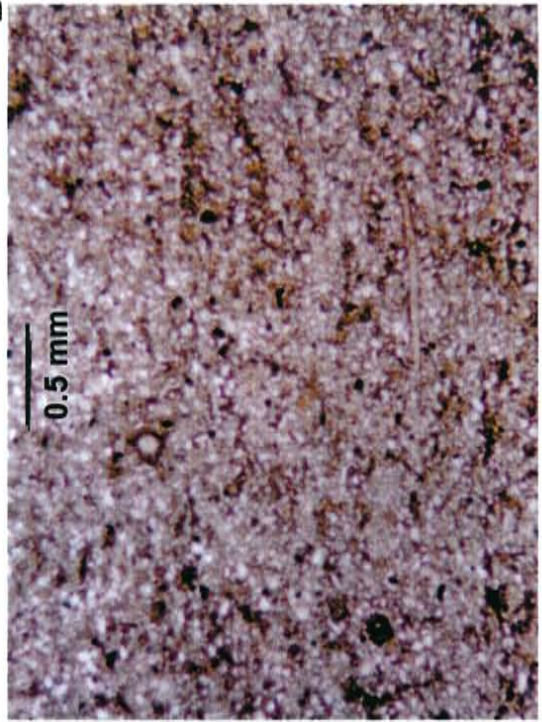
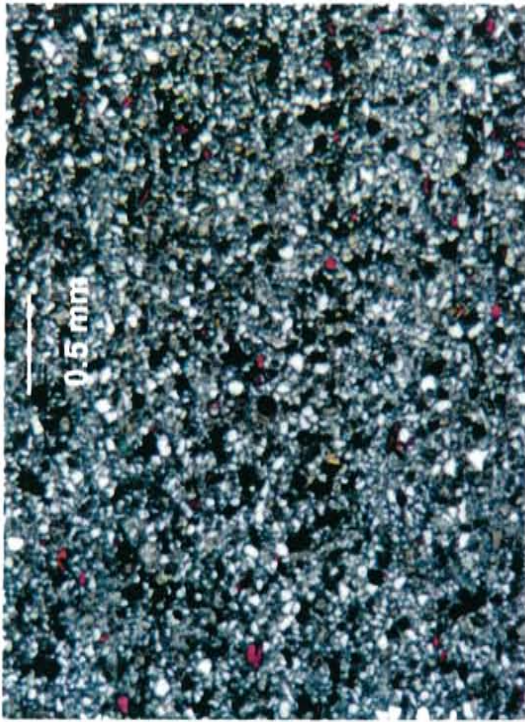


Fig. 4.11 – Photomicrographs of Patchy Dolomitic Siltstone – SSL-D:

Coarse siltstone highly cemented by sparse patches of dolomite cement (cross-nicols). Poikilotopic dolomite cement is observed in sparse patches all over the sample. Porosity has been considerably reduced by carbonate cementation.

Shackelford 138A cored well

Depth, ft: 7090.5

Sample No.: Plug 25

SSL: D

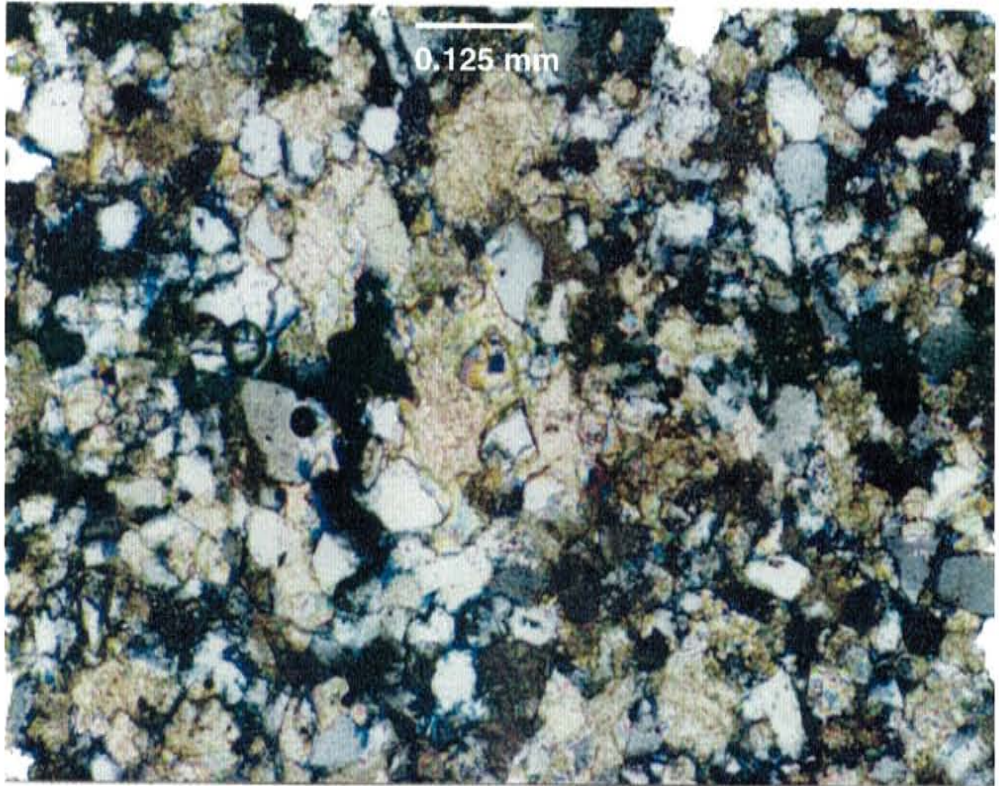


Fig. 4.12 - Photomicrographs of Shale and Silty Shales – SSL-E:

A and B: Laminated, burrowed, silty shale, moderately well sorted, and rich in organics. The rock is strongly laminated. Quartz, feldspar, and mica are the dominant grains. Due to the lack of fluid conduits this rock should present a good seal to fluids.

Shackelford 138A		
Depth, ft:	7093.65	Sample No.: SPX15
Grain Size:	28 μm	Sorting: MWS to WS
Porosity:	0.1 %	SSL: E

C and D: This thin section shows the sharp contact between a shale and an overlying siltstone. Note data below are given for both parts of the sample.

Shackelford 138A		
Shale-Siltstone Contact		
Depth, ft:	7065	Sample No.: SPX18
Grain Size:	28 μm (shale) 56 μm (siltstone)	Sorting: Well Sorted
Porosity:	Traces	SSL: E and F

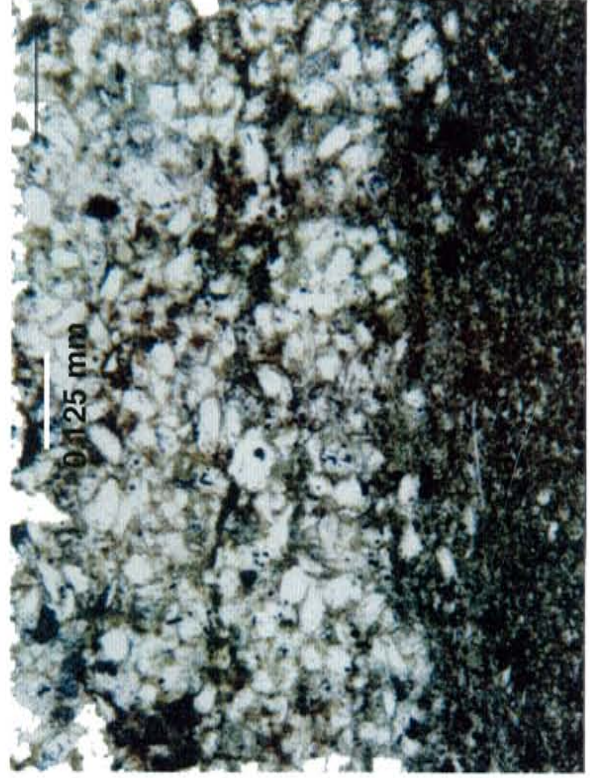
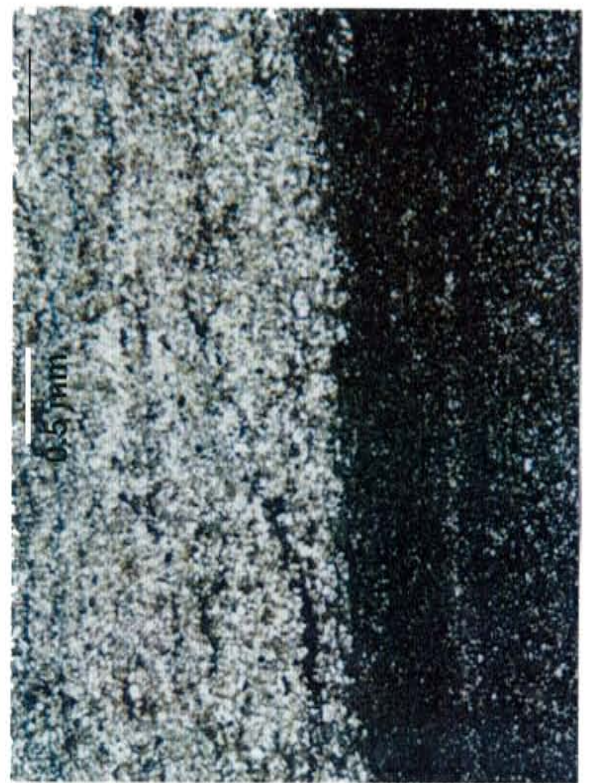
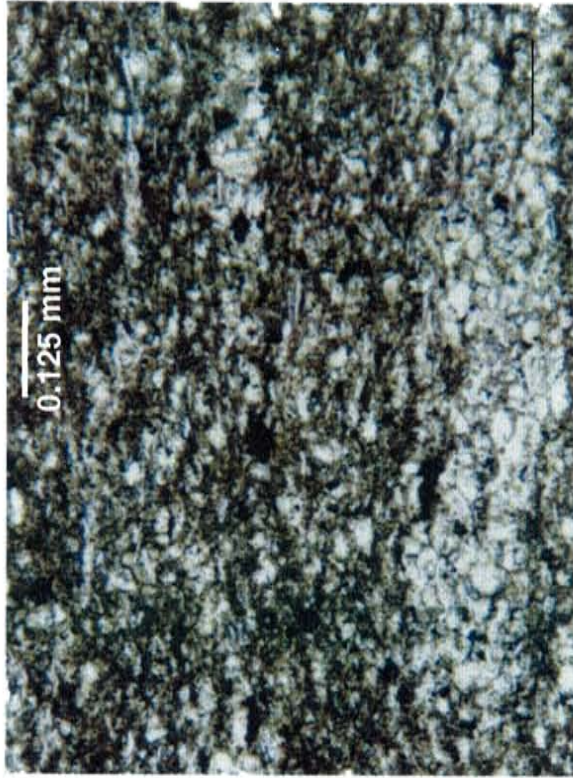
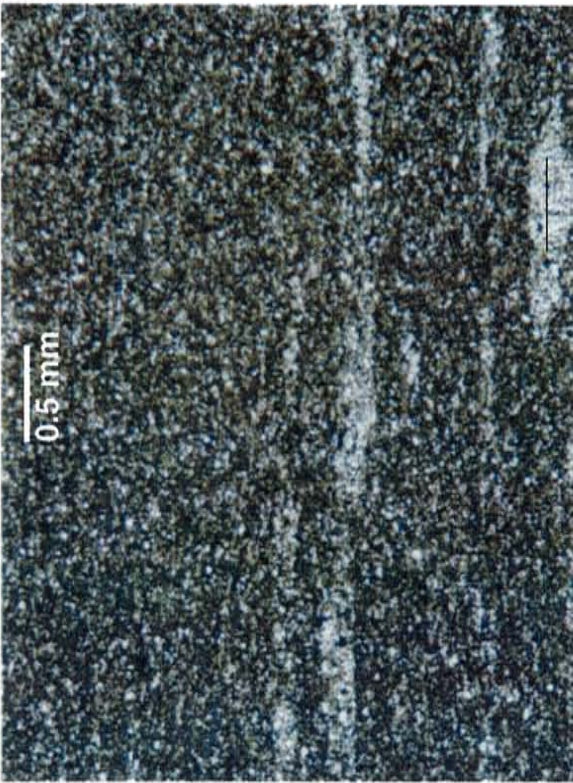


Fig. 4.13 – Photomicrographs of very Argillaceous Laminated Siltstones – SSL-F:

A: Clay rich, bioturbated and/or convoluted, poorly laminated, coarse siltstone. Abundant clay and organic rich matrix is present. Burrowing, and/or possible water escape features formed relatively clean siltstone lenses. Cements, including dolomite and quartz destroyed porosity within these relatively clean lenses.

E.T. O'Daniel 37 cored well		Sample No.:	ET21-1
Depth, ft:	7238.7	Sorting:	WS
Grain Size:	40 μm	SSL:	F
Porosity:	0.7 %		

B: Laminated, burrowed, coarse grained arkosic siltstone, moderately well to well sorted, arkosic. Although it is difficult to see, clay and organic-rich laminae alternate with thin, relatively clean, dolomite cemented laminae. Undifferentiated clays, quartz overgrowths, and dolomite severely disrupt pore interconnections.

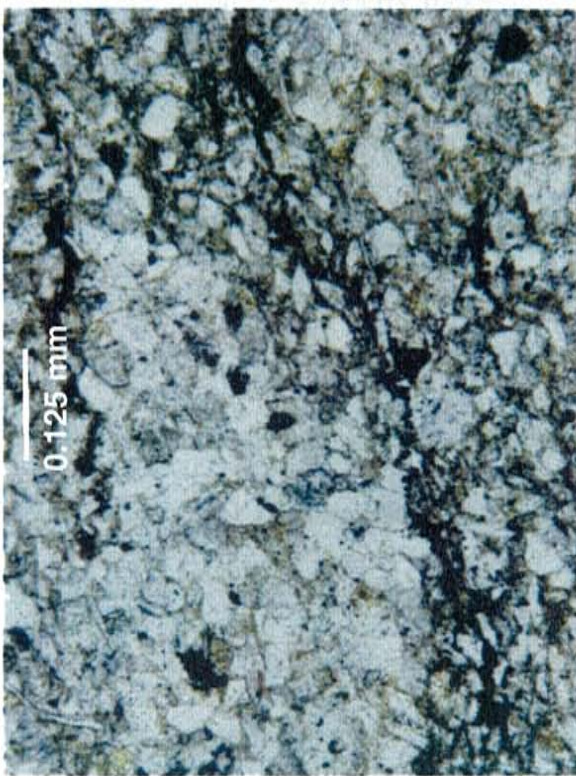
E.T. O'Daniel 37 cored well		Sample No.:	ET3
Depth, ft:	7093.5	Sorting:	MWS to WS
Grain Size:	58 μm	SSL:	F
Porosity:	5.7 %		

C: Laminated, burrowed, very shaly siltstone, moderately well to well sorted, and rich in organics. The strongly laminated rock shows abundant clay matrix rich in organics is the dominant pore filling material. Quartz, feldspar, heavy minerals, and mica are the dominant grains forming the rock fabric.

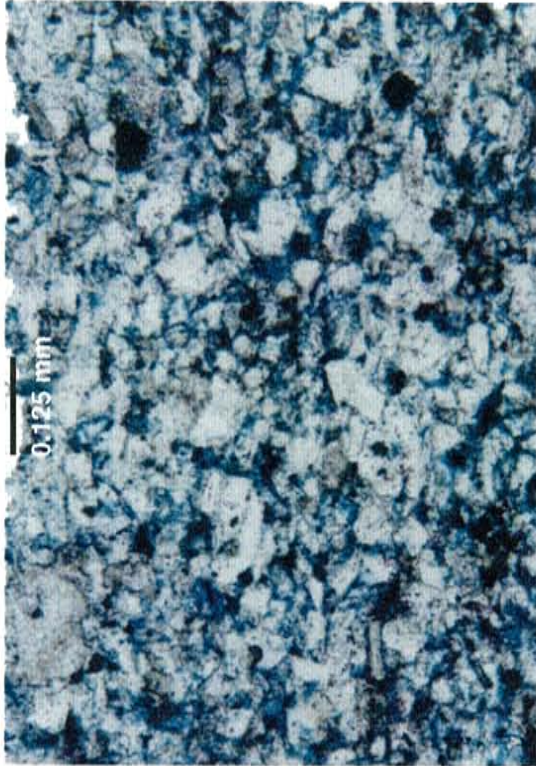
Shackelford 138A		Sample No.:	SPX10
Depth, ft:	7088.0	Sorting:	MWS to WS
Grain Size:	32 μm	SSL:	F
Porosity:	Traces		

D: Matrix supported fabric with abundant, poorly crystalline or recrystallized clays (CL). Micropores are the dominant pore type observed.

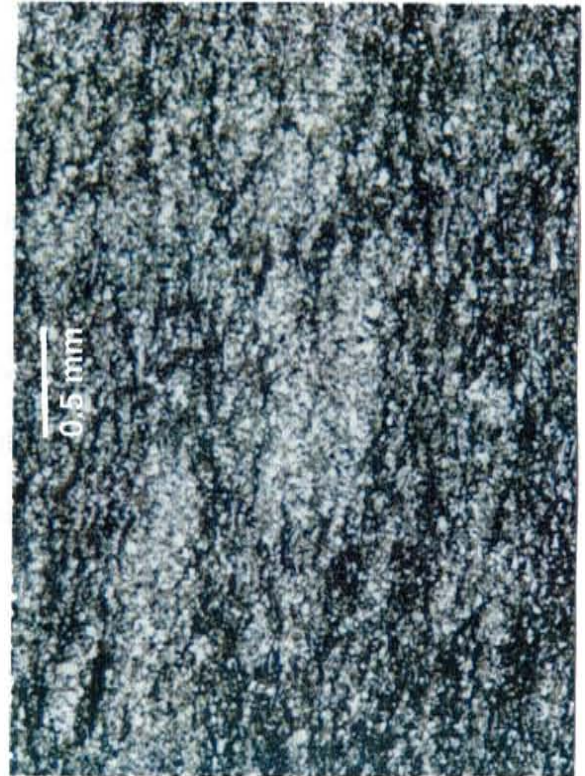
E.T. O'Daniel 37		Sample No.:	
Depth, ft:	7174.9	Sorting:	
Porosity:	6.1 % (from helium injection)	SSL:	F



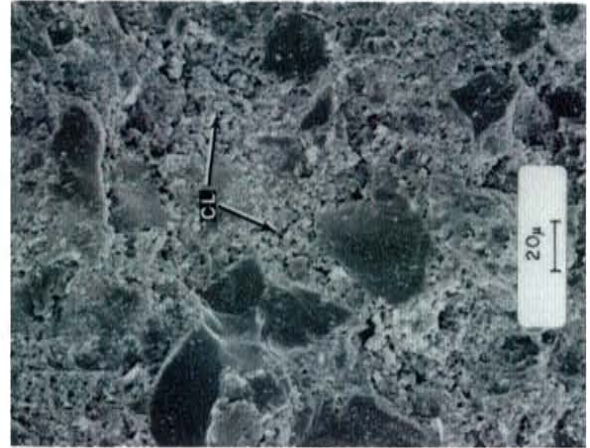
A



B



C



D

sedimentological analysis. Data used in this section are based on tables of point count data included in the appendix (Tables 1,2 and 3 of appendix); the table of average and ranges (Table 4.1); and a corresponding plate of photos that follows each category.

4.3.2 Small Scale Lithofacies “A”

Moderately good porosity, very fine sandstones and coarse siltstones - Very fine sandstones and siltstones are the best reservoir rocks within the Spraberry Formation (Fig. 4.8-a). These light-colored, massive to poorly laminated sediments are the highest porosity rocks among all six small scale-lithofacies (SSL). These rocks range from very fine sandstones to coarse siltstones with an average grain size of 61 μm . Porosity ranges from 19% to 10% and averages 14.3%. Lithofacies “A” contains most of the different types of pores noted in Spraberry rocks; however, the dominant pore types are reduced intergranular macropores (primary pore types 1 and 2; Fig. 4.8-b) and secondary pores of type 5 (dissolution pores; Figs. 4.8-c). Even for SSL-A, porosity is only moderately good, due to compaction, clay content and typical very fine grain size of the Spraberry sandstones and siltstones. The pore assemblage is moderately well interconnected, as observed with scanning electron microscopy. Dissolution of feldspar grains, carbonate grains and dolomite cement was observed. Dissolution effects can be recognized by the presence of remnant undissolved partial grains and grain molds in polygonal shapes. Although the SSL-A category is a well-sorted rock, in some cases isolated grains are three or four times the average grain size of the sample (Fig. 4.8-d). Grains are subangular to subrounded and somewhat elongate, showing a subtle subhorizontal orientation with respect to the plane of deposition. Original bedding has been slightly

affected by one or more of the following events: dewatering, burrowing, and/or diagenetic processes. The effect of compaction is suggested by the presence of long, sutured, and concavo-convex contacts. Quartz is the most abundant framework mineral. Fluid inclusions are common, seen to form chains across the grains, or lining the boundaries between grain and overgrowth. After quartz, fresh and altered grains of twinned plagioclase, primarily albite, and K-feldspar are the most abundant framework grains. Alteration and dissolution occurring along twin planes and corrosion of grain margins and interiors make recognition difficult. Illite, kaolinite and chlorite are only clearly detectable in XRD patterns, showing low crystallinity peaks for clays in sandstones. It is possible to observe illite flakes by using scanning electron microscopy (SEM) in some cases, although most of the clays observed on thin section are described as masses of laminated, disperse or undifferentiated clays. Relatively minor amounts of carbonate cement are present. SEM photomicrographs show euhedral dolomite rhombs of approximately the same size as clastic grains, suggesting dolomite replacement of precursor carbonate or unstable silicate grains.

4.3.3 Small Scale Lithofacies “B”

Slightly shaly laminated and/or patchy siltstones and very fine sandstones (low quality reservoir) – This type of lithofacies SSL-B (Fig. 4.9-a) presents overall lower porosity than SSL-A. Dissolution porosity within SSL-B is less abundant than in SSL-A rocks, being affected by organic/clay laminae (Fig. 4.9-b). Figure 4.9-c shows the effect of probable dewatering phenomena or burrowing, which produce a local increase in porosity. Quartz and feldspar grains are again the main mineral species. The sandstones

are arkose and subarkose. Detrital grains are generally subrounded to subangular and grain size averages 58 μm . Relatively larger amounts of clay, organics, and carbonate matrix and cements, and relatively lower porosity characterize this facies. Quartz cement (Fig. 4.9-d) is abundant in this lithofacies. Facies “B” rocks are typically associated with facies “A”. In general facies “B” has the same depositional, textural, and compositional characteristics of facies “A” (grain sorting, fine grain size, and subarkosic mineralogy), but exhibits considerably more laminations than facies “A”. Facies “B” rocks also occur as single thin layers in non-pay zones.

4.3.4 Small Scale Lithofacies “C”

Silty dolomite mudstone “dolostone” (good seal rocks for reservoirs) - From the observation of core macro-samples these sedimentary rocks are described as dark gray, very fine grained dolomites (possibly mudstones in “*Lithofacies LSL-5*”; Chapter 3). Thickness varies from a few centimeters to several tenths of centimeters. They are commonly massive (Figs. 4.10-a and b) but can show some laminae formed of a mixture of carbonate mud, clays, and organics.

Thin section specimens show that micritic dolomite (probably dolomitized mud) is the major component of this facies (Fig. 4.10-a). Micritic matrix varies to sparry dolomite in many cases (Fig. 4.10-c). Dolomitized carbonate muds averages 31% and dolomite cement counts for an average of 26%. Other mineral species are ferroan dolomite and fossil fragments. Foraminifers are the most common fauna found (Fig. 4.10-a). Echinoid spicules and fragments, crinoid columnals, and calcispheres are found as sparry spherical grains within the dolomitic micrite (Fig. 4.10-d). Radiolarian tests are

considered by other studies (Folk, 1989 and Martha Cather, pers. com.) to be a common type of fossil in the Spraberry Formation.

Quartz and feldspar of silt size (avg. 55 μm) are the major clastic grains, ranging in abundance from 20% to 24%, thus these carbonate muds are classified as a silty wackstone to packstone in composition. Muscovite occurs in trace amounts. Some thin sections were stained for recognition of ferroan dolomite and siderite, which has helped to detect possible recrystallization to ferroan dolomite (Fig. 4.7-a). These rocks lack porosity and form non-reservoir rocks, probably with good seal characteristics.

4.3.5 Small Scale Lithofacies “D”

Very “patchy” dolomitic siltstone – These samples, like SSL “A” and “B”, are arkosic to subarkosic in composition. The major detrital grains are quartz, followed by feldspars and minor rock fragments. Average grain size is 59 μm . The average amount of dolomite cement is 16 %, and for calcite 3 %. These are dominantly pervasive cements forming patches scattered throughout the rock. Porosity amounts to an average of 6 % and ranges from a high of 7 % to a low of 3 %. A higher percentage of dolomite cement distinguishes type “D” patchy dolomitic siltstones from the similar, but less dolomitic, type “B” rocks (Fig. 4.11).

4.3.6 Small Scale Lithofacies “E”

Shales and silty shales - Shales and silty shales, together with the silty dolomite mudstones (SSL-D) have the lowest porosity of the six categories described (Fig. 4.12-a). The maximum porosity found in samples from SSL-E is 1%, whereas clay matrix

(laminar and dispersed clays, organics, and depositional carbonate mud) is abundant, ranging between 35% and 57%. Detrital monocrystalline quartz ranges from 21.0% to 44.3% depending on the amount of silty laminae present in each sample. Color varies from gray to black. Among all petrographic categories, muscovite averages the highest in shales (5.5%). Fig. 4.12-b shows a higher magnification view of burrows (same sample as Fig. 4.12-a) within shale. Notice the reduction in organic content within burrow lenses. Alteration of feldspar grains makes it difficult to differentiate them from clay matrix, mixed with organics, carbonates, and accessory minerals like mica and pyrite. Framboidal pyrite is especially visible in the SEM photomicrographs for both shales (SSL-E) and argillaceous laminated siltstones (SSL-F). Pyrite, as well as mica, tends to increase in abundance with the increase of clay material. Phosphatic nodules are common in shale (SSL-E) and also in highly laminated argillaceous siltstones (SSL-F). Figures 4.12-c and 4.12-d present low and high magnification views of a contact between a very laminated argillaceous siltstone (SSL-F) and an underlying shale bed (SSL-E).

4.3.7 Small Scale Lithofacies “F”

Argillaceous highly laminated siltstones - Argillaceous highly laminated siltstones form a category that can grade from relatively clean laminated siltstones to very poor reservoir quality, laminated shaly siltstones (Figs. 4.13-a and b). Depending on the relative amounts of clays, organics, pyrite and other argillaceous materials, sediments will present thinner or thicker laminae between silts and shales. This is the most common lithology occurring throughout the upper Spraberry Formation in the three cores examined. Clean laminated siltstones (Fig. 4.13-b) are associated with the high porosity,

massive, very fine sandstones of SSL-B. The more silty parts of these rocks are cleaner, with coarser grain size and little argillaceous material (Fig. 4.13-a and Fig. 4.13-c). Grains are subangular to subrounded and closely packed. Quartz is dominant and altered or fresh feldspars are also visible. Some feldspar grains are altered to illite or kaolinite. Laminated shaly siltstones (SSL-F) are darker, and differ from the cleaner siltstones (SSL-B) in having significantly larger amounts of argillaceous matter. The effects of alteration and difficulties in distinguishing grain types are greater in this lithology (SSL-F) than in the analogous cleaner lithologies (SSL-B), especially for feldspar grains. Laminated shaly siltstones tend to be matrix-supported (Fig. 4.13-d). Argillaceous matrix is comprised of illite, chlorite, kaolinite, organics, pyrite, and some micritic carbonates.

4.4 DIAGENETIC INTERPRETATION

Spraberry diagenesis has resulted in an overall reduction of original porosity and permeability. Variations in the amount of compaction, cementation, and dissolution have overprinted the original rock fabric, and have asserted a certain control over spatial variations in reservoir quality within the upper Spraberry Formation. This study documents the relationship between lithofacies and diagenetic effects within the Spraberry Formation in a qualitative manner, and offers an explanation of how diagenetic events may have affected the quality of the reservoirs.

4.4.1 Arkosic sandstones, quartz overgrowths, and pressure solution of quartz grains

Silica cement volume is independent of stratigraphic position; however, it is more common in clean and porous, very fine sandstones and coarse siltstones (Fig. 4.3). Silica cement has three distinct morphologies as follow:

1. relatively continuous overgrowths developed on framework grain surfaces;
2. isolated, small (10-15 μm), euhedral silica crystals with bases attached to framework quartz grains; and
3. microquartz (<5 μm) crystals occurring as pore lining and pore filling cement.

Warn and Sidwell (1953) stated that opal cement is the more important pore-filling material within the sandy units. They also concluded that chalcedony replaced most of the carbonates. Warn and Sidwell also pointed out that grains are closely packed with numerous contacts showing the result of limited pressure solution of grain margins. Most of these previous findings discuss samples from the southern parts of the Permian Basin. Our area of work is located approximately 40 to 50 miles to the north. Some differences among the areas are to be expected. Little opal or chalcedony are seen in samples used in this study. Also, feldspar is an important constituent. Source rocks and diagenetic history vary somewhat; however, the overall fine-grained nature of the Spraberry, the general depositional sequences, and the basic rock composition are similar in both regions.

Quartz Overgrowths: Wilson, et al. (1994) and McBride (1989) cited the following sources of silica for quartz overgrowths:

- pressure solution of quartz and feldspars
- illitization of smectitic clays
- dissolution of quartz grains in shales and mudstones
- dissolution of siliceous microfossils or spicules
- dissolution of volcanic glass

For Spraberry sands, all of the above cases are possible sources of silica. Each case presents a different degree of possibility to have occurred. Overgrowths of quartz and feldspar within the sands probably cause little net reduction in porosity because equivalent amounts of dissolved silica account for precipitation in a closed system. This is possible for overgrowth dissolution, but not for quartz cement derived from pressure solution because such a mechanism is accompanied by considerable grain rearranging, which indeed reduces porosity substantially. In most cases, it is also difficult to define an open or closed system. Studies conducted by Heald and Renton (1966) documented a considerably greater degree of quartz cementation for finer grained, monocrystalline quartzose sands, like the Spraberry SSL-A and SSL-B (sandy, clean and porous lithofacies). Small-scale lithofacies "A" contain slightly higher average amounts of quartz overgrowths than SSL-B ("A" - 5.2%; "B" - 4.5%). The last may be due to the higher presence of cement coatings (clays and dolomite) and laminations in SSL-B that may have inhibited nucleation of quartz cement.

In the absence of pressure solution, dissolution of quartz is regarded as uncommon unless the pH of the interstitial fluids is strongly alkaline. Folk (1989) found

that quartz cements in the Spraberry Formation are much more soluble than the actual grains, perhaps due to an Al-rich basal part of the overgrowths that causes lattice distortion and enhances solubility.

In general, abundant cements in certain parts of the Spraberry Formation might have prevented quartz from being dissolved. Instead, due to the relative absence of preserving carbonate cements within the clean sands, radiolarian fossils were probably dissolved and then served as the silica source for overgrowths (Folk, 1989). This is probably why radiolaria have not been found in the clean sandstones. This idea is supported by the presence of numerous well-preserved radiolarian skeletons within early-cemented phosphate nodules and carbonate cemented layers (Folk, 1989).

Pressure solution and quartz overgrowth development are important causes of porosity loss in sandstones, and this is more pronounced with rocks rich in quartz grains (Wilson and Stanton, 1994). The typical Spraberry, very fine sandstones and siltstones match most of the accepted models for precipitation of silica cements. Burial depths greater than 7000 ft have produced enough compaction stress concentrated at points of grain-to-grain contact to create suturing and concavo-convex contacts between grains (Fig. 4.3). It is thought that solubility is increased at the grain contacts with the increase in stress. Silica liberated by dissolution can then precipitate on nearby contiguous surfaces where a lower degree of stress is present.

Bjørkum (1994) presented another hypothesis explaining that pressure might not be a significant factor in the dissolution process. Instead, diffusion transport might be controlled by the action of overpressuring. This process is probably a major source of silica for quartz overgrowths.

The presence of materials like micas and clays may enhance pressure solution within adjacent quartz grains (Thomson, 1959). Very small increases of pH at quartz-mica interfaces can produce dissolution of silica, which is caused by the preferential attraction of OH⁻ ions to negatively charged mica surfaces (Oelkers and others, 1992). The pH of saline pore waters adjacent to micas may increase as much as 0.6 log units (Boles and Johnson, 1983). Potassium-rich mica and illite clays are probably giving away K⁺ during this process. The cleavage surfaces of micas and clays exhibit faster ionic exchange than other areas of the rock fabric. The pH change is another possible mechanism for quartz dissolution, because pH can increase with the formation of fluids rich in potassium carbonate (K₂CO₃) when potassium is released from illite clay. Subsequent precipitation of quartz might occur in areas of lower pH, accompanied by suturing of quartz grains in zones of high pressure and high pH (Fig. 4.14).

Small amounts of clays might allow the precipitation of considerable silica cement. But if the amount of clays increases to an intermediate level, this can produce sufficient grain coating to prevent cementation and porosity reduction. This process of quartz cementation is probably related to the clean sands of the Spraberry Formation, which show the highest amount of quartz cement among all lithofacies, whereas content of clay minerals remain low.

As noted above, quartz overgrowths are believed to be inhibited by clay material coating grains of quartz, thus suppressing nucleation points (Pittman et. al, 1992). Different types of coats can effectively reduce the development of quartz overgrowths, detrital or diagenetic clays being the most common (Heald and Larese, 1974). In the Spraberry Formation the sandy and cleaner units have the maximum amounts of quartz

sedimentological analysis. Data used in this section are based on tables of point count data included in the appendix (Tables 1,2 and 3 of appendix); the table of average and ranges (Table 4.1); and a corresponding plate of photos that follows each category.

4.3.2 Small Scale Lithofacies “A”

Moderately good porosity, very fine sandstones and coarse siltstones - Very fine sandstones and siltstones are the best reservoir rocks within the Spraberry Formation (Fig. 4.8-a). These light-colored, massive to poorly laminated sediments are the highest porosity rocks among all six small scale-lithofacies (SSL). These rocks range from very fine sandstones to coarse siltstones with an average grain size of 61 μm . Porosity ranges from 19% to 10% and averages 14.3%. Lithofacies “A” contains most of the different types of pores noted in Spraberry rocks; however, the dominant pore types are reduced intergranular macropores (primary pore types 1 and 2; Fig. 4.8-b) and secondary pores of type 5 (dissolution pores; Figs. 4.8-c). Even for SSL-A, porosity is only moderately good, due to compaction, clay content and typical very fine grain size of the Spraberry sandstones and siltstones. The pore assemblage is moderately well interconnected, as observed with scanning electron microscopy. Dissolution of feldspar grains, carbonate grains and dolomite cement was observed. Dissolution effects can be recognized by the presence of remnant undissolved partial grains and grain molds in polygonal shapes. Although the SSL-A category is a well-sorted rock, in some cases isolated grains are three or four times the average grain size of the sample (Fig. 4.8-d). Grains are subangular to subrounded and somewhat elongate, showing a subtle subhorizontal orientation with respect to the plane of deposition. Original bedding has been slightly

affected by one or more of the following events: dewatering, burrowing, and/or diagenetic processes. The effect of compaction is suggested by the presence of long, sutured, and concavo-convex contacts. Quartz is the most abundant framework mineral. Fluid inclusions are common, seen to form chains across the grains, or lining the boundaries between grain and overgrowth. After quartz, fresh and altered grains of twinned plagioclase, primarily albite, and K-feldspar are the most abundant framework grains. Alteration and dissolution occurring along twin planes and corrosion of grain margins and interiors make recognition difficult. Illite, kaolinite and chlorite are only clearly detectable in XRD patterns, showing low crystallinity peaks for clays in sandstones. It is possible to observe illite flakes by using scanning electron microscopy (SEM) in some cases, although most of the clays observed on thin section are described as masses of laminated, disperse or undifferentiated clays. Relatively minor amounts of carbonate cement are present. SEM photomicrographs show euhedral dolomite rhombs of approximately the same size as clastic grains, suggesting dolomite replacement of precursor carbonate or unstable silicate grains.

4.3.3 Small Scale Lithofacies “B”

Slightly shaly laminated and/or patchy siltstones and very fine sandstones (low quality reservoir) – This type of lithofacies SSL-B (Fig. 4.9-a) presents overall lower porosity than SSL-A. Dissolution porosity within SSL-B is less abundant than in SSL-A rocks, being affected by organic/clay laminae (Fig. 4.9-b). Figure 4.9-c shows the effect of probable dewatering phenomena or burrowing, which produce a local increase in porosity. Quartz and feldspar grains are again the main mineral species. The sandstones

are arkose and subarkose. Detrital grains are generally subrounded to subangular and grain size averages 58 μm . Relatively larger amounts of clay, organics, and carbonate matrix and cements, and relatively lower porosity characterize this facies. Quartz cement (Fig. 4.9-d) is abundant in this lithofacies. Facies “B” rocks are typically associated with facies “A”. In general facies “B” has the same depositional, textural, and compositional characteristics of facies “A” (grain sorting, fine grain size, and subarkosic mineralogy), but exhibits considerably more laminations than facies “A”. Facies “B” rocks also occur as single thin layers in non-pay zones.

4.3.4 Small Scale Lithofacies “C”

Silty dolomite mudstone “dolostone” (good seal rocks for reservoirs) - From the observation of core macro-samples these sedimentary rocks are described as dark gray, very fine grained dolomites (possibly mudstones in “*Lithofacies LSL-5*”; Chapter 3). Thickness varies from a few centimeters to several tenths of centimeters. They are commonly massive (Figs. 4.10-a and b) but can show some laminae formed of a mixture of carbonate mud, clays, and organics.

Thin section specimens show that micritic dolomite (probably dolomitized mud) is the major component of this facies (Fig. 4.10-a). Micritic matrix varies to sparry dolomite in many cases (Fig. 4.10-c). Dolomitized carbonate muds averages 31% and dolomite cement counts for an average of 26%. Other mineral species are ferroan dolomite and fossil fragments. Foraminifers are the most common fauna found (Fig. 4.10-a). Echinoid spicules and fragments, crinoid columnals, and calcispheres are found as sparry spherical grains within the dolomitic micrite (Fig. 4.10-d). Radiolarian tests are

considered by other studies (Folk, 1989 and Martha Cather, pers. com.) to be a common type of fossil in the Spraberry Formation.

Quartz and feldspar of silt size (avg. 55 μm) are the major clastic grains, ranging in abundance from 20% to 24%, thus these carbonate muds are classified as a silty wackstone to packstone in composition. Muscovite occurs in trace amounts. Some thin sections were stained for recognition of ferroan dolomite and siderite, which has helped to detect possible recrystallization to ferroan dolomite (Fig. 4.7-a). These rocks lack porosity and form non-reservoir rocks, probably with good seal characteristics.

4.3.5 Small Scale Lithofacies “D”

Very “patchy” dolomitic siltstone – These samples, like SSL “A” and “B”, are arkosic to subarkosic in composition. The major detrital grains are quartz, followed by feldspars and minor rock fragments. Average grain size is 59 μm . The average amount of dolomite cement is 16 %, and for calcite 3 %. These are dominantly pervasive cements forming patches scattered throughout the rock. Porosity amounts to an average of 6 % and ranges from a high of 7 % to a low of 3 %. A higher percentage of dolomite cement distinguishes type “D” patchy dolomitic siltstones from the similar, but less dolomitic, type “B” rocks (Fig. 4.11).

4.3.6 Small Scale Lithofacies “E”

Shales and silty shales - Shales and silty shales, together with the silty dolomite mudstones (SSL-D) have the lowest porosity of the six categories described (Fig. 4.12-a). The maximum porosity found in samples from SSL-E is 1%, whereas clay matrix

(laminar and dispersed clays, organics, and depositional carbonate mud) is abundant, ranging between 35% and 57%. Detrital monocrystalline quartz ranges from 21.0% to 44.3% depending on the amount of silty laminae present in each sample. Color varies from gray to black. Among all petrographic categories, muscovite averages the highest in shales (5.5%). Fig. 4.12-b shows a higher magnification view of burrows (same sample as Fig. 4.12-a) within shale. Notice the reduction in organic content within burrow lenses. Alteration of feldspar grains makes it difficult to differentiate them from clay matrix, mixed with organics, carbonates, and accessory minerals like mica and pyrite. Framboidal pyrite is especially visible in the SEM photomicrographs for both shales (SSL-E) and argillaceous laminated siltstones (SSL-F). Pyrite, as well as mica, tends to increase in abundance with the increase of clay material. Phosphatic nodules are common in shale (SSL-E) and also in highly laminated argillaceous siltstones (SSL-F). Figures 4.12-c and 4.12-d present low and high magnification views of a contact between a very laminated argillaceous siltstone (SSL-F) and an underlying shale bed (SSL-E).

4.3.7 Small Scale Lithofacies “F”

Argillaceous highly laminated siltstones - Argillaceous highly laminated siltstones form a category that can grade from relatively clean laminated siltstones to very poor reservoir quality, laminated shaly siltstones (Figs. 4.13-a and b). Depending on the relative amounts of clays, organics, pyrite and other argillaceous materials, sediments will present thinner or thicker laminae between silts and shales. This is the most common lithology occurring throughout the upper Spraberry Formation in the three cores examined. Clean laminated siltstones (Fig. 4.13-b) are associated with the high porosity,

massive, very fine sandstones of SSL-B. The more silty parts of these rocks are cleaner, with coarser grain size and little argillaceous material (Fig. 4.13-a and Fig. 4.13-c). Grains are subangular to subrounded and closely packed. Quartz is dominant and altered or fresh feldspars are also visible. Some feldspar grains are altered to illite or kaolinite. Laminated shaly siltstones (SSL-F) are darker, and differ from the cleaner siltstones (SSL-B) in having significantly larger amounts of argillaceous matter. The effects of alteration and difficulties in distinguishing grain types are greater in this lithology (SSL-F) than in the analogous cleaner lithologies (SSL-B), especially for feldspar grains. Laminated shaly siltstones tend to be matrix-supported (Fig. 4.13-d). Argillaceous matrix is comprised of illite, chlorite, kaolinite, organics, pyrite, and some micritic carbonates.

4.4 DIAGENETIC INTERPRETATION

Spraberry diagenesis has resulted in an overall reduction of original porosity and permeability. Variations in the amount of compaction, cementation, and dissolution have overprinted the original rock fabric, and have asserted a certain control over spatial variations in reservoir quality within the upper Spraberry Formation. This study documents the relationship between lithofacies and diagenetic effects within the Spraberry Formation in a qualitative manner, and offers an explanation of how diagenetic events may have affected the quality of the reservoirs.

4.4.1 Arkosic sandstones, quartz overgrowths, and pressure solution of quartz grains

Silica cement volume is independent of stratigraphic position; however, it is more common in clean and porous, very fine sandstones and coarse siltstones (Fig. 4.3). Silica cement has three distinct morphologies as follow:

1. relatively continuous overgrowths developed on framework grain surfaces;
2. isolated, small (10-15 μm), euhedral silica crystals with bases attached to framework quartz grains; and
3. microquartz (<5 μm) crystals occurring as pore lining and pore filling cement.

Warn and Sidwell (1953) stated that opal cement is the more important pore-filling material within the sandy units. They also concluded that chalcedony replaced most of the carbonates. Warn and Sidwell also pointed out that grains are closely packed with numerous contacts showing the result of limited pressure solution of grain margins. Most of these previous findings discuss samples from the southern parts of the Permian Basin. Our area of work is located approximately 40 to 50 miles to the north. Some differences among the areas are to be expected. Little opal or chalcedony are seen in samples used in this study. Also, feldspar is an important constituent. Source rocks and diagenetic history vary somewhat; however, the overall fine-grained nature of the Spraberry, the general depositional sequences, and the basic rock composition are similar in both regions.

Quartz Overgrowths: Wilson, et al. (1994) and McBride (1989) cited the following sources of silica for quartz overgrowths:

- pressure solution of quartz and feldspars
- illitization of smectitic clays
- dissolution of quartz grains in shales and mudstones
- dissolution of siliceous microfossils or spicules
- dissolution of volcanic glass

For Spraberry sands, all of the above cases are possible sources of silica. Each case presents a different degree of possibility to have occurred. Overgrowths of quartz and feldspar within the sands probably cause little net reduction in porosity because equivalent amounts of dissolved silica account for precipitation in a closed system. This is possible for overgrowth dissolution, but not for quartz cement derived from pressure solution because such a mechanism is accompanied by considerable grain rearranging, which indeed reduces porosity substantially. In most cases, it is also difficult to define an open or closed system. Studies conducted by Heald and Renton (1966) documented a considerably greater degree of quartz cementation for finer grained, monocrystalline quartzose sands, like the Spraberry SSL-A and SSL-B (sandy, clean and porous lithofacies). Small-scale lithofacies "A" contain slightly higher average amounts of quartz overgrowths than SSL-B ("A" - 5.2%; "B" - 4.5%). The last may be due to the higher presence of cement coatings (clays and dolomite) and laminations in SSL-B that may have inhibited nucleation of quartz cement.

In the absence of pressure solution, dissolution of quartz is regarded as uncommon unless the pH of the interstitial fluids is strongly alkaline. Folk (1989) found

that quartz cements in the Spraberry Formation are much more soluble than the actual grains, perhaps due to an Al-rich basal part of the overgrowths that causes lattice distortion and enhances solubility.

In general, abundant cements in certain parts of the Spraberry Formation might have prevented quartz from being dissolved. Instead, due to the relative absence of preserving carbonate cements within the clean sands, radiolarian fossils were probably dissolved and then served as the silica source for overgrowths (Folk, 1989). This is probably why radiolaria have not been found in the clean sandstones. This idea is supported by the presence of numerous well-preserved radiolarian skeletons within early-cemented phosphate nodules and carbonate cemented layers (Folk, 1989).

Pressure solution and quartz overgrowth development are important causes of porosity loss in sandstones, and this is more pronounced with rocks rich in quartz grains (Wilson and Stanton, 1994). The typical Spraberry, very fine sandstones and siltstones match most of the accepted models for precipitation of silica cements. Burial depths greater than 7000 ft have produced enough compaction stress concentrated at points of grain-to-grain contact to create suturing and concavo-convex contacts between grains (Fig. 4.3). It is thought that solubility is increased at the grain contacts with the increase in stress. Silica liberated by dissolution can then precipitate on nearby contiguous surfaces where a lower degree of stress is present.

Bjørkum (1994) presented another hypothesis explaining that pressure might not be a significant factor in the dissolution process. Instead, diffusion transport might be controlled by the action of overpressuring. This process is probably a major source of silica for quartz overgrowths.

The presence of materials like micas and clays may enhance pressure solution within adjacent quartz grains (Thomson, 1959). Very small increases of pH at quartz-mica interfaces can produce dissolution of silica, which is caused by the preferential attraction of OH^- ions to negatively charged mica surfaces (Oelkers and others, 1992). The pH of saline pore waters adjacent to micas may increase as much as 0.6 log units (Boles and Johnson, 1983). Potassium-rich mica and illite clays are probably giving away K^+ during this process. The cleavage surfaces of micas and clays exhibit faster ionic exchange than other areas of the rock fabric. The pH change is another possible mechanism for quartz dissolution, because pH can increase with the formation of fluids rich in potassium carbonate (K_2CO_3) when potassium is released from illite clay. Subsequent precipitation of quartz might occur in areas of lower pH, accompanied by suturing of quartz grains in zones of high pressure and high pH (Fig. 4.14).

Small amounts of clays might allow the precipitation of considerable silica cement. But if the amount of clays increases to an intermediate level, this can produce sufficient grain coating to prevent cementation and porosity reduction. This process of quartz cementation is probably related to the clean sands of the Spraberry Formation, which show the highest amount of quartz cement among all lithofacies, whereas content of clay minerals remain low.

As noted above, quartz overgrowths are believed to be inhibited by clay material coating grains of quartz, thus suppressing nucleation points (Pittman et. al, 1992). Different types of coats can effectively reduce the development of quartz overgrowths, detrital or diagenetic clays being the most common (Heald and Larese, 1974). In the Spraberry Formation the sandy and cleaner units have the maximum amounts of quartz

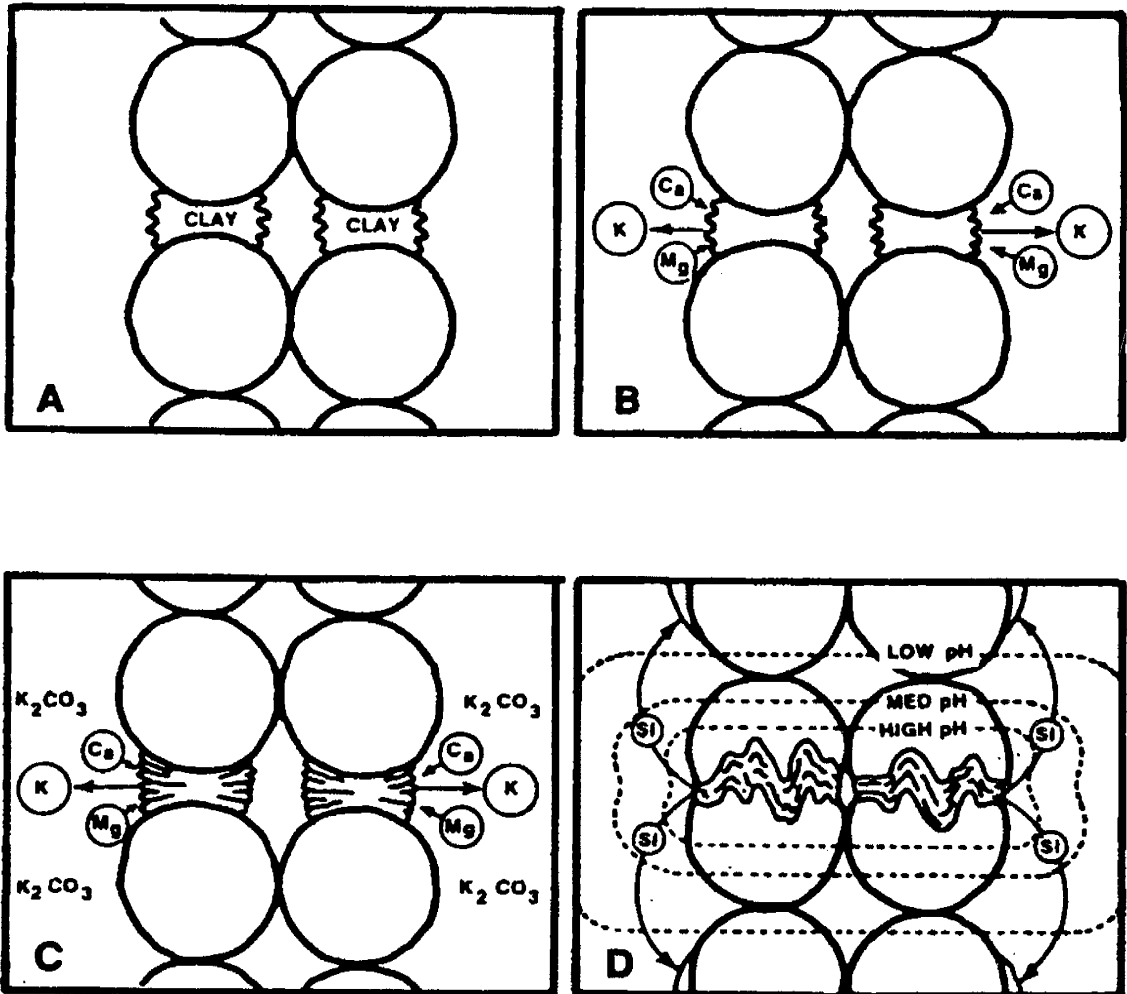


Fig. 4.14 – Model developed by Thomson (1959) for the effect of clay intercalation near quartz dissolution and precipitation. (A) Shows simplified original mineralogical distribution. (B) Exchange of K^+ by Ca^{2+} and Mg^{2+} starts next to the borders of the mica and illite sheets. (C) Cleavage surfaces exhibit faster ionic exchange. Fluid solution in the surroundings becomes richer in K_2CO_3 , thus pH rises in clay rich areas. (D) Increases in pressure promote Si^{4+} dissolution close to the high pH areas and precipitation in the regions of lower pH.

overgrowths with average values of 5% (SSL-A and SSL-B) (Table 4.1). Units with higher clay content show a gradual reduction in silica cement in general. Patchy dolomitic siltstones (SSL-D) average 4% quartz overgrowths as do shaly laminated siltstones. Muddy lithofacies such as shales and dolostones do not contain appreciable quartz overgrowths.

The Spraberry Formation contains abundant laminated and massive shales. Lesser amounts of sandstones and siltstones are intercalated with those shales. Illitization within shale layers is regarded by Mullis (1992) as a major source of silica for quartz precipitation within the sandy units. He concluded that a sandstone/mudstone model with thicknesses of 10 to 20 ft can export considerable amounts of silica by diffusion transport from mudstones to sandstones.

Similarities are found between the Mullis (1992) model and the Spraberry Formation. Extensive alteration and dissolution of feldspar is observed within the shaly facies. Pressure-temperature conditions are sufficient to fit the model. As the model predicts, precipitation of quartz occurred within the sandstones, but it is not evident in the shales, which should be the source for exporting material. Spraberry shales are particularly rich in micas and clays (sources of potassium) that can serve as catalysts in the dissolution process, as explained above (Thomson, 1959). Thicknesses of 10 to 20 ft agree with the Mullis model. Further evidence for a shale source comes from a Spraberry thin section immediately above a shale/sandstone boundary. In this thin section the abundance of quartz overgrowths decreases dramatically as the distance from that boundary increases (Martha Cather, pers. com.). This sequence of similarities is

important because they explain a consistent process for precipitation of quartz cement within Spraberry rock matrix and on fracture surfaces.

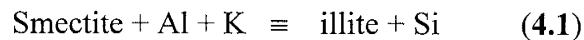
4.4.2 Clay Diagenesis

Most of the clays in the Spraberry Formation are detrital, although diagenesis must have affected the majority of the clay minerals. Diagenesis has a different effect in the argillaceous facies than in the cleaner sandstones and siltstones (Fig. 4.6). Burial diagenesis for clays in sandstones and shales differ due to differences in starting materials, rock porosity and permeability, and level of compaction. Clay detritus in shales is related to the clay mineralogy of the source area. The authigenic transformation of clays in the sands and shales depends on how much the sediments have been affected by time, temperature, and pressure during burial. Usually, clay sediments exposed to considerable amounts of overburden pressure and temperature suffer total transformation of their lattice structure (George Austin, pers. com.). Commonly, chemical composition remains the same, but the pattern of ordering of the clay lattice increases toward more crystalline clay. The increase of lattice crystallinity is a result of rearrangement of the different atoms of oxygen and silicon in a single tetrahedron and/or rearrangement of a whole layer of tetrahedral cells. Increase in crystallinity level is also accompanied by the reordering of the different stacked layers of tetrahedral.

Spraberry siltstones and very fine sandstones with moderate to high porosity show several different modes of clay mineral occurrence. Fluids carrying dissolved detrital clays (mechanical infiltration) were probably primarily infiltrated during early shallow stages of burial in the Spraberry Formation. Also, neoformed clays from sources

outside of the system (i.e. shales) precipitate within the sandstones. The process of alteration of feldspar may also have produce clay minerals within the Spraberry sandstones and siltstones.

A trend of disappearance of kaolinite and smectite, and appearance of chlorite and illite, has been commonly observed with a gradual increase in burial depth, approaching the chlorite and muscovite mica mineralogy of greenschist (Eslinger and Pevear, 1988). Given the conditions of burial depth, temperature, pressure, time and clay assemblage in the Spraberry Formation, the above sequence of events is probably relevant. Both shale and sandstones present this general trend of illitization of precursor clay minerals, summarized with the following equation from Hower et al., (1976):



Alteration and dissolution of feldspar is very common in the Spraberry Formation, especially in the argillaceous lithofacies. In part of the argillaceous samples, it is difficult to determine whether the clay matrix is originally detrital or if it formed as the result of alteration of the detrital feldspar grains. Houde (1979) found that fresh and altered plagioclase feldspar commonly occurs in the Spraberry Formation, with the altered variety being more common. He said that the feldspar alteration probably turned into formation of illite and sericite clays. The X-ray diffraction data (Table 4.2) shows the dominant presence of illite, but no sericite has been detected.

In order to assess the significance of illitization processes, it is necessary to understand the effect of paleotemperatures during the burial history of the Spraberry Formation. Some data on paleotemperatures for the Spraberry Formation have been

obtained in the past. Houde (1979) includes an investigation with a very thorough analysis of source bed geochemistry of shales in the Spraberry Formation.

Houde (1979) calculated temperatures from the present geothermal gradient of the area, which indicate that the minimum temperature to which the Spraberry has been exposed ranges from at least 63°C up to approximately 77°C close to the base of the core he studied. Also, his kerogen coloration data agrees well with the previous geothermal gradient calculated temperatures. These data from the geothermal gradient and kerogen coloration strongly suggest that the Spraberry was exposed to temperatures at which initial generation of oil begins. Hound (1979) suggested that these temperatures could have been even higher during the end of the Paleozoic due to orogenic activity. Ranges of vitrinite reflectance data presented by Dutton (1980) cover temperatures between 60-65°C. These various temperature estimations are dependent on the length of time the rocks and organics have been exposed to a given temperature. Organic matter techniques are more accurate to estimate level of oil maturation (oil window) rather than indicate maximum paleotemperature exposure. This means that more or less how mature rocks are can be estimated more accurately than to obtain precise values of paleotemperature exposure. Similar level of organic maturation can be achieved at lower temperatures over long periods of time and also at higher temperatures over shorter periods of time. For this reason, and until better data is available, the temperature ranges shown above should be considered in view of the accuracy of the methods used to estimate them. The following analysis will explain how these temperatures are related to the illitization process of Spraberry clays.

In general, the illitization reaction appears to occur by successive transformations within the mixlayer illite/smectite toward increasing ordering. The process involves either: (1) the transformation of smectite layers accompanied by the uptake of potassium and aluminum or (2) the neoformation of illite (Eslinger, et al. 1988). When aluminum is inserted in the tetrahedral lattice, the layer charge increases and allows potassium to be fixed in the interlayer position. Eslinger et al. (1988) described how neoformation requires the dissolution of smectite and other phases, and the precipitation of thin illite crystals, which have smectite-like swelling interfaces. The process of neoformation is the most probable one for clays formed in the porous clean sandstones and siltstones of the lithofacies "A" and "B".

In order to understand the significance of the process of diagenesis for clays in the Spraberry Formation, first we have to take a brief look at the possible burial diagenesis of the type of clay assemblage found in the upper Spraberry Formation. Jadgozinski (1949) originally introduced a classification of different levels of ordering for successive combinations or stacking of layers of illite and smectite. Each species of clay mineral has a different order of stacking the individual layers of clay, and each pattern corresponds to a different specific clay polytype. In other words, each clay species can present several polytypes. Because Spraberry clays are dominantly illite with minor amounts of smectite, in this study, interest is focused on the various polytype arrangements for mixed-layer illite/smectite.

The terminology commonly used is based on the term Reichweit ("the reach back"; Moor and Reynolds, 1989), presenting ordered levels $R=0$, $R=1$ and so on for the distinct stacking patterns. The general burial sequence of ordering starts with a shallow-

depth, smectite-rich, random pattern of stacking layers that corresponds to I/S R=0. Illite content in the I/S interlayer and order of stacking layers increases successively with deeper burial and higher temperature (Fig. 4.15). The following is the generalized sequence of increasing ordering that has often been noted in Gulf Coast sandstones/shale sequences:

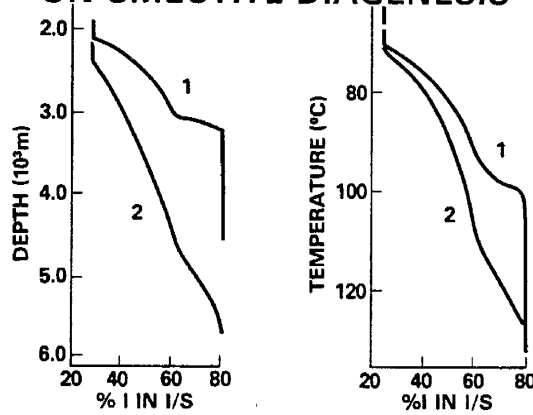
$$\begin{aligned} \text{Smectite} &\equiv \text{I/S random (R=0)} \equiv \text{I/S ordered (R=1)} \\ &\equiv \text{I/S ordered (R=3)} \equiv \text{illite (1M)} \equiv \text{mica (2M)} \end{aligned} \quad (4.2)$$

(Eslinger et al., 1988)

A mixed-layer I/S with illite content from 0 to 60% is considered random R=0. If the percentage of illite ranges from 65 to 85%, then it is ordered R=1, and those with 85-100% percent illite are ordered R=3 (Eslinger, et al., 1988). At a temperature of 60 to 80°C the smectite-dominated composition of random ordered mix-layers I/S R=0 begins changing into a more ordered type with a parallel increase in the amount of illite. At about 10,000 ft of burial depth and approximately 100 °C with the illite/smectite ratio of about 35:63, it commonly suffers an abrupt change from the random stacking pattern to the ordered R=1 (Hoffman and Hower, 1979; Moore, 1989). This specific interval of illitization from R=0 to R=1 might be directly related to the diagenesis of Spraberry clays. This transition may be more or less drastic from one well to another.

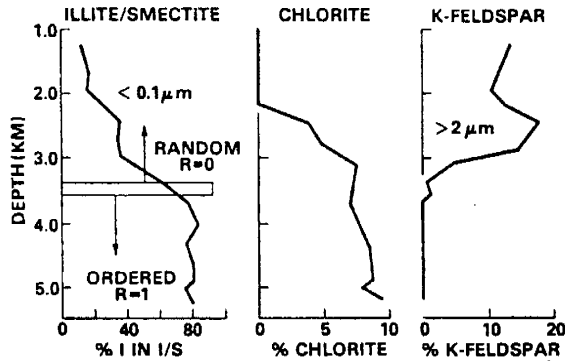
Hoffman and Hower (1979) proposed a general time-temperature general model for the illitization of smectite with increasing depth (Fig 4.15), which is probably relevant for the Spraberry clays. This model is applicable to most geologic and petroleum studies of sedimentary rocks and basins of Miocene age or older, and relates to timing of oil maturation. The Spraberry Formation is Permian (Adams, 1951). The temperature and

DEPTH/TEMPERATURE CONTROLS ON SMECTITE DIAGENESIS



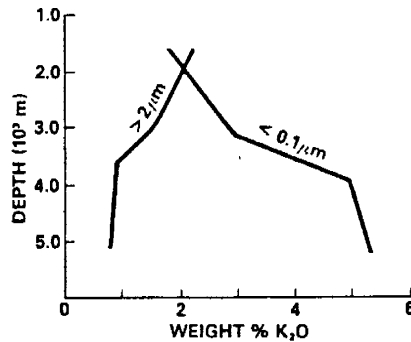
HOWER, (1981)

MINERALOGICAL CHANGES RESULTING FROM SHALE DIAGENESIS



HOWER, (1981)

TRANSFER OF POTASSIUM TO CLAY FRACTION



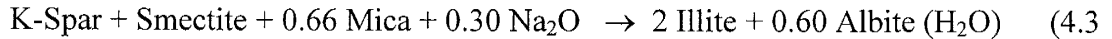
HOWER, (1981)

Fig. 4.15 – The Hower model (1981) for illitization (above) has a number of similarities with the diagenetic characteristics observed in the Spraberry Formation.

age information shown above suggest that the clays in the Spraberry Formation should be around the smectite rich to R=1 (I/S) region. However, assemblages of clays that we have found (Table 4.2) show very small amounts of smectite and I/S mixlayer. These clay assemblages, with significantly small amounts of expandable layers (smectite), are supposed to occur at greater depths and higher temperatures (R=3). As no further studies of polytype orders have been performed, this type of research would be most useful. Without more complete information on polytype assemblages, clay mineralogy, and temperature data from younger and older rocks within the Spraberry stratigraphic sequence, it is difficult to properly interpret illitization events.

Several observations can be made that may relate the clay mineralogy of Spraberry sediments to diagenetic alteration of detrital clays caused by an increase in burial depth and temperature. Similarities are found with interbedded shales and sandstones from the Gulf Coast Tertiary sediments with an open system during diagenesis (Boles et al., 1979; Eslinger et al., 1988). Following deposition, Spraberry sediments contained abundant clay and organic matter. Such deposits commonly are highly smectitic (Eslinger, et al., 1988), giving an original composition for diagenetic transformations that occurred with subsequent burial. Potassium necessary for illitization was available from dissolution of K-feldspar and detrital mica that are abundant in the Spraberry Formation. Shales are good sources of potassium released during the compaction and migration of great amounts of fluid into more porous sandstones. The transformation of smectites and dissolution of feldspar both provide sources for silica that give way to substantial quartz overgrowth precipitation. These are trends that appear to match the Spraberry diagenetic sequence.

An additional trend is found in the albitization of plagioclase. Microprobe and SEM analysis have documented an unusual concentration of Na-plagioclase (Cather, pers. com.). The following reaction given by Lynch (1986) illustrates the production of albite and illite from an original rock composition containing smectite, K-spar and mica:



Eslinger et al. (1988) noted that in the coarser size fractions of shales, K-feldspar is either dissolved or albitized at depths typically below about 8,000-10,000 ft. Depths for samples in the present study are somewhat shallower than those proposed by Eslinger.

The temperatures found in the Spraberry Formation are considered high enough for the first stage of ordering polytypes (from smectite to random R=0 I/S and approaching the ordered R=1). However, the assemblages of clays found in the current study with dominant amounts of illite and chlorites and absence of many expandable layers, better resembles a polytype group of higher temperatures (R=1). It seems that the Spraberry system closely fits the Hower model with trends for illite and chlorite contain, potassium dissolution, amount of heat and depth (Fig. 4.15). However, the question still remains of exactly where the Hower model and the Spraberry illitization process coincide. Pursuing XRD analysis of unoriented samples and examination of samples of younger and older strata should solve this ambiguity.

It is important to realize that the original composition of sediments at the time of deposition is not known. For instance, we do not have precise information for the amounts of smectite, illite and feldspar that were originally deposited within the shale beds. This information is crucial because the determination of a particular diagenetic

course is based on this composition. The following are a number of factors and hypotheses that should be taken in consideration.

- 1) The original amount of smectite might have been small enough so that high amounts of potassium from the different sources described above have been added to most of the smectite present, producing transformation of its lattice to become illite. But these types of shale/sand sediments are typically characterized by presenting high amounts of smectitic clays during deposition (Eslinger et al., 1988). For this reason it is difficult to expect that smectite was not overwhelmingly present in the shale-dominant facies of the Spraberry Formation and other horizons within the basin.
- 2) Reaction kinetics are probably a major factor in diagenesis of Spraberry clays. Reaction kinetics are believed to be important in the illitization process, but have not been studied in detail in the Spraberry Formation.
- 3) The fact that hydrocarbons actually exist in these deep marine, low permeability sequences suggests that the rocks have been exposed to heating and time sufficient to produce illitization. It is far more difficult to expect hydrocarbon migration from deeper units, considering how slowly fluids move in these extremely low permeability rocks (0.1 md, average).

Clay mineral reactions should be studied within the whole geological context of the basin. Besides original composition of detrital clay assemblages at paleotemperatures, potassium availability, time, and relationship with hydrocarbon generation, the hydrological regimes and structural evolution also should be considered. In summary, an overall

understanding of the basin geology has to be reached to thoroughly understand clay diagenesis.

4.4.3 Hydrocarbon Emplacement and Relation to Clay Diagenesis

An interesting relationship exists between the progressive increase in crystallinity (lattice order) and amount of illite with the simultaneous thermal maturation of hydrocarbons in potential source rocks. The term “catagenesis” is used by petroleum geochemists for the transformation of kerogen and humic material into oil and gas during reactions between temperatures from 50 to 200°C (Eslinger and Pevear, 1988). This range seems to parallel the abrupt transformation of illite/smectite sequences into the ordered R=1 polytype. Eslinger *et al.*, (1988) theorized that clays might act as catalysts that speed up the cracking or decarboxylation that occur during hydrocarbon generation.

The relation between maturation of oil and alteration of clays is still not well understood. There is a temperature range from approximately 100°C (abrupt change to the ordered rectorite type of I/S; R=1) to 175°C where a higher stage of ordering of I/S is produced (R≥3). The “oil window”, or temperature range where hydrocarbon maturation occurs (65° to 175°) roughly coincides with the rectorite range of illitization discussed above. The temperature of oil maturation is above the random I/S (R=0). But this is yet just below the range of temperature for a very ordered “Kalkberg” (I/S, R≥3) and closely coincides with the rectorite range (I/S, R=1) of temperatures. Spraberry rocks coincide with the typical assemblage of clays for ordered polytypes; however, possible Spraberry paleo temperatures found by others (from 60° to 77°C; Houde, 1979; Dutton, 1980) may only reach the initial part of the oil maturation stage. These temperatures are not enough to

account for the lack of expandable smectite layers noted in the Spraberry, unless the time and kinetics with rocks of Permian age have worked in favor of the illitization processes. Another possibility is that an unusually low amount of smectite was present initially in the Spraberry Formation.

Dutton (1980) regarded Spraberry organic matter as mostly amorphous material containing high amounts of lipids, probably derived from algae or from Radiolaria. This is an important point since Radiolaria were very common in Spraberry sediments (Folk, 1989; Cather, pers. com.) and may have served as a silica source for quartz cement and also ultimate hydrocarbon generation.

A source rock, an impermeable seal, and a porous rock are needed to form a reservoir trap containing hydrocarbons. The Spraberry sequence of shales, porous sandstones and siltstones form a good seal/reservoir system. Spraberry shales are probably good hydrocarbon source rocks (Houde, 1979). Many arguments in the literature exist on the idea that as a post-trapping effect, maturation of hydrocarbons ceases and most diagenetic reactions are retarded (Wilson et al., 1994). In turn, further precipitation of cements and clays is discontinued. This is important because the migration of oil to the sandy units of the Spraberry Formation might be considered as a time limit for diagenetic reactions. Oil and gas are non-conductive with respect to most ions present in formation waters, thus the newly immigrated fluids impede the diffusion of ions and pore water movement (Wilson, et al., 1994). Also, there is an increase in tortuosity throughout the thin pellicular rim of pore waters that remain as non-removable or connate water after hydrocarbons have invaded the reservoir rocks. This rim of water surrounding grains makes it still more difficult for diagenetic alteration to continue. Much disagreement is still found

between investigators on this point. For example, there are suggestions from MacGowan and others (1990) that aluminum has a higher solubility in liquid hydrocarbons than in water.

4.4.4 Pyrite Cement

Authigenic pyrite occurs in small quantities in all lithologies and is especially abundant in shales and shaly siltstones. Pyrite has both framboidal and octahedral morphologies. Pyrite probably formed within basinal deposits at the interface between the sediments and anoxic, sulfate-bearing seawaters through the activity of sulfate reducing bacteria within organic matter (Krumbein et al., 1952; Gautier, 1985).

4.4.5 Carbonate Diagenesis

Most of the carbonates found in the upper Spraberry Formation are detrital. Dolomitization seems to have occurred due to the effect of burial. The dolomitic matrix varies from micritic to sparry matrix as the result of replacement of carbonate mud. The origin of ferroan dolomite is probably due to recrystallization and replacement of preexisting dolomite and calcite.

The authigenic character of most dolomite is quite clear when observed as large patches of poikilotopic cement and replacement of detrital grains (Fig. 4.7). Brief descriptions have been given by Folk (1989) of poikilotopic dolomite, and other carbonate cements (ferroan dolomite, calcite, ankerite) with variable iron content, that were probably formed prior to much compaction.

It is possible that dolomitic sediments were transported from the arid environments of mud-rich sabkha and salt pan. These sediments probably prograded to the shelf margins and throughout channels to the marine basin floor. The last combine the sabkha model of dolomitization and Handford's (1981) carbonate-dominated system of deposition presented in Chapter 1. The chemistry of waters incorporated into the sediments during burial played a major role in the creation of the proper environment for dolomitization (Houde, 1979). Houde suggested that dense magnesium-rich brines formed in the shelves surrounding the basin as the result of intense evaporation and the precipitation of calcite and evaporitic minerals (CaSO_4). However, this mechanism does not always work. Saline density currents subsequently transported these magnesium and iron-rich fluids to the deep marine basin, where they precipitated as dolomite and other iron-rich carbonate cements.

Ferroan dolomite cannot be synthesized at low temperatures. Thus, it is considered to be of high-temp authigenic origin (Katz, 1971). A possible explanation for precipitation of ferroan dolomite is that poorly circulated interstitial water in the sediments created an anaerobic environment with the increase in burial depth. Progressively, the anaerobic environment facilitated the reduction of ferric iron (Fe^{3+}) into ferrous iron (Fe^{2+}). A possible source of iron and magnesium is the conversion of smectite to illite (Boles and Franks, 1979) within the interbedded argillaceous facies of the Spraberry or surrounding formations.

In addition, SEM, microprobe, cathodoluminescence, and XRD analysis show that several generations of carbonate cement are present (Cather, 1998). At least three phases of carbonate are present in some 1U samples, with dolomite being the first-formed

phase followed by ankerite, then a ferroan dolomite (Cather, 1998). Ferroan dolomite is the most common phase seen within the 1U fractures (Fig. 4.7). In general it appears possible that original sediments deposited in the basin floor were mostly calcite and dolomite muds derived from the sabkha plains surrounding the shelf, or at least these were sediments and fluids rich in magnesium and iron. Evidence of detrital origin are observed on faintly laminated cores. Such large amount of fine carbonate material can be originated only during sediment deposition. Further dolomitization probably occurred with the gradual increase in burial temperature. A later stage of ferroan dolomitization occurred when the temperatures were sufficiently elevated.

4.4.6 Origin and Mineralization of Spraberry Fractures

Fracturing mechanism: In this section a structural diagenetic model is presented for the fracturing of the Spraberry Formation. Macro-observations of core samples, microscopic analysis of thin sections, and information extracted from XRD and SEM analysis of clays have helped construct a history of burial, compaction, lithostatic pressure buildup for vertical and horizontal stresses, pore pressure increase, reduction of unconfinement, and fracturing. Fractures in the Spraberry Formation are extensional, which means that they formed by opening perpendicular to the fracture strike (Lorenz, 1997). In other words, Spraberry fractures do not show evidence of shear stress. Only a process of compaction stress could form this type of extensional fracture patterns (Lorenz et al., 1991).

A gradual increase in burial depth increased compaction, pore pressure, and temperature. The clay-rich Spraberry Formation, with only a minor amount of fine

interbedded sands and siltstones, provided a favorable environment for overpressuring. Clay sediments mixed with organic matter are characterized by having the highest initial porosity and contain very large amounts of fluid. Burial compaction and diagenesis of these types of sediments usually results in significant loss of porosity within the clay and organic rich sediments (e.g., shales) accompanied by a tremendous loss of fluids (Miall, 1990). At the same time that the principal vertical stresses are being increased, the pore pressure mainly within the sandy part of the formation is expected to increase due to the migration of large amount of fluids into the sands (Miall, 1990). Pressure solution features, typical of overpressured sands (McBride, 1989; Boggs, 1995), were found during petrographic analysis (Fig. 4.3). High pore pressure probably caused the necessary reduction of principal effective stresses to a level at which enough unconfinement (Lorenz et al., 1991) was created and fractures were produced. Lorenz et al. (1991) explains the unconfinement effect showing how regional fracturing can form when a substantial increase in pore pressure acts as an opposite force to the principal compressive stresses (Figs. 4.16 and 4.17). The increased pore pressure increases the brittleness of the rock. He shows that an effect of unconfinement is produced by adequate differential stress created between the vertical stress (σ_1 = major principal stress) and the smaller horizontal stresses (σ_3 = smaller principal stress). Stress anisotropy between the two horizontal minimum stresses (σ_2 and σ_3) is also needed; then, fractures will propagate preferentially parallel to the plane formed by the major vertical (σ_1) stress and the intermediate horizontal (σ_2) stress directions. Then the rock is said to have reached the point of failure. For this to occur a source of compressive regional stress is needed that should be located in the same direction as the fracture orientation. The Laramide

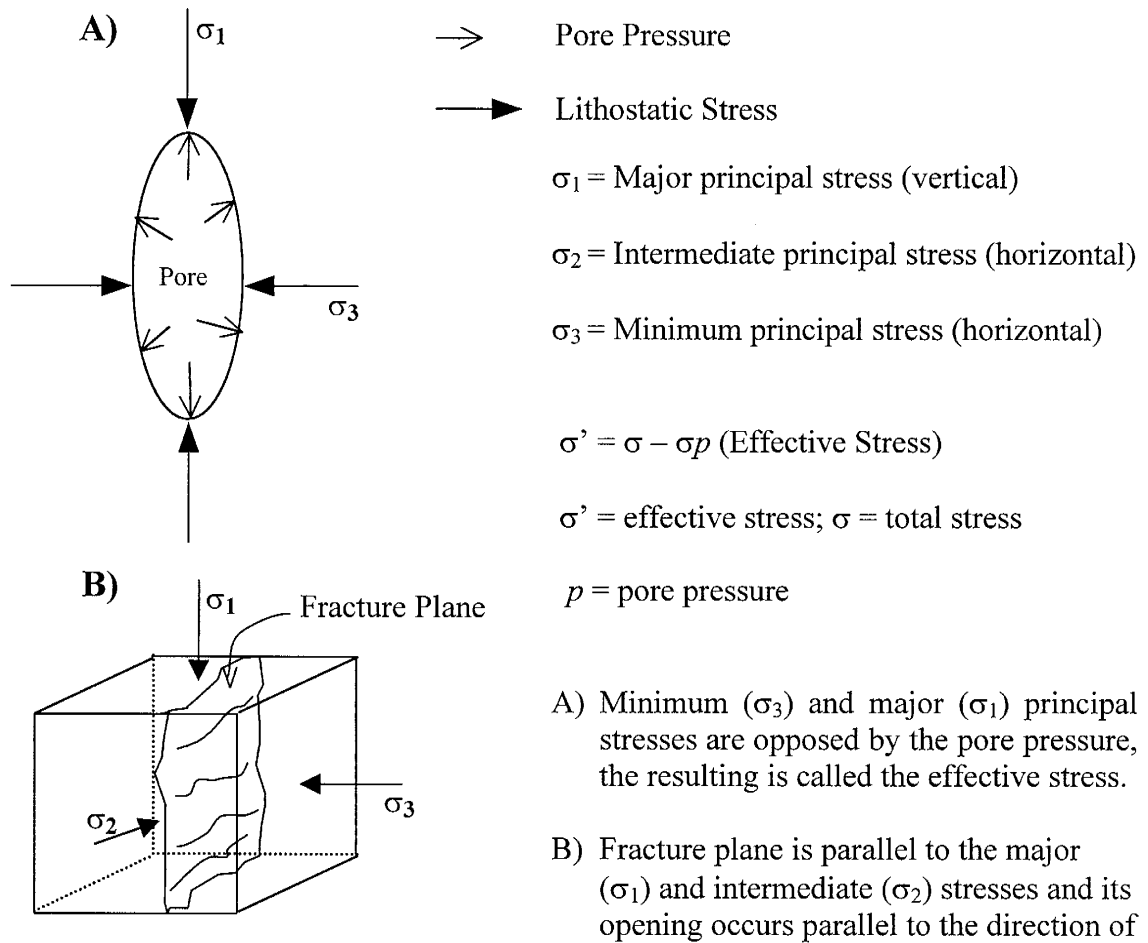


Fig. 4.16 – The effective stress at depth is the sum of the external stresses minus the pore pressure. See fracture plane direction parallel to σ_1 and σ_2 .

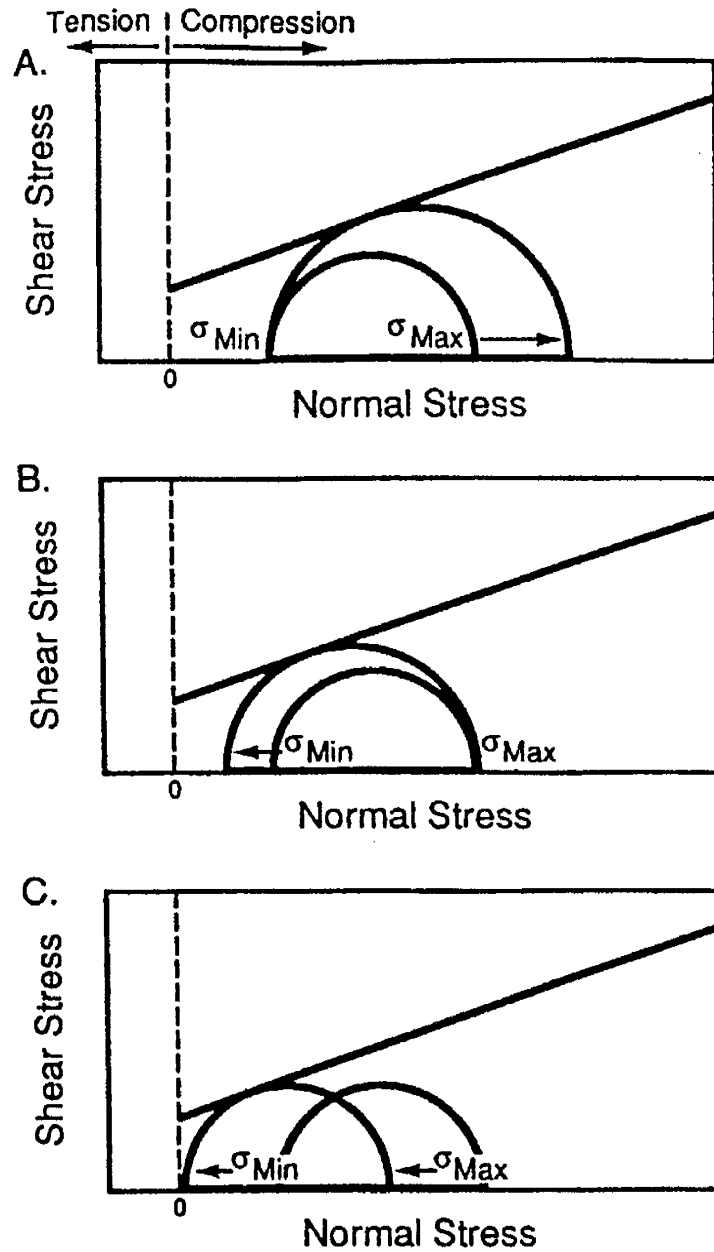


Fig. 4.17 – Three possible models for regional fracturing. (A) An increase in the maximum stress enlarges the stress circle to where it touches the yield envelope. (B) A decrease in the minimum stress also enlarges the stress circle reaching the point of failure. (C) An increase in pore pressure shifts the position of the stress circle to where it may touch the yield envelope (compiled from Lorenz, Teufel, and Warpinski, 1991)

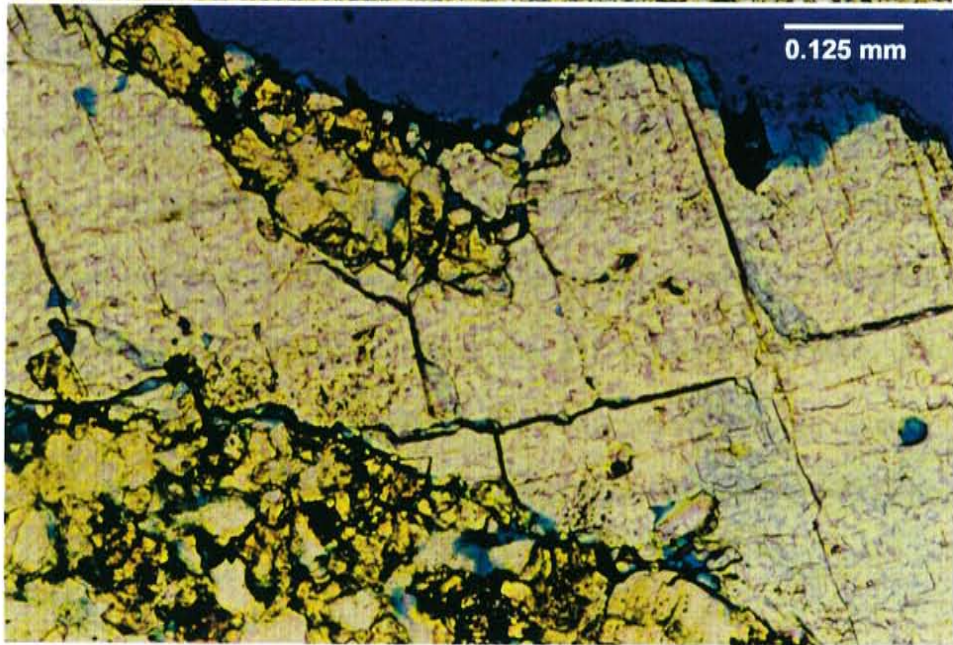
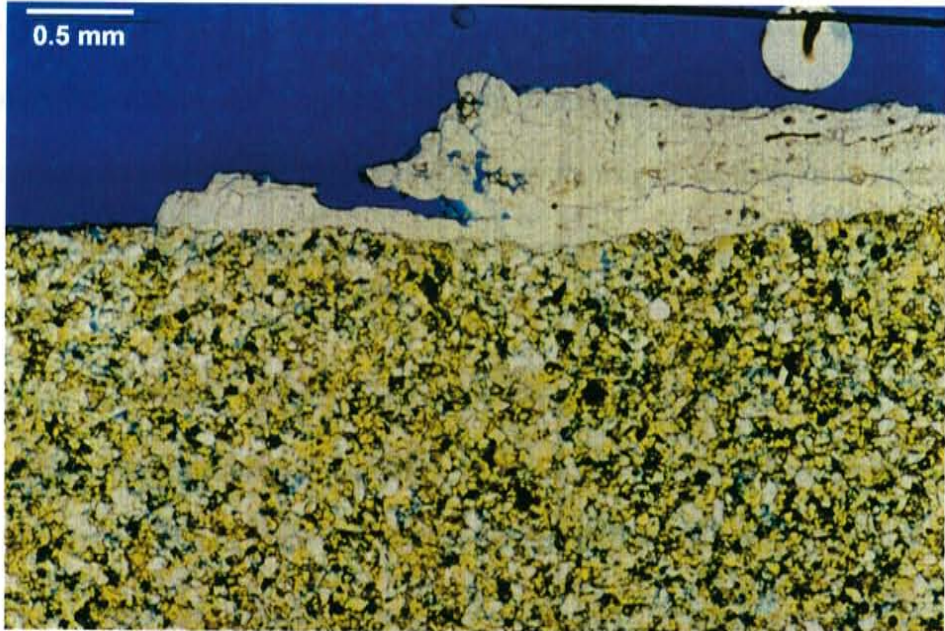
orogeny is regarded as the only tectonic event that could have possibly supplied the horizontal compressive stress necessary for fracturing in the Spraberry Formation (Winfree, 1995; Cherney, 1998).

Winfree (1995) presented an interesting study with evidence for the area's fracturing that is interpreted to occur through a process of folding and also regional fracturing with parallel orientation. Because the orientation of the folding and the regional fractures is similarly northeast trending, these are probably related to the Laramide deformation. The Laramide orogeny during the end of the Cretaceous until the Eocene is the only regional compressive tectonic event that occurred after the Paleozoic in west Texas (Horak, 1985; Winfree, 1995). Winfree (1995) explained that the folds appear to be the result of compressional uplift of faulted-bounded basement blocks, and that circumstantial evidence suggests that regional fractures, folding, and fractures related to the folding occurred simultaneously. Maximum burial at the end of the Cretaceous (Horak, 1985) possibly coincided with the peak generation of hydrocarbons, higher pore pressure, and the northeast compressive stress produced by the Laramide Orogeny.

Fracture mineralization: Calcite, barite, and quartz precipitated within the fractures (Saleta et al., 1996; Cather et al., 1997). Figure 4.18 shows barite cement on a fracture surface for the Shackelford 138A core (1U unit, vertical well). Barite crystals can partly to completely cover the surfaces of 1U fractures and may be responsible for reducing the crossflow of fluids and gas between rock matrix and fracture porosity (Cather et al., 1997). Cather and Schechter (1997) observed quartz crystals on fracture surfaces. She also suggested that the presence of abundant euhedrally-terminated quartz helped to keep fractures open during certain periods of diagenesis. Indeed, although

Fig. 4.18 – Two Photomicrographs showing barite mineralization on fracture surface.

This is a thin-section sample from the Shackelford 138A well, 7088.8 ft depth. Naturally fractured interval, very fine sandstone and siltstone (SSL-A and SSL-B). Notice the large dimensions of barite crystals.



quartz crystals seem insignificant in terms of abundance and size, they provide numerous asperities that may prevent these fractures from closing even at reservoir pressure conditions.

Horizontal cores from upper Spraberry 1U and 5U units provided invaluable data on fracture orientation, spacing, aperture, and mineralization (Cather et al., 1997); however, many questions still remain concerning the origins of the various fracture sets, the relationship of the fracture network to rock matrix, and its effect on oil production. At least three sets of fractures occur within the upper and middle Spraberry cores. These sets have distinct orientations, spacing, mineralization, distribution with respect to lithology, and surface characteristics (Cather et al., 1997). Cather used scanning cathodoluminescence microscopy to analyze cements in the fractures and in the rock matrix. Non-luminescent quartz cement is seen both within fractures and rock matrix showing similar appearance, which suggests that fracturing and precipitation of quartz occurred at the same time. The same type of analysis is drawn from microprobe data (Cather et al., 1997) for ferroan dolomite. These data show that ferroan dolomite cement in the fractures and in rock matrix have similar compositions. Precipitation of barite within 1U fractures and possibly within the 5U fractures followed. Microscopic examination of 1U fracture surfaces shows that barite occurs in large crystals (1mm or more) with very smooth tabular faces. Cather also observed that barite was formed at a later time, as there is little or no barite within the rock matrix.

4.4.7 PARAGENESIS

Upper Spraberry sandstones have been subjected to several stages of diagenesis. Diagenesis has resulted in both the occlusion and, more rarely, the enhancement of porosity. The relative timing of the various diagenetic events is estimated by examination of the spatial relationship of cements in thin section or with the scanning electron microscope. However, accurate superposition of one mineral component on another, or the total or partial absence of a detrital grain or cement in these very fine-grained rocks are very difficult to determine. The following diagenetic sequence (Fig. 4.19) has been determined for upper Spraberry rocks examined in this study.

1. Deposition of sediments with initial primary intergranular porosity. Some interstitial space occurred within more porous sands filled by detrital clays, probably during early stages of post depositional infiltration of fines. However, there is no conclusive evidence that shows that well defined illite is not the product of late infiltration of clays during the migration of large amounts of brines from the argillaceous lithofacies. Also another possibility is that early infiltration of smectitic clays would then be altered to illite.
2. Basinal sediments that were deposited in anoxic bottom-water conditions experienced varying degrees of pyrite precipitation due to the production of H_2S by sulfate-reducing bacteria at the sediment-seawater interface prior to burial (Krumbein et al., 1952; Gautier, 1985).
3. Shallow burial. Minor adjustments in grain packing occurred in response to burial loading. Some rocks, particularly clean sandstones of submarine channel origin, were subject to an early stage of silica overgrowth cementation helped by pore space

Diagenetic Event	Early	Late
Infiltration of Fines	---	
Pyrite	---	
Compaction	—————	—————
Quartz Overgrowths	—————	-----
Fluid Migration	—————	-----
Calcite Cement	———	
Dolomitization	-----	
Ferroan Dolomite		—————
Illitization		—————
Chlorite		-----
Pressure Solution		—————
Oil Window		—————
Dissolution		—————
Fracture Formation		—————
Fracture Cements:		
Quartz		———
Ferroan Dolomite		———
Barite		———

Fig. 4.19 – Generalized paragenetic sequence for the Upper Spraberry Formation

subject to an early stage of silica overgrowth cementation helped by pore space originally available (Figs. 4.3-C, D, E and F). Quartz overgrowth must have preceded the precipitation of the calcite cements overlying them (Fig. 4.7-B). Although volumetrically insignificant in controlling reservoir quality variations, these overgrowths aided in arresting compactional effects and preservation of porosity and permeability during later stages of compaction.

4. Fluid migration from argillaceous and organic rich lithofacies to the more resistant sandstones. Compressional forces tend to affect quartz-rich composition to a lesser extent than clay rich lithofacies (ductile). This stage of fluid migration is much earlier than maturation of hydrocarbons.
5. Precipitation of calcite cement. Figure 4.7-B shows calcite cement (red-stained) covering quartz grains and quartz overgrowths. This is probably an early diagenetic event after precipitation of quartz cement. There is little evidence of early quartz cement in the Spraberry Formation. McBride (1989) cited as possible sources of early quartz cement the decomposition of feldspars and silica precipitated from descending water associated with silicate minerals in the zone of weathering.
6. The majority of the carbonates appear to be detrital, although burial dolomitization has occurred. The poikilopic texture of dolomite cement (Fig. 4.11) suggests the authigenic effect (burial) on most of the dolomite. Ferroan dolomite is probably of authigenic origin as it cannot be synthesized at low temperatures (Katz, 1971). This suggests that considerably increased burial temperatures have produced the conditions for ferroan dolomite nucleating precursor dolomite crystals (Fig. 4.7) or other grain types. However, better data are needed in order to further constrain the timing of

formation of these cements. Cather (1997) has shown results from SEM, microprobe, cathodoluminescence, and XRD analysis with samples from horizontal cores. Four phases of carbonate are present with calcite being the first-formed phase followed by dolomite, ankerite, and ferroan dolomite.

7. Most of the illite probably originated from late alteration of detrital feldspar and smectite. Most of the clays are part of argillaceous laminae rich in organic matter. These are believed to be originally smectitic sediment masses because shale deposition is commonly rich in smectite and detrital illite is more rare in these types of sediments (Eslinger, et al., 1988). Certainly some of the illite must have been present during deposition but the considerable lack of smectite clay in the samples studied can only be explained by illitization. Because the original composition of the sediments is not known, it is necessary to perform distribution studies of clay components along larger depth intervals. This way the timing of occurrence of the different clay materials can be determined more accurately. Figures 4.5-A and B, 4.7-E, and 4.20 suggest that quartz and dolomite cement preceded precipitation of authigenic clays (mainly illite). Late-stage precipitation of fibrous illite clay occurs on pore walls and within pore throats. Illite cement, while volumetrically insignificant, bridges pore throat openings, dramatically reducing formation permeability.
8. Chlorite is only detected in the XRD patterns. No recognizable chlorite is observed in the masses of clays in thin sections or SEM. Occurrence of chlorite is commonly more pronounced at later stages of burial diagenesis (Hower, 1981; Fig. 4.15). Most authors agree that abundance of chlorite increases as temperatures approach those of low-grade metamorphism (Boles et al., 1979). The present study shows localized

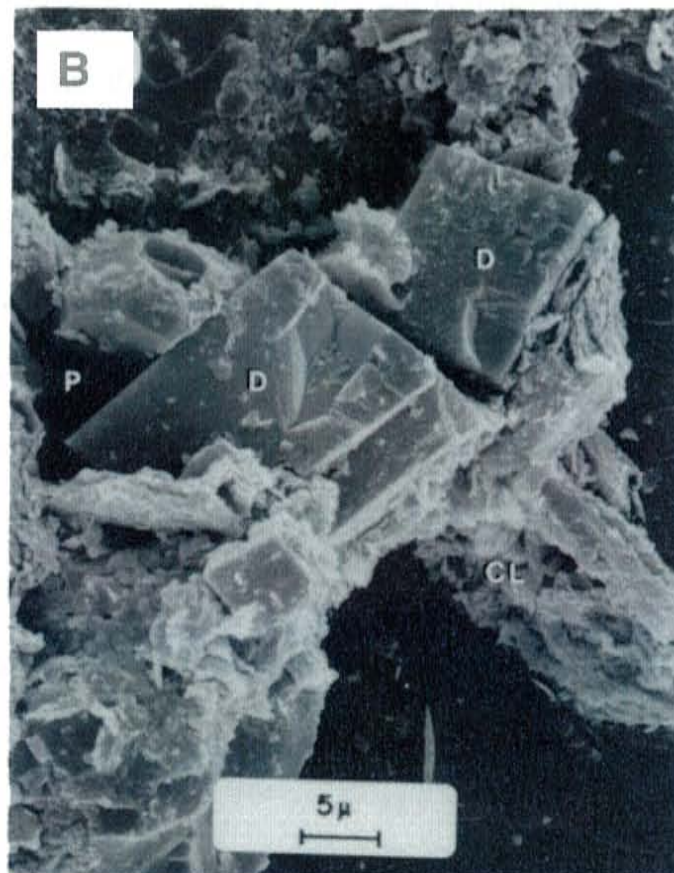
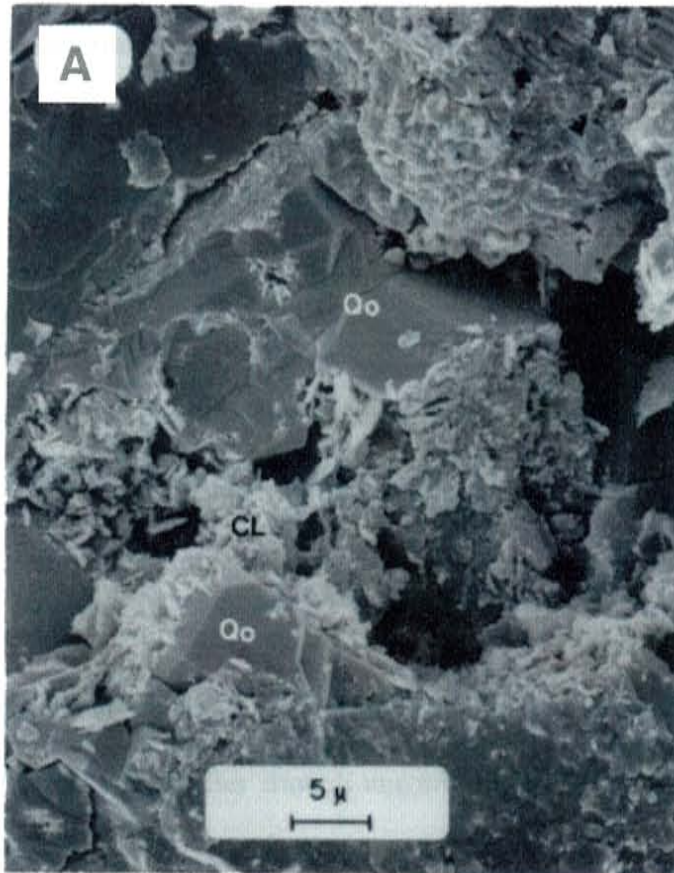
Fig. 4.20 – Photomicrographs showing diagenetic sequence for dolomite cement, quartz overgrowths and clays.

A: Quartz overgrowths (Qo) coated by clays (CL). Clays are probably illite.

Depth, ft:	7102.6	Sample No.:	SPX26
Grain Size:	58 μm	Sorting:	MW
Porosity:	7.7%	SSL:	B

B: Crystals of dolomite cement are coated by clay (probably illite).

Depth, ft:	7109.5	Sample No.:	Plug 44
Grain Size:	50 μm	Sorting:	M
Porosity:	6.3%	SSL:	B



abundance of chlorite from XRD analysis. The small chlorite amounts found are consistent with temperatures of early to intermediate stages of illitization. For this reason chlorite is interpreted as associated with the illitization process. For more accurate interpretations, distribution studies of clay components along larger depth intervals are needed.

9. After considerable burial, high lithostatic pressure among grain contacts, mainly in very fine sandstones and siltstones, produced pressure solution (Figs. 4.3-A and B).
10. Burial temperatures reach the oil window and generation of corrosive organic acids from the process of hydrocarbon maturation. These acids favor secondary porosity by dissolution of cements and grains.
11. Fracture formation occurs after enough unconfinement is produced. To produce the effect of unconfinement a considerable increase in pore pressure is necessary. The higher the pore pressure, the more strength is withdrawn from the horizontal and vertical stress; thus, the effective stress approaches the point of failure. This event is contemporaneous with late stages of quartz overgrowth and ferroan dolomite precipitation on rock matrix and on fracture surfaces (Cather, 1997).
12. Considerable amounts of barite cement precipitate on fractures (Fig. 4.18). Very small amounts of barite cement have been found on the rock matrix. Barite is considered to be of a later stage than other cements found. Barite cement on fracture walls occurred after little precipitation of other cements was taking place due to oil migration. Large barite crystals occurred on fractures surfaces favored by large fracture apertures.

CHAPTER 5

PETROPHYSICS

Rock and Fluid Flow Analysis

Assessing Reservoir Quality

Integration of geological and petrophysical data allows rock-fluid flow characterization for upper Spraberry rocks. The small-scale lithofacies (SSL) from Chapter 4 are considered here in light of the petrophysical data to define interrelations between the lithological character and the fluid flow and saturation behavior. The six small-scale lithofacies comprise the subject reservoirs, marginal reservoirs and non-reservoir rocks of the upper Spraberry Formation.

Petrophysical data from core plugs combined with thin section information is presented. One small-scale lithofacies is assigned to each core plug sample that has a thin section match. The SSL represent flow units defined as intervals of rock with unique pore geometry and mineralogical composition and are related to certain fluid flow characteristics.

Analytical techniques used to develop this research include porosity-permeability measurements of core plugs, air minipermeameter measurements on core slabs, thin section analysis, scanning electron microscope analysis of pore structures, air-mercury capillary pressure, pore body and pore throat size distributions, and GR log of each well.

Integration of results from these analytical techniques reveals that the six small-scale lithofacies (SSL) described using thin-section analyses are consistent with the petrophysical analysis shown in this section.

5.1 DESCRIPTION OF PETROPHYSICAL PROPERTIES

Four different methodologies were used to analyze petrophysical properties: 1) a computer-controlled scanning air-minipermeameter (CCSAM), (2) imbibition experiments with air, oil and synthetic brine, (3) water and oil saturation determination from core plugs using the Dean Stark method, and (4) petrophysical properties with injection of nitrogen, helium and mercury. The proposed petrophysical techniques in combination with the petrographic analysis (Chapter 4) are used to confirm and improve the conventional formation evaluation that uses GR logs.

5.1.1 Gamma Ray Log Resolution

Operators of the Spraberry oil reservoirs implement a method of using GR logs to distinguishing among shale, clay-rich siltstone and very fine sandstone units (Figs. 3.1 and 3.2) in the field. This method has provided good differentiation of lithological characteristics in many investigations (Guevara, 1988; Tyler and Gholston, 1988). Figures 5.1 and 5.2 show data from different analytical techniques (petrography and petrophysics) combined with the gamma ray log response for the cores E.T. O'Daniel 37 and Shackelford 138A. Notice the definition of reservoir units 1U and 5U.

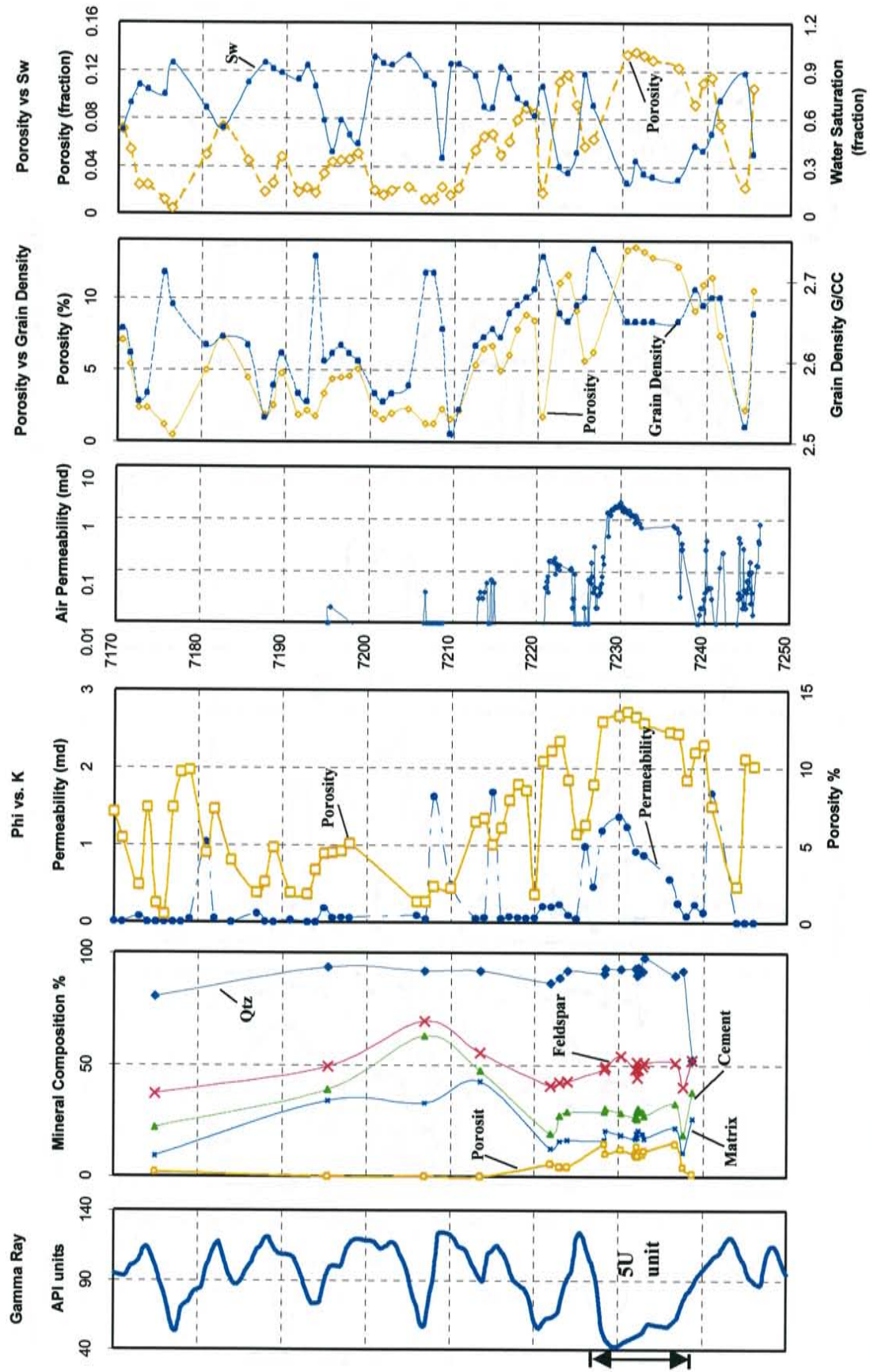


Fig. 5.1 - Core E.T. O'Daniel 37. Integration of petrographic and petrophysical data. Note the 5U unit, sandstone reservoir interval in the Upper Spraberry Formation. Heterogeneous character is well defined by most curves where sufficient sampling was included.

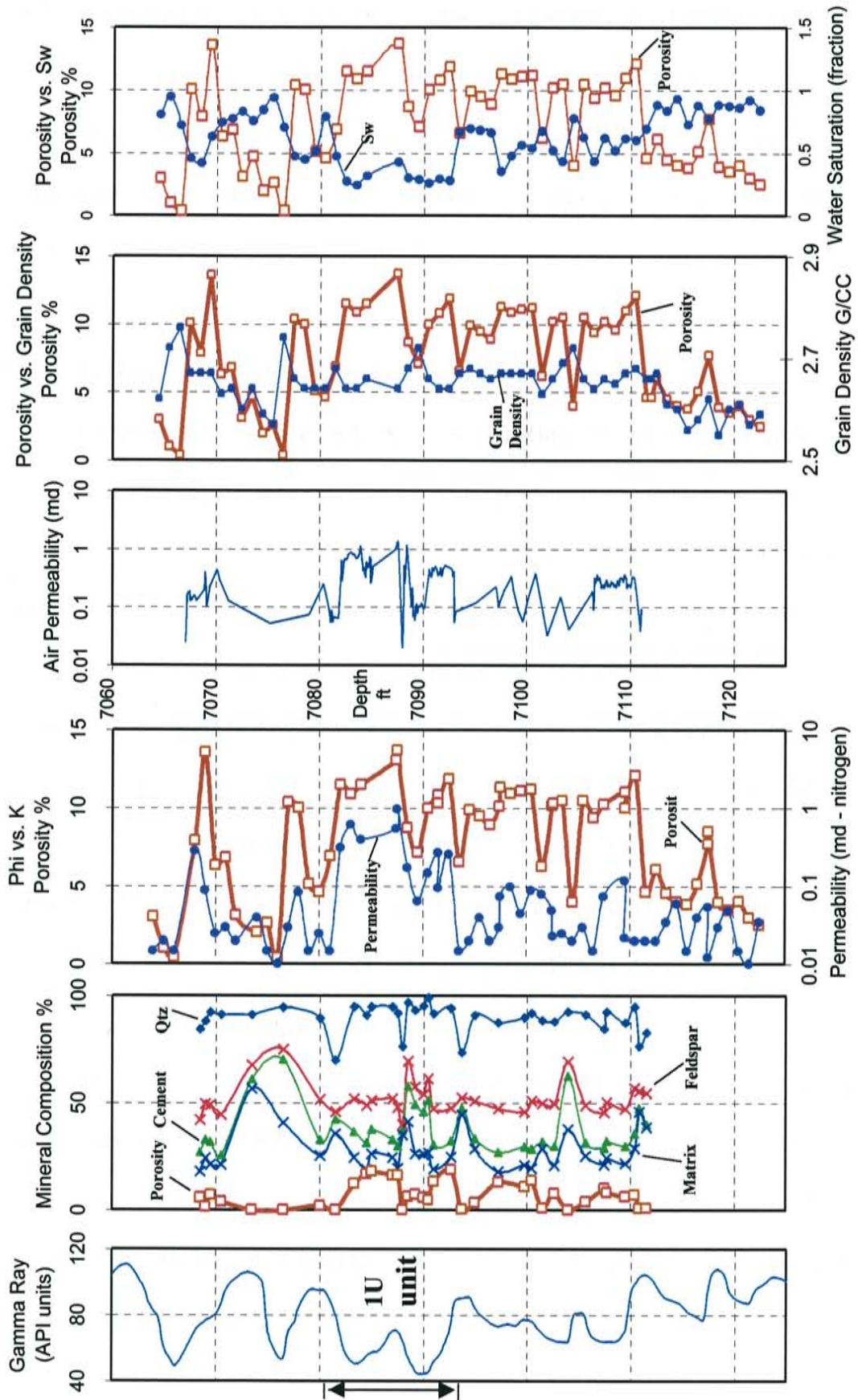


Fig. 5.2 - Core Shaekelford 138A. Petrographic and petrophysical data integration. 1U unit divided by a shale streak. Heterogeneous character as well as in Fig. 5.1 is well defined. GR curve resolution is good to describe major lithological contacts.

5.1.2 Computer-Controlled Scanning Air-Minipermeameter (CCSAM)

Figures 5.1 and 5.2 show detailed profiles of permeability measurements made at a spacing of 0.5-1.0 in. on core slabs. Although the air permeability curves show a good relationship with gamma-ray curves and core descriptions, the vertical air permeability variation is much more complex in character.

5.1.3 Permeability, Porosity, Water Saturation, Grain Density and Capillary Pressure from Flow-Through Rock Analysis and Dean Stark

Accurate representation of rock-fluid properties is necessary when obtaining petrophysical data. Laboratory techniques that implement injection of nitrogen, helium and mercury into core plug samples are very accurate in determining reservoir properties. This section presents permeability and porosity data (compiled from Reservoirs Inc., 1996) from nitrogen and helium injection, respectively. These are incompressible and chemically inert gases. Helium is capable of filling all connected space inside a rock sample, thus giving accurate porosity values. Mercury, also a non-compressible fluid, is a non-wetting fluid that does not react with the rock and also has the ability to completely occupy pore spaces. Thus, measurements using injection of mercury are very accurate in determining pore throat values.

The goal of this work was to define reservoir rock character and to distinguish it from all other types of SSL encountered within the Spraberry. The different data sets were analyzed to determine correlations between porosity/permeability and lithologic controls on reservoir quality. Capillary pressure analysis is presented to define pore throat systems for each rock type.

Core plug samples selected for detailed analysis in this study have a wide dynamic range of porosity (13.7 to 0.4 %) and permeabilities (1.97 to 0.01 md). The dispersion of porosity permeability data is such that permeabilities range over an order of magnitude for any given value of porosity (Fig. 5.3).

Figures 5.1 and 5.2 presents the variation for water saturation (S_w) and porosity along the depth profile (S_w from Dean Stark). This depth profile shows a strong increase of water saturation within the non-pay, low porosity muddy zone. With any increase in porosity or, in other words, with a decrease in clay matrix and carbonate cements and mud, the oil saturation increases and amounts of water saturation become less.

5.1.4 Analyzed Cores

Two cores have been sampled with core plugs (cores E.T. O'Daniel 37 and Shackelford 138A; Figures 5.1 and 5.2). Several sets of petrophysical data have been extracted from core plug measurements and then correlated to mineralogical composition from thin sections. The E.T. O'Daniel 37 core covers an interval that goes from 7080 to 7250 ft (5U unit). The Shackelford 138A core includes samples from depth 7060 to 7122 ft (1U unit). Integrated depth profiles with all data sources were constructed in order to establish the degree of heterogeneity and the level of correlation between different data sets.

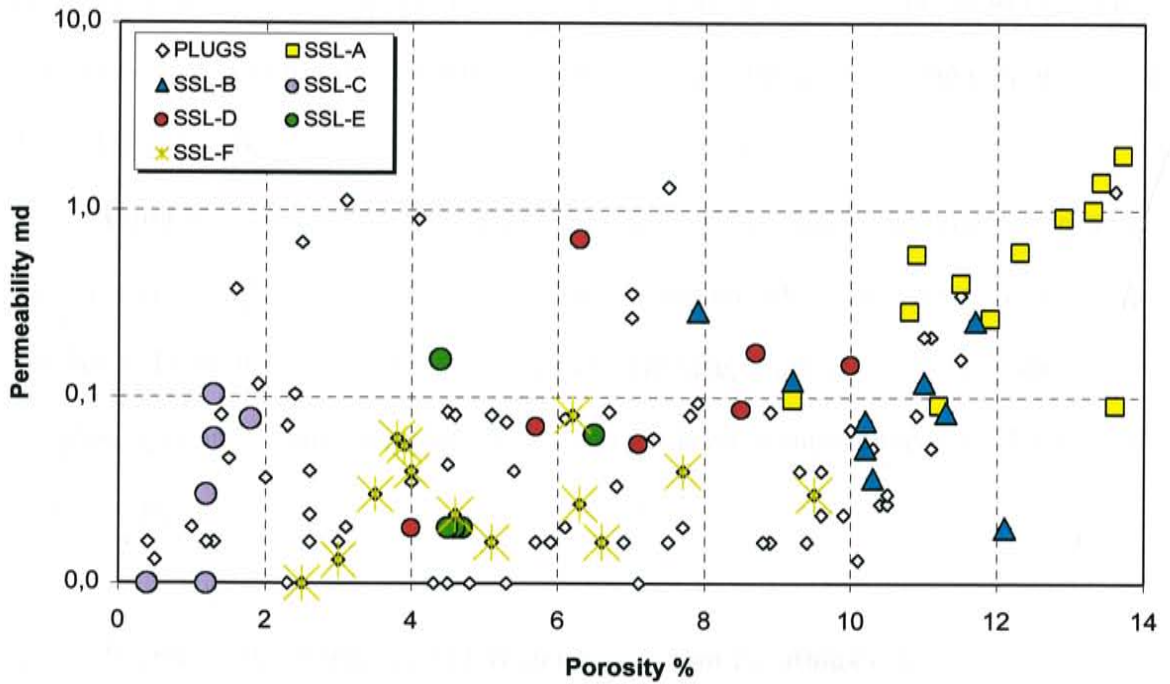


Fig. 5.3 – Porosity-permeability from core-plug measurements. Colored dots represent different core plugs lithofacies in correlation with thin section information. Note the clusters of points for each lithological distribution. SSL-A (yellow dots) shows good correlation for porosity and permeability.

5.2 DISCUSSION OF PETROPHYSICAL PROPERTIES

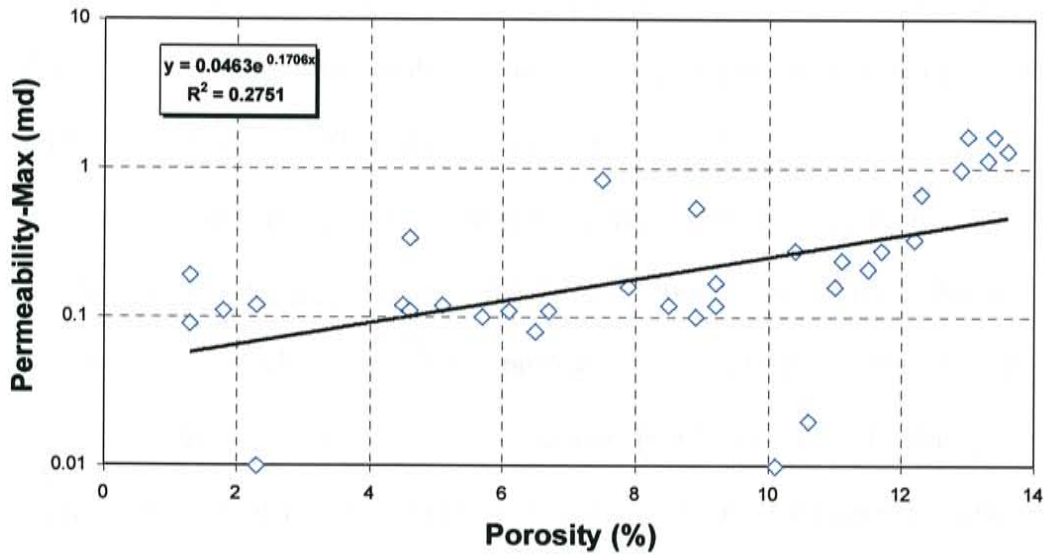
The gamma-ray deflection curves correlate well with the core descriptions. Thickness for sandy beds are fairly well predicted by the deflection to the left; however, peak heights do not define facies characteristics very accurately. This is due to the limited sensitivity of the GR tool to differentiate mineralogical sources other than clay amount in the rock framework.

Complex permeability behavior is depicted with the use of air minipermeameter measurements (Figs. 5.1 and 5.2). A number of factors affect the heterogeneity of the Spraberry Formation: clay and organic-rich laminae, burrowing, cementation, pore morphology, pore distribution, pore throat aperture, level of interconnection of pores, and rock wettability.

5.2.1 Permeability, Porosity, and Water Saturation Relationships

The wide dispersion of porosity permeability data reflects changes in the volumetric distribution of pore types within the reservoirs. The relationship between porosity and permeability is related in part to stratigraphic position in the wells. In E.T. O'Daniel No.37 there is a difference in correlation match for samples approximately below and above the 7195-ft depth (Fig. 5.4). Above this depth there is a poor match between porosity and permeability due to great variation in lithology. A number of heterogeneities at various scales tend to decrease fluid conductivity. These include dispersed and laminated clay matrix, abundant organic matter, bioturbation, soft sediment deformation within shaly laminae, and silica cement within sandy laminae. In this way

(only samples from depths range 7195-7245 ft)



(only samples from depths range 7080-7195 ft)

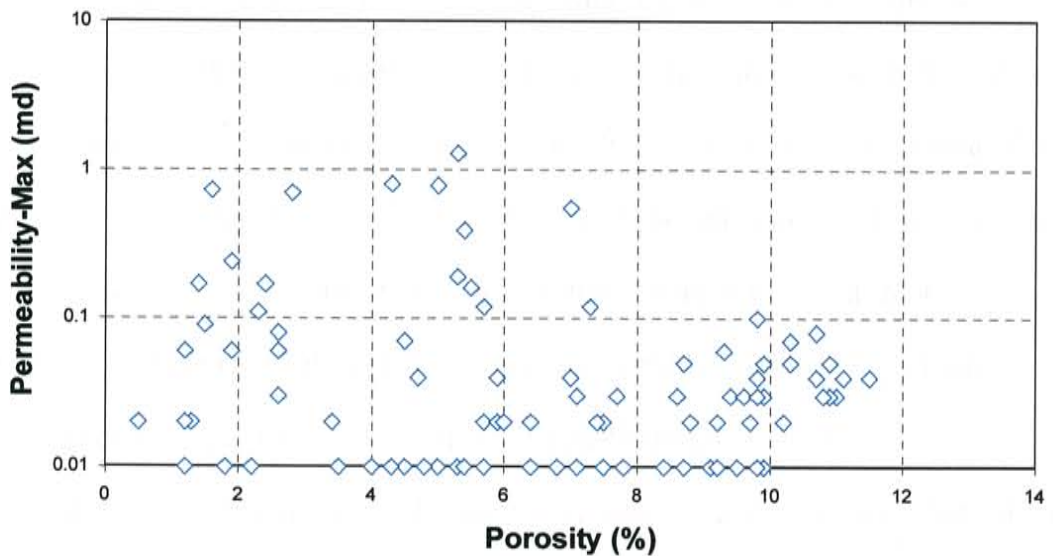


Fig. 5.4 – Cross plots showing differences in porosity-permeability correlation for samples above and below 7195-ft depth for E.T. O'Daniel 37 core.

pore interconnection is considerably reduced for many samples, although total porosity remains relatively high. However, the more sandy areas that comprise the reservoir interval 5U unit (below 7175 ft) exhibit a better correlation between porosity and permeability. Better fluid conductivity is related to bigger pore spaces and pore throat radius present in SSL-A and SSL-B within this area.

Permeability depends on rock properties such as grain sorting, amounts of clays and cements, pore throat size, pore size distribution, pore connectivity, tortuosity, and rock-fluid properties such as capillary pressure and wettability. For this reason mineralogically complex lithologies show greater point scattering in the porosity-permeability cross-plot of Fig. 5.4, whereas cleaner and more homogeneous sandstones show a better trend.

Figures 5.5 and 5.6 present contiguous intervals of fluorescing pay zone and non-pay argillaceous zones (from core images) with permeability, porosity and water saturation relationships that suggest strong mineralogical control. Commonly, areas of non-fluorescence contain higher amounts of clays although they may appear quite similar to fluorescent rocks when viewed in normal light. Although some porosity exists, non-fluorescent intervals exhibit much less permeability than fluorescent zones. The low permeability in these relatively porous intervals is probably related to higher amounts of dispersed clay minerals and laminae that affect pore throat connectivity.

The depth profiles for Sw and porosity (Figures 5.1 and 5.2) further indicate that lithological control is strongly related to fluid-rock behavior. Figure 5.7 shows data from two cores, Shackelford 138A and E.T. O'Daniel 37 that correlate porosity with Sw measurements. The linear relation with a negative slope clearly indicates the trend of

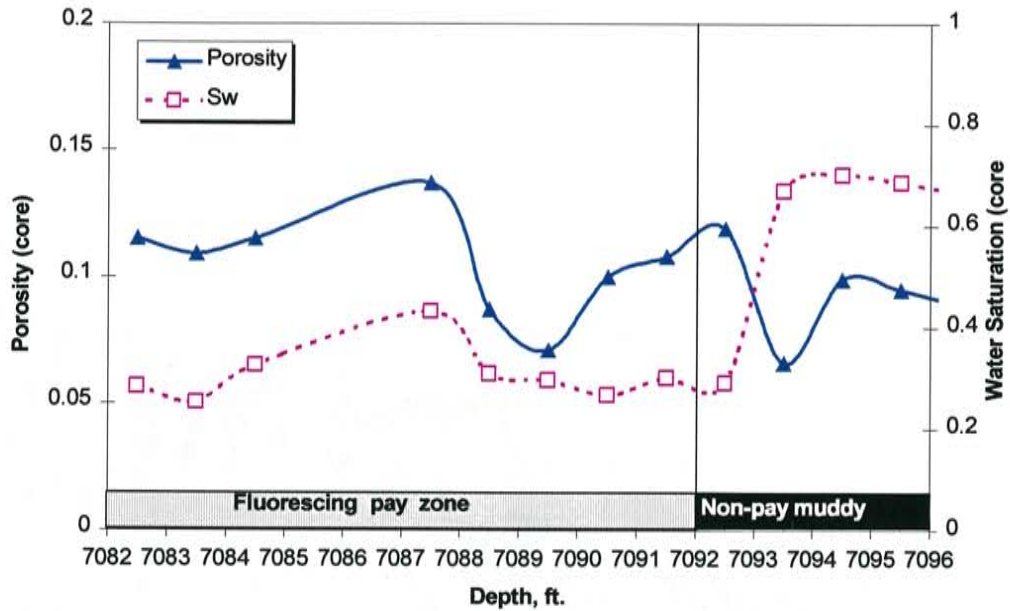


Fig. 5.5 – Core plug data (Sw and porosity) for Shackelford 138A - 1U unit, Upper Spraberry Formation. Relatively similar sandy units do not show obvious evidence of major heterogeneity in core samples. Petrophysical properties measured in the lab show important variations between fluorescing pay zones and non-pay zones richer in clay.

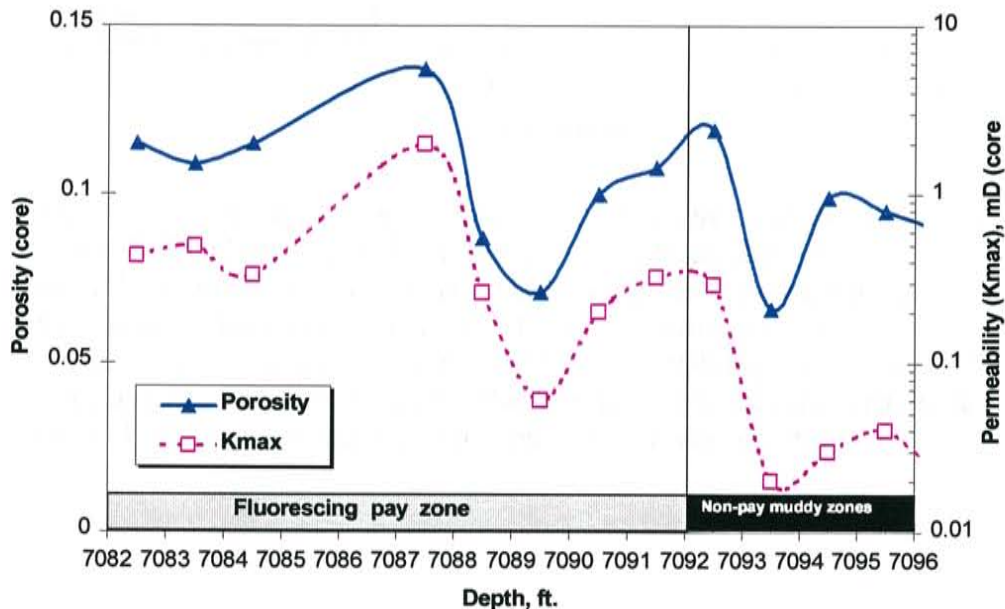


Fig. 5.6 – Core plug data (permeability and porosity) for Shackelford 138A - 1U unit, Upper Spraberry Formation. Non fluorescent zones are commonly lower quality reservoirs and non-reservoir rocks strongly affected by pore lining and pore bridging clays.

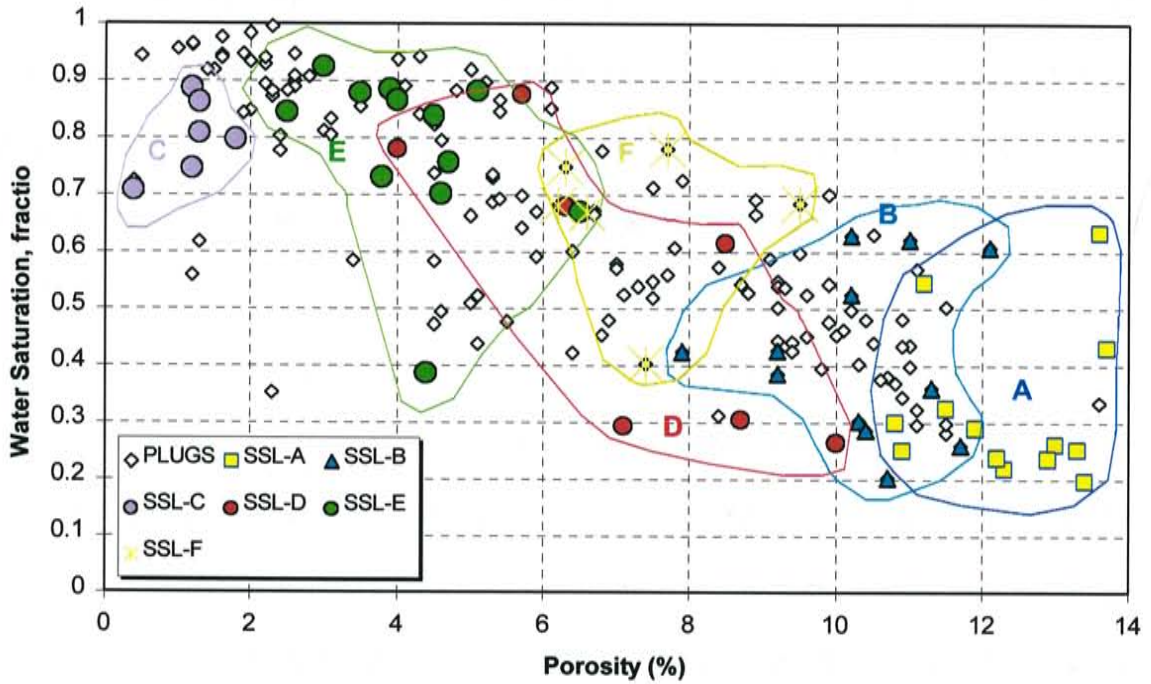


Fig. 5.7 – This figure shows core plug data (S_w and porosity) from cores Shackelford 138A and E.T. O'Daniel 37. Colored dots represent thin section control for small-scale lithofacies. There is a general increase in water saturation with gradual decrease of porosity. From this cross-plot the close relationship between water saturation and lithological variability is obvious. This S_w -mineralogical interaction suggests that capillary pressures and wetting behavior of the rock-fluid system are important controls on water/oil saturation.

decreasing water saturation with increasing porosity. For the same figure (Fig. 5.7), thin sections have been used in relation to core plug measurements as a control to determine if trends of small-scale lithofacies with water saturation are present. The outcomes are well-defined clusters for each of the six SSL. A good correlation of S_w and porosity shows clean porous sandstones (SSL-A and SSL-B) at the lower end of the S_w trend. Subsequent increases in clay matrix and carbonate cements through shaly laminated and patchy dolomitic siltstones (SSL-D and SSL-F) lead to increases in S_w . The less porous, finer grained, argillaceous and dolomitic mudstones of SSL-E and SSL-C are at the upper level of S_w .

Depth profiles (Fig. 5.1 and 5.2) show drastic changes in S_w and porosity at lithological boundaries. Moreover, changes in clay content and laminae within the same lithologic group can lead to a considerable increase in S_w . This evidence suggests that the small pore spaces and pore throats of the Spraberry Formation control fluid saturation through capillary pressure and wetting character, not by means of gravity forces. A parallel investigation (Yanfidra, 1998) has analyzed wettability data from Spraberry core plug samples using brine and oil injection and spontaneous imbibition of brine. From these measurements, initial water saturation, core permeability, and core wettability have been determined. These are very important factors because of their effect on final oil recovery.

When some mineral facies are characterized as water-wet, it means that these facies possess a hydrophilic character; thus, water will preferentially be attached to the surface of this mineral. If this were the case of a hydrophobic mineral facies, it would probably be preferentially electrochemically related to the oil phase.

Pore walls in the Spraberry sands are formed by a variety of different minerals including quartz, different types of feldspar, micas, accessory minerals, carbonate cements, clays, organic matter, pyrite and other less abundant minerals. These different mineralogical species give to the rock matrix a distinct wetting behavior at the microscopic level. In this way a single large pore that is surrounded by clay, quartz and dolomite may exhibit more than one wetting character. The illite-rich zones tend to be water-wet and adsorb water into the clay interlayer, which contrasts with the weakly water-wet behavior of clean siltstones and sandstones. The Amott wettability index to water (I_w) has been determined to be between 0.22 and 0.35 for very fine Spraberry sandstones and siltstones (Yanfidra, 1998). This weakly water-wet behavior is a result of the heterogeneous mineralogical character of the Spraberry reservoirs.

Robin et al. (1995) performed a good example of a study that concerns wettability and level of mineralogical heterogeneity. He utilizes a microscopic technique called Cryo-SEM to study the wettability of reservoir rocks from fluid distribution at irreducible water saturation, S_{wi} , and residual oil saturation, S_{or} . In the research performed by Robin et al. (1995) brine is associated with illite and oil is trapped within booklets of kaolinite. The Cryo-SEM technique used by Robin et al. (1995) also confirmed the influence of wettability on fluid distribution in porous media. These results and analysis explain how illite, which is present in considerable amounts in the Spraberry Formation (especially within the clay/organic rich lithofacies) tends to induce a water-wet behavior to the samples. Thus, due to illite content, the water-wet behavior as well as the water saturation is probably more pronounced within the argillaceous lithofacies than within the cleaner sandstones and siltstones.

Due to the mineralogical complexities, cleaner siltstones and sandstones rocks from the studied intervals in the Spraberry Formation exhibit relatively low *irreducible* or *non-movable* water saturation (S_{wi}). Pore throat and capillary pressures are probably related to this problem. Tentatively, we can say that pore throat and pore systems are so tight in clay/organic rich lithologies (SSL-E and SSL-F) and in dolostones (SSL-C) that strong capillary forces are holding the totality of the fluids in the form of non-movable water. In turn, the total water saturation in these rocks is expected to be relatively high. A question raised by this analysis is the possibility of a relationship between preferential migration of hydrocarbons out of the argillaceous porous media into the more weakly water-wet sands and silts during very early stages of maturation. In other words, the strong hydrophilic character of the clay-rich rocks might have promoted the expulsion of hydrocarbons and the partial retention of water.

Figure 5.8 shows an example of different curves created calculating capillary pressure and S_w from flow through rock experiments (Yanfidra, 1998). Due to variations in composition from one core plug to another, the behavior of the capillary pressure- S_w curves shows considerable differences.

Oil imbibes spontaneously into Spraberry sandstones without requiring any pressure input; this is due to the weakly water-wet character of the rocks. This behavior does not favor water-flood oil recovery methods, since water injected into the formation will not sweep the oil particles that are attached to the rock. At a certain point, water injection would not be able to move any more of the oil that is trapped in hydrophobic intergranular pore cavities. For this reason other methods of oil recovery should be examined (CO_2 flooding).

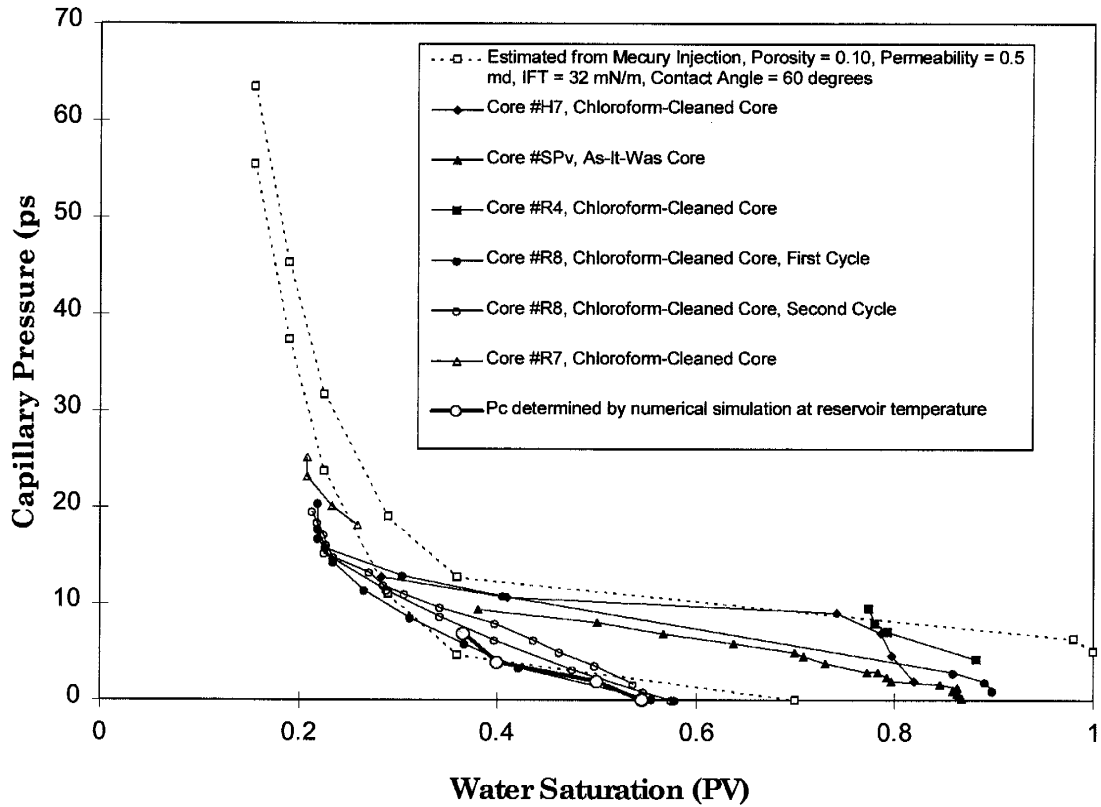


Fig. 5.8 – This graph shows several curves for S_w and capillary pressure from imbibition experiments done with core plugs from various depths in the Spraberry sandstones. Note the variability from one core plug to another.

5.2.2 Grain Density and Porosity Relationships

Figure 5.9 shows additional analyses of lithological controls on reservoir quality. Grain density is strongly related to lithological character. Porosity and grain density data from the two cores analyzed show a hyperbolic relation with a positive slope. Two main trends are observed in this graph. One trend involves porosity and grain density increasing with decreasing amounts of clays and organic matter (from SSL-E to SSL-A). A second trend shows that an increase in porosity occurs with a progressive decrease in micritic dolomite mud, dolomite cements, and grain density (from SSL-C to SSL-A). A cluster of points in the top left corner can be discriminated as dolomite mudstone, due to their typical high grain density, very low porosity and petrographic characteristics. Table 5.1 summarizes the general trends found in the petrophysical data for three major subdivisions of rock types: 1) clean sandy rocks, 2) shaly and silty non-fluorescent rocks, and 3) dolostones.

Notice that these three subdivisions represent the major lithological and flow units that occur in the Spraberry Formation: SSL A, B, C, E, and F. Patchy dolomitic siltstone (SSL-D) is a flow unit that falls between SSL-B and SSL-F (Fig. 5.9). This category shows a slightly higher grain density range and lower porosity than SSL-B due to the higher amounts of dolomite cement present. The significance of the observed lithological trends that correlate grain density (mineralogy dependant parameter) with porosity derived from petrophysical measurements (helium injection) is due to a strong natural classification of the different lithofacies. It is important for the utilization of geophysical well logs to recognize lithological character and reservoir quality. Physical properties

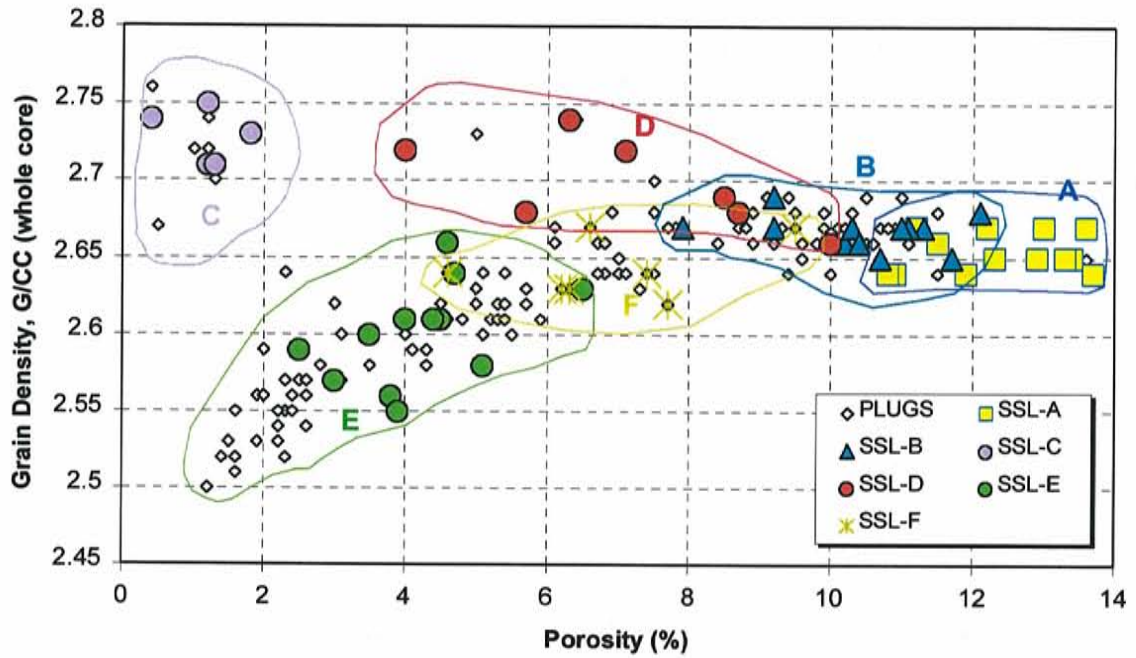


Fig. 5.9 – This is a chart of porosity vs. grain density data from core plugs from Shackelford 138A and E.T.O'Daniel 37. The grain density and porosity cross-plot further suggest the strong lithological controls on porosity. The classification of this database in different lithofacies is based in observations of core plugs and thin sections in association with their porosity and grain density characteristics.

MAJOR LITHOLOGIC TYPES – SMALL SCALE LITHOFACIES			
UPPER SPRABERRY FORMATION			
THREE MAIN GROUPS	1. CLEAN SANDY ROCKS	2. SHALY AND SILTY NON-FLUORESCENT ROCKS	3. DOLOSTONES
Description	Mostly massive structure, low clay amounts, good porosity and pore throat radius, main mineral component is quartz. Include SSL “A” and “B”	Laminated, bioturbated, or convoluted, very low porosity, main mineral component are clays and quartz. Include SSL “E” and “F”	Mostly massive carbonate rich mudstones, poor porosity to total absence of pore space, main mineral components are dolomite mud, and quartz. Include SSL “C”
Fluorescent Capacity	Fluorescent	Non-Fluorescent	Non-Fluorescent
Grain Density	2.70 to 2.64 g/cc	2.60 to 2.51 g/cc	2.75 to 2.73 g/cc
Porosity (helium)	12 % (“A”) 9.95 % (“B”)	3.8 % (“E”) 7.3 % (“F”)	1.0 %
Permeability (nitrogen)	0.64 md (“A”) 0.12 md (“B”)	0.056 md (“E”) 0.034 md (“F”)	0.048 md
Sw (from Dean Stark)	35 % (“A”) 44 % (“B”)	75 % (“E”) 61 % (“F”)	79 %

Table 5.1 – This table summarizes grain density data in relation to the major flow units. Patchy dolomitic siltstone (SSL-D) is a flow unit that falls between SSL-B and SSL-F. SSL-D shows slightly higher density range and lower porosity than SSL-B due to the amounts of dolomite cement present.

such as grain density can affect the response of geophysical logs in such a way that rock properties can be estimated.

5.2.3 Pore Throat Relationships Based on Mercury Capillary Pressure

Mercury injection data from core plug samples from the Shackelford 138A and E.T.O'Daniel 37 are presented in this section. Figure 5.10 shows a set of cross-plots that correlate porosity, permeability and pore throat data. The results show consistency between rock-fluid parameters and those obtained in the petrographic study. Once again a good separation of clusters for each lithofacies is observed. The better correlation of pore throat to permeability, compared to the more scattered points in the pore throat vs. porosity graph, suggest that reservoir quality is better controlled by pore throat apertures than by the amount of pore space. This in turn is related to the very fine grain size and the small pore spaces of the Spraberry Formation where capillary pressure exerts strong influence over fluid mobility.

Table 5.2 summarizes the results (average values) for each SSL from helium, nitrogen and mercury injection. The analysis of petrophysical data emphasizes the heterogeneous nature of the deposits in the Spraberry Formation. From these data, one can see distinct differences among SSL occurring in the upper Spraberry Formation. As expected from thin section analysis, SSL-A and SSL-B have the best potential as reservoir rocks. These consist of very fine sandstones and siltstones with variable pore structures. Small-scale lithofacies C, D, E, and F required higher pressures to pass fluid through a tight pore systems with very small pores and pore throat radii. SSL-C, SSL-D, SSL-E and SSL-F are considered to be marginal reservoirs to poor or non-reservoir rocks.

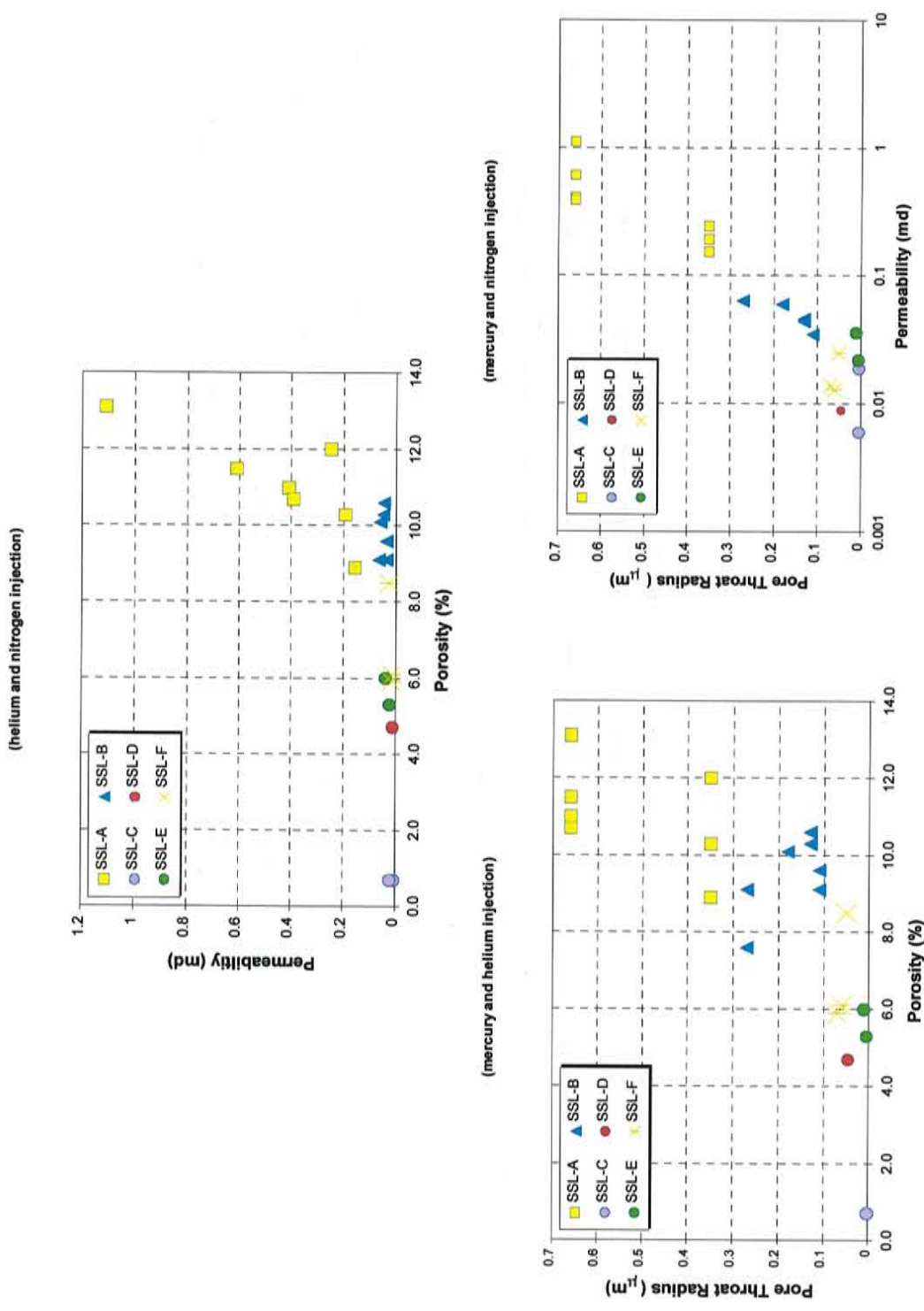


Fig. 5.10 - These three cross-plots of mercury injection data (porosity-permeability and pore throat radius) from cored wells Shackelford 138A and E.T. O'Daniel 37. Cross-plots suggest that rock-fluid behavior is tied to lithological variability for the six small-scale flow units (SSFU) under study.

SSL	POROSITY helium (%)	PERMEABILITY nitrogen (md)	MODAL PORE THROAT RADIUS mercury (μm)	DISPLACEMENT PRESSURE RANGE, mercury (psia)	NUMBER OF SAMPLES (in mercury injection only)
A	12	0.64	0.53	74.8-161	7
B	9.95	0.12	0.16	300-602	7
C	1.0	0.05	0.0035	11,943-4,980	2
D	8.0	0.18	0.045	987	1
E	3.8	0.06	0.0075	3,491	2
F	7.2	0.03	0.06	1,434	3

Table 5.2 – This table summarizes helium, nitrogen and mercury injection data for plugs of different SSL that occur in the Spraberry Formation.

They are dolostones and patchy dolomitic siltstones, and shales and shaly siltstones with variable organic content.

CHAPTER 6

CONTROLS ON RESERVOIR QUALITY IN THE UPPER SPRABERRY FORMATION

6.1 FACTORS CONTROLLING POROSITY, PERMEABILITY AND OTHER PETROPHYSICAL PARAMETERS

A number of factors have been determined that exert more or less control on porosity, permeability, pore throat diameter, capillary pressure and wetting behavior of the rock-fluid system. This chapter presents a discussion of all the important factors that affect reservoir quality in the Spraberry Formation. These factors are subdivided as primary controls and secondary controls, for factors related first to the detrital origin of the rocks and secondly to those related to the diagenetic changes suffered by sediments after deposition. This chapter also includes a discussion of the processes of generation of secondary porosity in Spraberry reservoirs. Other important topics covered in this discussion chapter are “the relation between overpressuring and preservation of rock fabric porosity and formation of fracture porosity” and also “the use of small-scale lithofacies in description of reservoir quality variability”. Finally insight on the significance of the small-scale lithofacies analysis is presented to explain the importance of this type of approach.

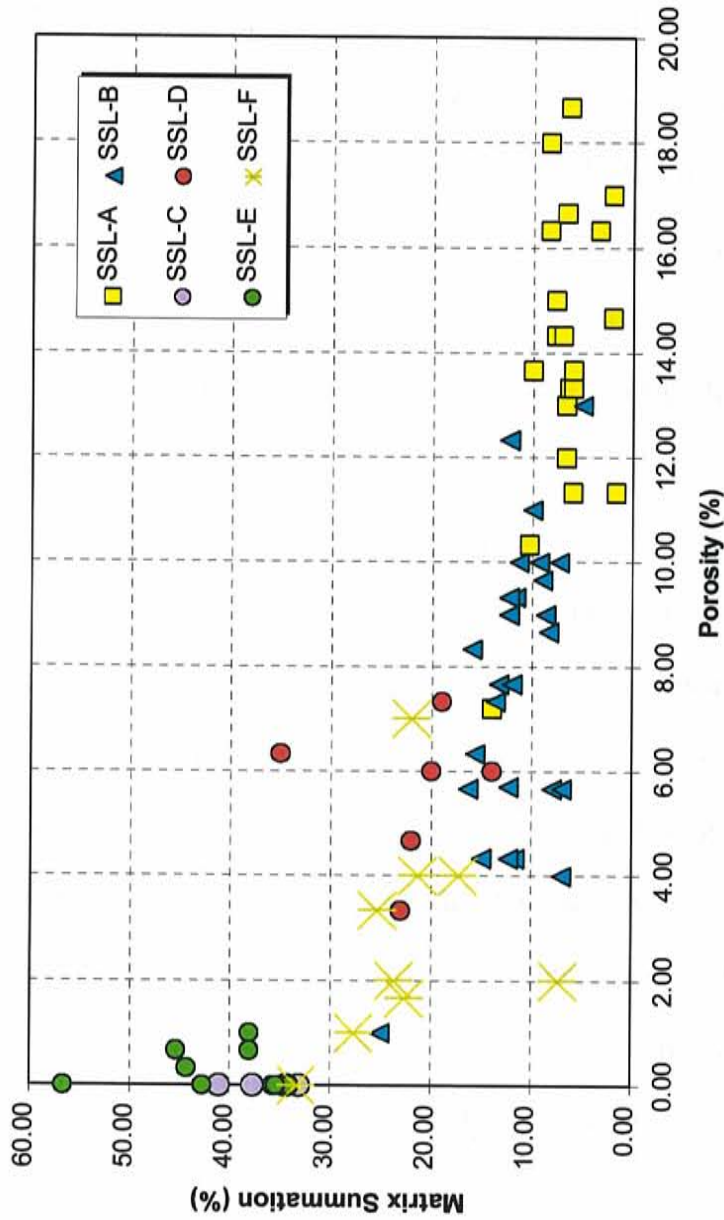


Fig. 6.1 – Point count data for porosity vs. matrix summation by small-scale lithofacies (include three cores under study). Matrix summation includes laminar clays, dispersed clays, organics, and depositional carbonate. The cross-plot shows that a considerable decrease in porosity is followed by an increase in depositional matrix.

6.1.1 Primary Controls

Diagenetic processes have obviously overprinted original depositional characteristics. However, mineralogical composition due to provenance, transport and depositional factors probably exerts the most important control on reservoir quality. Figure 6.1 shows porosity against a summation of originally deposited, pore filling and fine-grained material (total matrix). These data were obtained from thin section point counts. The matrix summation includes laminar clays, dispersed clays, organics, and depositional carbonates. The graph shows a correlation, with porosity decreasing with gradual increases in total amount of matrix. Clusters of points with different symbols and colors belong to groups of distinct lithofacies (SSL), suggesting lithological control on the amount of pore space.

Original rock texture - This element includes grain size and sorting. Very fine grained, poorly sorted sandstones of submarine channel abandonment, distal turbidite, and basinal origin have smaller pore and pore throat sizes than coarser grained and better-sorted sandstones of submarine channel origin. Pore size distribution is more heterogeneous within the low energy, basinal siltstones and sandstones: a function of lamination and bioturbation.

Sorting - Original low porosity after deposition was probably further reduced by authigenic cements and compaction. Bloch and McGowen (1994) stated that “porosity is essentially independent of grain size, but it is strongly controlled by sorting and decreases progressively from very well-sorted to poorly sorted sand.”

Grain size, pore throat diameter and capillary pressures - An indirect depositional control on quality is the very fine grain size of these sands and silts, which probably causes marginal permeability in Spraberry reservoirs (Bloch and McGowen,

1994). Reducing the size of grains produces a proportionally equal decrease in pore and pore throat size. Total porosity amounts for a given volume of rock does not depend on grain size. However, reservoir quality depends less on total porosity than it relies on the size of individual pores. Considerable reduction of grain size does cause a direct decrease in pore throat aperture and the size of individual pores, causing higher capillary pressures that further damage the conductivity of fluids throughout the reservoir. Bloch and McGowen (1994) have stated that at the reservoir scale, grain size is the primary control of permeability, and a decrease in grain size from proximal to more distal facies is generally accompanied by decreasing permeability.

Mineralogy – This is a very important factor that partially controls wetting behavior. Wetting behavior is a relationship between a specific mineral phase and a fluid type. Since the Spraberry formation has a complex mineralogy in contact with two fluids, water and hydrocarbon, the expected wetting behavior is also complex. The wettability index for Spraberry reservoir rocks is considered weakly water wet. This is probably due to the minor presence of water absorbent illite clay and mixture of other mineral phases that are either water wet or oil wet. The exact microscopic wetting behavior for each mineral has not been determined. However information from plug wettability (Yanfidra, 1998) and studies performed by other authors with mineralogically complex formations (Robin, 1995) indicate that the Spraberry reservoirs are strongly affected by heterogeneities. Abundant illite is related to high water saturation found in argillaceous non-reservoir lithofacies.

Burrows - Often, burrows are more porous and permeable than the surrounding matrix, which is thought to be a product of the cleaning effect of browsing organisms.

Observations of burrows in thin-section usually show higher amounts of pore space than the surrounding framework (Fig 4.6-C). Folk (1989) described burrows in the Spraberry Formation as particularly permeable portions of the rock. He suggested that more permeable burrows might have provided a pathway for early migration of hydrocarbons. However, in many instances it appears that the cleaner burrows tend to be more affected by pressure solution (less cement, higher stress instability), thus showing considerable reduction of porosity by silica cement. Mottled sedimentary fabric is not rare in the Spraberry and it is associated with burrowing and/or the dewatering phenomena. A lack of connectivity between the burrows and surrounding clay-rich matrix precludes an increase in effective permeability.

Expandable Clays - The amount of expandable clays is small and restricted to minor quantities of interlayer illite/smectite. The possibility that the expansion and high cation exchange capacity of smectites damaged porosity and/or permeability is relatively low. Low amounts of expandable clays suggest that the distorting effect on any type of electric or porosity logs from bound water in interlayers between successive lattices of smectite is very low. However, structural water contained in illite and chlorite should still affect the response of electric logs. The main effect of the clays present in the Spraberry rocks is in the damage of reservoir pore space and fluid conductivity by forming pore lining, pore bridging, and pore filling types.

6.1.2 Secondary Controls (Diagenetic)

To observe the effect of cements on reservoir quality, the same type of cross plotting was done for porosity and diagenetic cements using data from point counts (Fig. 6.2).

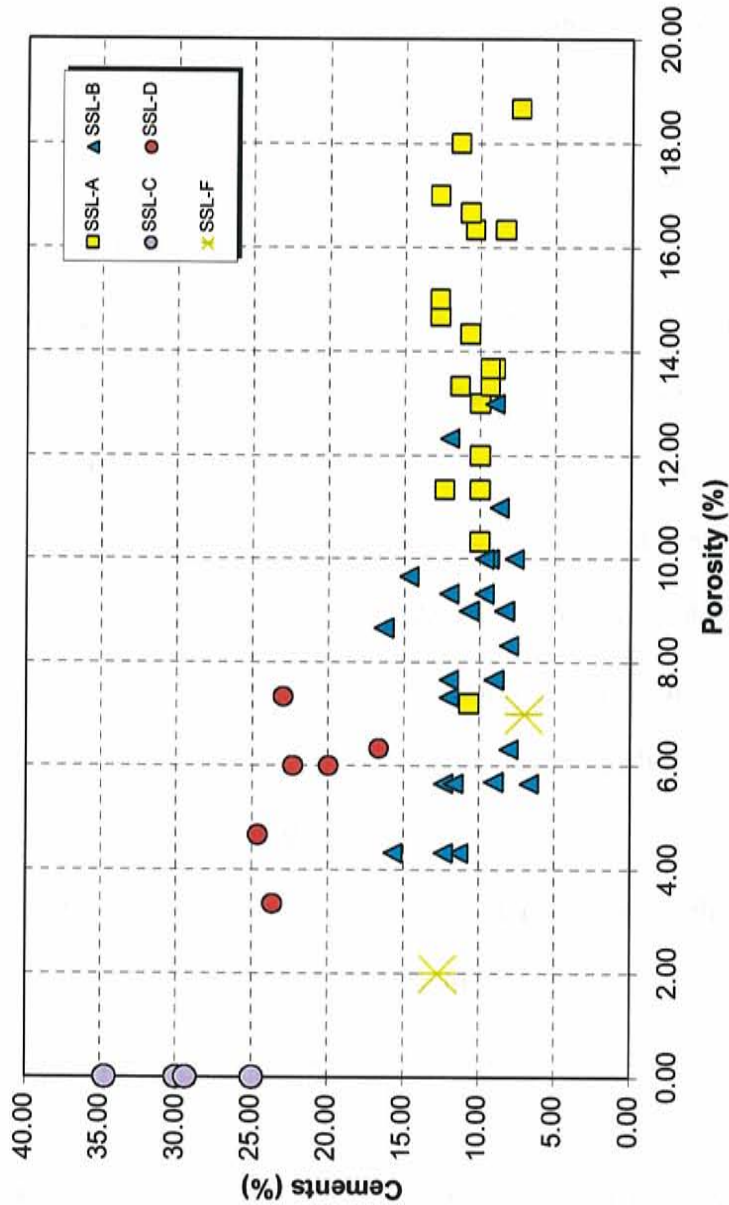


Fig. 6.2 – Point count analysis data for porosity and cement summation by small-scale lithofacies (include three cores under study). Cement summation includes quartz overgrowths, calcite, dolomite and pyrite. There is a correlation between decreasing porosity and increase of cements although the dispersion of points is more scattered than the cross-plot for matrix-porosity. Cements for Rock Type “E” (shale) are not considerable.

Cement summation includes quartz overgrowths, calcite, dolomite and pyrite. The plot shows a similar trend with otherwise more scattered points and clusters that belong to different lithological groups (SSL). These suggest that cements exert control on porosity amounts and distribution to a somewhat lesser extent than depositional matrix.

Compaction - This controls grain packing and the degree of deformation of ductile grains. Compaction has resulted in a reduction of the original size of pores and pore throats, and therefore has contributed to a general reduction in porosity and permeability during burial. Compaction must have significantly affected the more clay rich lithofacies and carbonate mudstones (L1, L2, L3 and L4 Chapter 3; SSL-C, SSL-E and SSL-F Chapter 4).

Cementation - This also results in reduced pore and pore throat size and increased pore system tortuosity (in the case of sandstones with microquartz, carbonate and clay cements). Precipitation of authigenic clay can produce a dramatic increase in pore surface area, and in partitioning of intergranular pore space near pore walls into micropores (pores $<5\mu\text{m}$ in diameter). Additionally, the bridging of pore throats by fibrous illite has an effect far in excess of the small volume of clay present, dramatically reducing formation permeability (Neasham, 1977 and Crocker, 1983).

Dissolution - Selective dissolution of chemically unstable framework grains produces secondary porosity within very fine-grained sandstones and siltstones, usually improving permeability (Lithofacies L6, L7 Chapter 3; SSL-A Chapter 4). Commonly dissolved grains in the Spraberry Formation are feldspars and carbonate grains.

Fabric rigidity - Despite being subject to burial loading, some of the Spraberry lithofacies examined in this study (Lithofacies L6, L7 Chapter 3; SSL-A and SSL-B Chapter 4) have retained significant amounts of original intergranular porosity, resisting grain

slippage and packing adjustments. Non-ductile fabric composition and early silica cementation in the very fine sandstones and siltstones should have arrested grain slippage by increasing the mechanical strength (rigidity) of the rocks. The dominantly arkosic composition of the sandstones and siltstones helped maintain reservoir quality. These types of arkosic sandstones have high framework stability, and are less easily altered by chemical processes. On the other hand, clean sandstones and siltstones tend to be more affected by precipitation of quartz and other types of cement into open pore spaces. Pressure solution is also more prevalent. In general, quartz cements have the double effect of reducing porosity by pore occlusion and also improve rigidity of the rock fabric. To some extent, the presence of argillaceous materials may prevent nucleation of quartz or carbonate cements on grain surfaces. Spraberry reservoir rocks represent a balance between the mechanisms of pore space preservation and destruction by quartz cement.

Fracturing – Fracturing is perhaps the single most important factor that enhances reservoir quality in the Spraberry Formation. Fractures in such type of tight reservoirs with extremely low permeabilities are the major contributors to the conductivity of fluids. These reservoirs are strongly fractured in a roughly northeast orientation, and this orientation gives the reservoirs an anisotropic fluid conductivity behavior (Lorenz, 1997 and Cherney, 1998).

6.1.3 Secondary Porosity Processes

Four types of primary porosity as well as secondary dissolution porosity have been recognized in this study. Folk (1989) pointed out that many pores and detrital silt grain sizes

were similar in the Spraberry sandstones, thus relating porosity to possible dissolution of silt-size clastic grains, as well as calcite.

A number of hypotheses based on experimental work, theoretical models, and geochemical and diagenetic models for secondary porosity enhancement have been developed mainly during the last 20 years. The more sound cases that relate to the deep burial diagenetic history of Spraberry sandstone reservoirs are as follows:

- secondary porosity generation by carbonic acid
- generation of secondary porosity by organic acids
- secondary porosity generation by silicate hydrolysis

The first hypothesis is a weak possibility, primarily because the Spraberry Formation is a system that probably reached a maximum temperature that was still too low to produce significant amounts of carbonic acid. The maximum temperature estimate to which Spraberry sediments in the northern Midland Basin were probably exposed to is about 77°C (Houde, 1979). Temperatures estimated for the generation of enough carbonic acid from kerogen need to be 100°C. The relationship between organic matter and porosity enhancement has

literature since the early 1980s (Surdam et al., 1989b, and 1989c). Organic matter is decomposed during burial under the influence of higher pressures and temperatures, thus producing organic acids and promoting dissolution of alumino-silicates. According to Surdam and others (1989), organic reactions occurring simultaneously with inorganic reactions (such as kaolinization, illitization) produce a significant control on those inorganic reactions. Complexing and transport of cations released from alumino-silicates by anions of organic acids are thought to be very important processes in the generation of dissolution porosity. Ideal conditions for these reactions occur in a range of temperatures from 80°C to 120°C (Surdam and others 1989). This mechanism of porosity development would then be possible if temperature estimates proposed by Houde (1988) for the Spraberry Formation were somewhat higher.

The so-called silicate hydrolysis model (Smith and Ehrenberg, 1989; Hutcheon and Abercrombie, 1990a) possibly affects deeply buried clastic sequences such as the marine basin sediments of the Spraberry Formation. Dissolution of carbonate minerals is thought to occur because aluminosilicate equilibria helps decrease pH above temperatures of 100°C to 120°C. However, below 100°C, organic acids may dissolve carbonates, but with subsequent carbonate precipitation due to the aluminosilicate system effect. Carbonate precipitation eliminates any excess CO₂ in this type of system, thus there is no reduction in pH.

Enhanced dissolution of framework silicate grains near grain boundaries can occur due to the increase of pH close to the borders of micas and clays adjacent to quartz or feldspar grains. However this type of pore space formation might be just re-distributional, rather than true enhancement.

The influence of secondary porosity in reservoir quality is important, but much porosity in closed systems is simply redistributed rather than newly produced (Bloch, 1994). Material dissolved in one place may be re-deposited only a short distance away. Pore space formed by the dissolution of framework grains in the Spraberry Formation may increase the total amount of porosity, but it is understood that an equally considerable improvement of permeability rarely occurs. Dissolution of very fine grained and intra-granular material may produce pores that are too small or isolated to increase effective porosity. Pore space formed by dissolution of pore filling cements is often more effective in substantially improving porosity and permeability. Physically and chemically stable arkosic and subarkosic rocks such as the Spraberry sandstones and siltstones are the typical type of lithology that can preserve relatively high amounts of dissolution porosity.

6.1.4 Preservation of Rock Fabric Porosity and Formation of Fracture Porosity due to Overpressuring

An important event that perhaps followed dissolution in the Spraberry Formation is the preservation of porosity due to significant increases in geopressures. High overburden effects are suggested by pressure solution characteristics such as long and sutured grain boundaries found within the very fine sandy units. The formation of regional vertical fracture systems, which are very important for fluid conductivity in these reservoirs, is also related in part to the occurrence of overpressure events within the reservoir sands (Lorenz, 1997). Other characteristics of the Spraberry Formation are common to overpressured formations. Highly compressible shales, rich in organic fluids, are overwhelmingly more abundant in the Spraberry Formation than the rigid, fine, clean, and porous sandstones. In

these clay-rich systems large amounts of fluids are gradually injected into more porous sandstones and siltstones from the shales by compactional dewatering. After lithification, shaly rocks and carbonates that presently have very low permeability formed a good seal preventing escape of fluids from the enclosed sandy units. Very high pore pressure must have been preceded by periods of high lithostatic compression that promoted dissolution of silica at grain contacts. With the final buildup of overpressuring and reduction in total stresses, both fracture formation and preservation of matrix porosity occurred. Migration of low compressibility hydrocarbons into the sandy units is an additional factor for a rise in pore pressure. Large amounts of fluids confined within a fixed amount of pore space give rise to high pore-pressure buildup.

6.2 USE OF SMALL-SCALE LITHOFACIES TO DESCRIBE RESERVOIR QUALITY VARIABILITY

As has been previously observed, the SSL represent flow units defined as intervals of rock with unique pore geometry, and mineralogical composition that have specific fluid flow characteristics. The petrographic and petrophysical data presented in Chapter 5 include an analysis of the interaction of the different small-scale lithofacies as a whole. In this section of Chapter 6 the data and analyses are presented as a detailed study of each SSL as a separate group. Information regarding pore and pore throat structures, capillary pressure and permeability is integrated along with data obtained from the petrographic analysis for each lithofacies. In this manner, reservoir quality variability is examined in light of the effect that clays, cements and other factors have on

permeability, and how permeability is related to pore and pore throat dimensions for each lithofacies.

6.2.1 Petrophysical Description of Small-Scale Lithofacies – SSL

SSL-A – The average values of porosity and permeability are 12% and 0.64 md respectively. This rock type is dominated by intergranular macropores of Pore Type 1 (30-40 μ m), Pore Type 2 (15-30 μ m), and secondary dissolution Pore Type 5 (50 μ m). Intergranular macropores (PT1) are relatively large and are well interconnected through large pore throats of relatively uniform size. Thin-section analysis reveals that the hydrocarbon-bearing samples classified as *SSL-A* have relatively well preserved intergranular pore systems. Quartz overgrowths, patchy dolomite cement, and dispersed pore-filling clays produce some reduction of total pore volume. Illite, chlorite and smectite have also reduced pore volume. These minerals have formed pore linings and caused pore throat bridging, which in turn has resulted in the partitioning of pore space near pore walls into micropores (Pore Type 4 <5 μ m in diameter). Type 2 pores are much less abundant than Type 1 pores. Type 3 pores are not significant components of the pore system. Capillary pressure data shows a relatively high range of pressures from 74.8 psia to 161 psia necessary to intrude the larger system of pore throat radii (0.53 μ m) reflecting moderate obstruction of the intergranular pore system. Figure 6.3 shows an example of a very uniform pore throat distribution with a dominant pore throat radius at 0.66 μ m for sandstones and very coarse siltstones (*SSL-A*). Relatively high displacement pressures for sandstones with moderate porosity are the product of small pore throats and significant amounts of pore-lining and pore-bridging illite and carbonate cements.

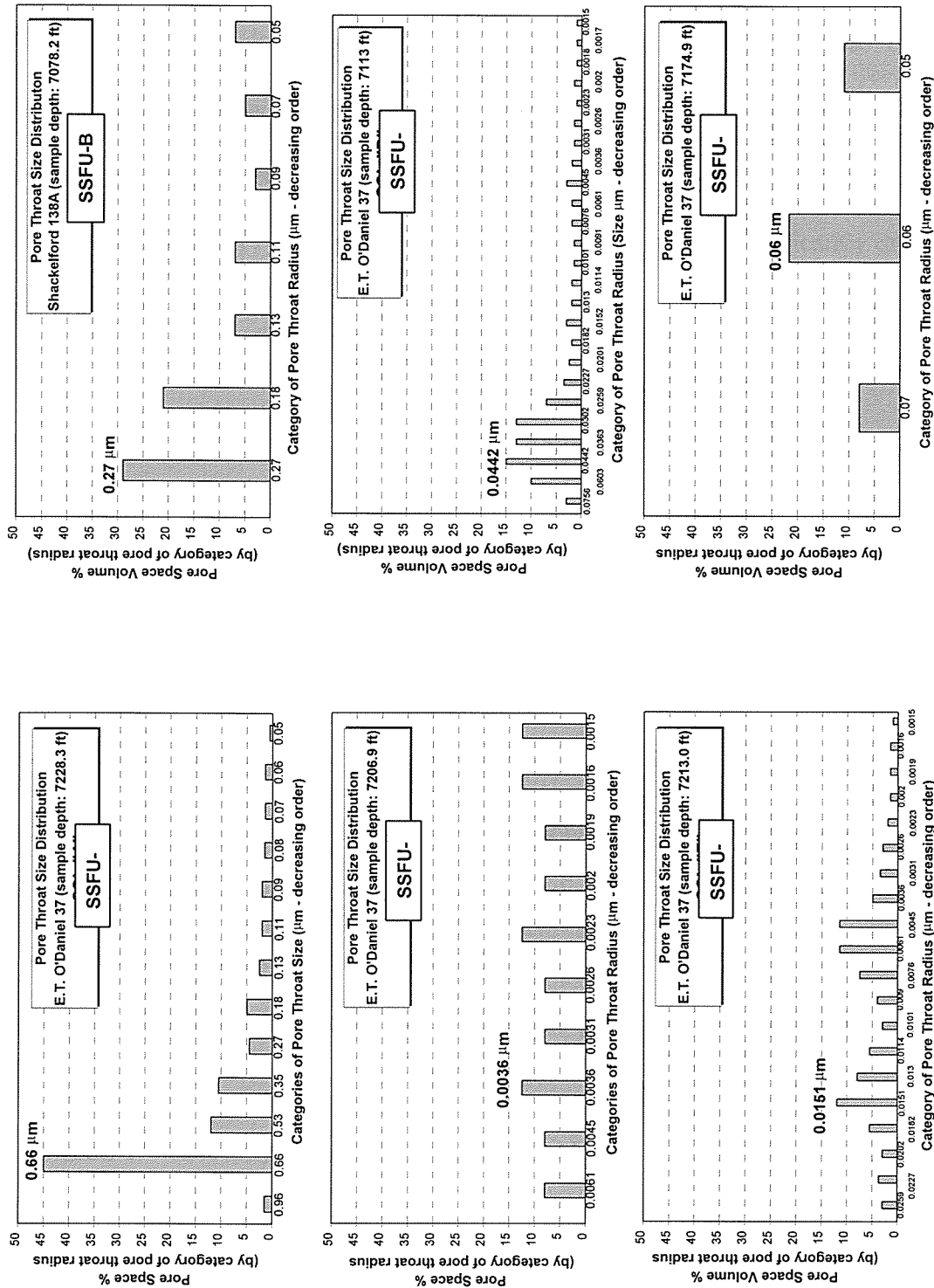


Fig. 6.3 – This series of cross-plots shows pore throat distribution for the six flow units cited before. Notice the variability in pore throat distribution from one SSFU to another. The more uniform pore throat distribution is SSFU-A with a dominant pore throat size of 0.66 µm (45% pore volume). SSFU-C exhibits the smallest pore throat and the more variable distribution.

SSL-B – These are lesser quality reservoir rocks with average values of 9.95% for porosity and 0.12 md for permeability. They are fine to very fine grained, moderately to well sorted siltstones dominated by Type 2 pores (intergranular macropores 15-30 μm diameter). Type 3 pores (intergranular mesopores 5-15 μm diameter) are less abundant, but common within these rocks. Clay cementation has partitioned pore space near pore walls into micropores (Type 4 pores). Pore Types 1 and 5 are not significantly developed. The larger pore throat radii average 0.16 μm and have a displacement pressure range of 300 psia to 602 psia. Pore throat radii distribution is log-normal with a relatively dominant pore throat size of 0.27 μm (Fig. 6.3; *SSL-B*).

SSL-C – These are carbonates muds (dolostones) equivalent to the carbonate debris flow deposits of LSL-1 (hand specimen from core, Chapter 3). These carbonates have very low porosity (1.0% avg.) and permeability (0.05 md avg.) and are not reservoir rocks. For this reason the pore structures of these rocks have not been studied in any detail (two core plugs samples studied). Very small pore throat apertures of 0.0035 μm need extremely high displacement pressures (11,943 psia to 4,980 psia) to intrude them. These are essentially moderate quality seal rocks rather than potential reservoirs. Pore throat distribution is shown in Fig. 6.3 (*SSL-C*) and shows the higher degree of pore throat heterogeneity with several pore throat sizes presenting a similar amount of pore space.

SSL-D – Porosity for these patchy dolomitic siltstones is 8% and the very low permeability averages 0.18 md. *SSL-D* rocks are moderately well to well sorted siltstones and sandstones dominated by Type 3 pores (intergranular mesopores 15 μm diameter). They display poorly preserved pore systems and have massive, laminated, or disturbed

sedimentary fabrics. Type 2 pores (intergranular macropores 15-30 μm diameter) are less abundant. Microporosity (Type 4 pores) is developed within clay cement rims on grains. The microporous clays tend to severely obstruct intergranular pores. Type 1 macropores scarcely occur within these rocks. Type 5 (dissolution) pores are also very rare. Pore throat radii (0.045 μm) are considerably obstructed; thus, moderately high displacement pressure (987 psia) is required to intrude them. The general pore throat distribution for patchy dolomitic siltstones (SSL-D) is lognormal and exhibits three dominant pore throat sizes that approach a maximum of 0.0442 μm (Fig. 6.3).

SSL-E – Porosity found for these samples averages 3.8% while average permeability is 0.06 md. These are very tight rocks with certain amounts of organic matter and carbonate mud mixed within an argillaceous matrix. Type 5 rocks are shales characterized by micropores (Pore Type 4) and very small modal pore throat radii. Due to their extremely low reservoir quality only two samples from capillary pressure mercury injection were run for these lithofacies. These rocks commonly form permeability seals, not reservoir rocks. An average for modal pore throat is 0.0075 μm . The pore throat distribution is bimodal with several pore throat sizes approaching similar pore space (Fig 6.3; SSL-E).

SSL-F – Average porosity and permeability for five samples are 7.2% and 0.03 md, respectively. Samples display massive, laminated, or disturbed sedimentary fabrics, and are characterized by the virtual absence of visible porosity. Intergranular pore space is severely occluded by abundant detrital clays or dolomite cement. Estimated microporosity is high for clay-rich samples, but low for the dolomite-cemented samples. The main pore types present are mesopores of 5 to 15 μm . Although porosities are

slightly higher than SSL-D (patchy dolomitic siltstones), the average value for modal pore throat radii is considerably smaller (Fig. 6.3; 0.06 μm) for SSL-F due to clays lining pores and bridging pore throats. Displacement pressure necessary to intrude the larger set of pore throats in SSL-F is 1,434 psia, more than double that used in the patchy dolomites (SSL-D). For these reasons, very shaly laminated siltstones (SSL-F) present a lower degree of permeability than the less porous SSL-D.

6.2.2 Interpretation of Petrophysical Properties of Small-Scale Lithofacies

Very fine sandstones and siltstones (SSL-A) were observed to be very clean and present the highest level of porosity among the distinct lithofacies groups. However, the detrimental effect of silica cement was found to be most notable with these clean sandstones as well as in thinner intervals with lower reservoir quality (SSL-B). Two clastic carbonate categories have been distinguished. A micritic dolomitic mudstone (SSL-C) with porosity below 1% is a well-indurated, dark and massive strata that comprises about one tenth of the column observed in the Spraberry Formation. Patchy dolomitic siltstones (SSL-D) having relatively high amounts of carbonate cements form a second category of carbonate rock. Substantial dissolution has taken place in some of these rocks; thus, they are considered moderately good quality reservoir rocks. Shales and shaly laminated siltstones (SSL-E and SSL-F) are the dominant lithofacies present in most of the cores examined. These are seen as rocks of very poor reservoir quality, as are SSL-C micritic dolomite mudstones.

Small-scale lithofacies "A" and "B" are potential reservoir rocks. These are distinguished from one another by different pore structures. SSL-A has the best reservoir

quality and is characterized by the largest intergranular and dissolution macropores and largest interconnecting pore throats. SSL “B”, “D” and “F” are characterized by progressively poorer reservoir quality, the result of reduced pore and pore-throat sizes. SSL “C” and “E” are carbonate muds and shales that completely lack reservoir properties and form moderate quality seal rocks.

The occurrence of the largest pores and pore throats in SSL “A” is a function of several factors:

1. SSL-A are the coarsest grained sandstones and siltstones
2. SSL-A very fine sandstones and siltstones are better sorted than other Spraberry rocks and contain smaller amounts of depositional micritic mud, carbonate cements, clay matrix, clay cements, and organics
3. SSL-A very fine sandstones and siltstones are characterized by relatively open grain packing (compactional effects are not pronounced)

Strong evidence was presented for depositional controls on porosity and permeability. For instance, in SSL-A (massive sandstone and siltstone), a product of high-energy deposition, shows the best reservoir properties in the porosity-permeability cross plots (Fig. 5.3 and 5.10). Massive dolostone (SSL-C) and shale (SSL-E), from low energy environments, show very low reservoir quality. Original porosity in low energy argillaceous lithologies tends to be considerably higher than sandy and silty sediments. But at the same time, the organic and clay-rich sediments are more susceptible to compaction, losing fluid and porosity when subjected to deep burial. For this reason quartz-rich facies are expected to better retain porosity and have better permeability levels, which should be related to depositional character.

However, the clusters of points for each lithofacies type are not totally distinct from each other. The overlapping of depositional lithofacies in these graphs probably is due to a number of causes, including diagenesis and similarity in pore-structure produced by different depositional environments.

The reservoir quality of SSL-A and SSL-B is strongly tied to mineralogical and textural properties such as grain size, grain sorting, clay type and content, and carbonate cement. These are parameters that strongly control pore and pore throat size, permeability, capillary pressure, and wettability. Individual pores and pore throats in Spraberry sandstones are of relatively small sizes; this quality, in turn is related to the very fine sand and siltstone grain size of these rocks (J. Neasham, 1977). Clay types and amounts can affect pore and pore throat partitioning even in relatively small quantities (Crocker, 1983).

SSL-B has a more complex pore structure than SSL-A. This complexity is a function of finer grain size, increased occurrence of depositional shale laminae (as well as some organics), carbonate and silica cements, and increased effects of compaction. Owing to the presence of shale laminations in some samples, substantially reduced vertical permeability is noted when compared with SSL-A. These factors contribute to produce small pore size (these rocks are generally characterized by pores of less than 30 μm diameter) and pore throat size as well as a large standard deviation of pore and pore throat sizes. While varying little in total porosity from SSL-A sandstones, reduced permeability in SSL-B sandstones is a function of this smaller pore and pore throat size and slightly higher amounts of clays and carbonates.

SSL-D and SSL-F siltstones present varying degrees of heterogeneities, thus, as a result binary, skewed, and uniform pore size distributions are all noted. Lithologies are a mixture of: 1) micropore-dominated, shale/organic layers (distorted in the case of bioturbated rocks) and 2) primary intergranular pore-dominated sand layers with dolomite patches and dispersed clays. The pore systems of SSL-D differ from good reservoir rocks in that most of the porosity in these rocks is poorly interconnected and consists of intergranular mesopores (generally 5-15 μm diameter).

SSL-C and SSL-E are essentially nonporous and impermeable seal rocks. High-pressure mercury injection capillary pressure data indicate that displacement pressures are very high, ranging from 1000 to 15,000 psia. These tightly cemented samples have very small modal pore throat radii, ranging from 0.004 to 0.05 microns.

6.3 SIGNIFICANCE OF SMALL-SCALE LITHOFACIES ANALYSIS

Detailed analysis of the different types of rocks that form a sedimentary sequence is important where there is either potential for existence of recoverable hydrocarbons or actual oil production exist. In the upper Spraberry Formation lithofacies variability is strong, which make determination of cut-off values and pay zones a complex task. In order to be able to determine an accurate relation between different types of rocks and log response it is needed first a precise understanding of the small-scale lithofacies. Eventually an adequate assemblage of log tools should report good estimates of porosity, cements, amounts of clays, and saturation of oil and brine. In order to do so, these parameter have to be well understood with tangible data obtained by using analytical

techniques that can examine the rocks and fluids in a direct manner. For this reason the detail separation of the lithologic groups that form the upper Spraberry Formation is so important. These analysis form part of an ongoing project where rock and fluid characteristics are investigated by using geophysical log techniques. Large amounts of data can be obtained fast and relatively inexpensive for a large array of wells by using log analysis.

A second very important issue in the Spraberry Formation is the interrelation between different lithologies and fracturing. The information obtained from the analysis of small-scale lithofacies will be used in future studies that relate them to mechanical behavior and susceptibility to fracturing. Variation of parameters such as mineralogical composition, grain size, bed thickness, stress history affect the mechanical behavior of rocks making them be more or less brittle or ductile.

The recovery mechanisms are also affected by rock variability in the Spraberry Formation. The Spraberry reservoirs are typical naturally fractured reservoirs with extremely low permeability and usually marginal production. These types of reservoirs are dependent on fracture porosity to provide fluid conductivity and a substantial part of the oil storage. After five decades of marginal production, hardly 12% of the original oil in place have been recovered, leaving a very large amount of hydrocarbons stored in the porosity of the rock framework. Reservoir pressure and permeability are very low, making production by conventional means a far from easy task. Capillary pressures, small pores and pore throats and the particular wetting behavior of the Spraberry Formation are closely related to lithological variability. The heterogeneous character is believed to affect oil recovery, consequently, these circumstances lead to an effort to

extract more accurate geological information from the Spraberry Formation and its reservoirs. This information will provide the basis for investigation into the development of CO₂ injection technology to improve the low productivity and expand the recoverable reserve of the Spraberry Trend area.

CHAPTER 7

SUMMARY, CONCLUSIONS, AND RECOMENDATIONS

This thesis provides detailed geological characterization of old, naturally fractured reservoirs in the upper Spraberry Formation. Such studies are necessary in order to understand complicated lithological and fluid properties that affect reservoir recovery. The upper Spraberry reservoirs are a particularly important case, because considerable amounts of remaining oil reserves are still unrecovered. Historically the Spraberry Formation has faced many problems regarding the producibility of its numerous reservoirs. These are related to the very tight nature of the rock framework, which has very low permeabilities ranging from 0.1 to 0.5 md. However, the intense fracturing of the formation provides conduits for fluid flow. A key point that is the objective of extensive investigation deals with the fluid ability to transfer from the rock framework to the fractures from which recovery is actually performed.

This study formed part of a Department of Energy (DOE) founded project named: “Advanced Reservoir Characterization and Evaluation of CO₂ Gravity Drainage in the Naturally Fractured Spraberry Trend Area”. To understand the fluid/rock interaction during oil recovery using CO₂ injection we need to have a clear view of the actual

rock/fluid system. Information concerning lithofacies distribution, mineralogy, pore and pore throat systems, fluid saturation, capillary pressure and wettability behavior were investigated in order to apply an optimum recovery program in the future.

7.1 LITHOFACIES INTERPRETATION OF CORES AND SEDIMENTOLOGICAL ANALYSIS

A representative group of seven large-scale lithofacies (LSL) was extracted from two conventional cores covering the upper Spraberry Formation. These are the main sedimentary textures, structures and other features found in the intervals examined. The group of lithofacies was examined in the context of a depositional model developed by previous studies. The different lithofacies encountered were classified into two textural groups: 1) mudrock lithofacies from low energy environments, and 2) sandstone lithofacies from higher energy environments. Finely laminated facies are interpreted as related to cyclical annual depositional events. Whereas, thicker and massive very fine sandstones and siltstones are related to non-cyclical temporally random events (e.g. turbidity currents, hurricanes, earthquakes, and storm currents).

7.2 PETROGRAPHY AND DIAGENESIS

A detailed mineralogical study of thin sections, scanning electron microscopy and X-ray diffraction was performed using samples from three cores that cover the upper Spraberry Formation. Six small-scale lithofacies were described and analyzed based on

distinctive petrographic characteristics. Pore morphologies, degree of dissolution, mineralogy, rock textures, degree of compaction, and cementation were examined for each of these petrographic categories. Two clean and porous sandstones facies with good reservoir quality were found. One carbonate mudstone; one low porosity, dolomitic cemented siltstone; and two clay rich lithofacies were also found. Primary and secondary pores were the two main pore types detected.

Diagenetic processes have overprinted original depositional characteristics. However, original rock composition exerts the most important control on reservoir quality. Post-depositional processes included precipitation of quartz cement, clay diagenesis, migration of hydrocarbons, pyrite cementation, carbonate cementation, dissolution mechanisms, and fracture formation and mineralization. Controls that affect porosity are as follows.

1) *Quality damaging controls*

Authigenic illite

Argillaceous laminae

Quartz cement

Dolomite and ferroan dolomite cement

Tight packing of rock fabric related to initial very fine grain size and compactional effects.

2) *Quality enhancing controls*

Quartz-rich composition makes reservoir rocks relatively more resistant to compression forces and chemical effects.

Dissolution of unstable grains and cements such as feldspar and carbonate cements.

As a synthesis for the study on post depositional events, I have presented a diagenetic time-sequence for the upper Spraberry Formation. This sequence is based on evidence found during the petrographic analysis and different information and theories obtained from previous research. The paragenetic sequence constructed in this investigation improves our understanding of the different processes that control the quality of the Spraberry reservoirs.

7.3 PETROPHYSICAL DATA INTEGRATION WITH THIN SECTION CONTROLS

The results obtained from the geological characterization were integrated with a comprehensive set of petrophysical data. Here the small-scale lithofacies were studied as flow units in light of the new data for fluid flow and fluid distribution. These data include porosity from helium injection, permeability from nitrogen injection, grain density from weight difference, water and oil saturation using the Dean Stark method, and pore throat size distribution from mercury injection.

Water and oil saturation data show a close relationship between water saturation, porosity and lithological variability. The relationship between water saturation and lithology suggests that wettability may control fluid distribution in the system. Lithological variability controls the different petrophysical parameters: porosity, permeability, capillary pressure, pore throat size, and water saturation.

An interesting question regarding this analysis is how the fluids migration from shale to sandstone lithofacies. This concerns the possible preferential migration of hydrocarbons expelled from the clay and organic rich non-reservoir lithofacies (strongly water-wet) into the more weakly water-wet, sandy and porous lithofacies. Such expulsion is inferred from the fact that water is the dominant fluid phase in the clay/organic rich lithofacies, whereas oil saturation is much more abundant in the sandy and porous rocks.

The relationship between grain density and water saturation leads us to conclude that lithological controls strongly affect distribution of fluids within the upper Spraberry Reservoirs. To successfully use geophysical well logs it is important to recognize lithological character and reservoir quality. Physical properties such as grain density can affect the response of geophysical logs in such a way that rock properties can be estimated.

7.4 GENERAL CONCLUSIONS

Mineralogy, grain size, sedimentary structures, the presence of matrix-supported or grain-supported fabric and ultimately, reservoir quality, vary with lithofacies type. These parameters are in part controlled by depositional factors and affected by diagenetic changes. Lithological controls over reservoir quality are clay matrix content, carbonate content, presence of quartz overgrowths, and pressure solution of grains by compaction. It appears that there is no single factor producing a dominant control on reservoir quality and distribution of porosity. However, the different depositional and diagenetic effects that shape each of the lithofacies act in combination to produce distinct lithofacies

qualities. These sets of different qualities seem to occur in a continuum trend. These types of lithological trends are closely related to and control permeability, fluid saturation, wettability and capillary pressures.

Pore throat sizes and the distribution of the different types of pores and pore throats control permeability. The connectivity between pores is also very important. These are factors that are controlled in a complex manner by the lithological characteristics of each lithofacies group. It is difficult to assess the exact value of each control. Thus it makes sense to first evaluate each lithofacies or rock/fluid system as a separate group with the particular characteristics that make each of them distinct. Then the group of rock/fluid systems has to be understood as part of a total that presents certain specific trends.

The relationship between water saturation, wettability and capillary pressure is also controlled by variability in lithofacies type. Fluid distribution is controlled by forces that hold fluids to the very small pores and pore throats, not by gravity forces.

The factors that control fluid distribution in the upper Spraberry Formation are the strong capillary forces and the wetting affinity of certain fluids to a given type of mineralogical composition. This analysis greatly differs from the reservoir compartmentalization defined by Guevara (1988). He implied that fine stratification with intercalation of terrigenous and carbonate muds separate sandstones reservoirs and that each of them could present their own water/oil contact. Guevara's study (1988) coincides with our analysis in asserting the importance of capillary forces in hydrocarbon recovery from Spraberry reservoirs. However, there is no evidence of reservoir compartmentalization in the upper Spraberry Formation.

The area of the upper Spraberry Formation examined in this study exhibits six different rock/fluid groups, each with a distinct and complex mineralogical composition. In this framework of very tight rocks with a complex mineralogy, it is easy to expect a low permeability character and mixed or weakly-water wet behavior of the different rocks. Total porosity in the samples observed from the upper Spraberry reservoirs averages 14% and reaches a maximum of 18%. Nonetheless, permeability levels could be higher if pores and pore throats were larger. In general, the total amount of porosity is not the significant factor; the size of individual pores and pore throat apertures is the main control on the quality of the Spraberry reservoirs.

7.5 RECOMMENDATIONS

Another important issue in reservoir characterization is the utilization of geophysical well log analysis — using adequate software packages — to perform faster and practical estimations of reservoir parameters. In the upper Spraberry Formation large amounts of lab data have been obtained providing a much better understanding of geological and petrophysical problems. However, the actual scale of investigation is reduced to a few wells and covers a small area.

At this point, further investigation should concentrate on the implementation of log models based on measurable data applied to a larger number of wells, in order to create a regional evaluation that can be more plausibly used in field practice. Additional cores should be retrieved in those areas to add verification data for the rock/fluid model. When sufficient data are available, mapping of lithological groups can be conducted. In

this way definition of an improved and more accurate depositional model can be obtained. Application of this rock/fluid model to log studies of a regional scale based on maps and cross sections would serve as input data for better reservoir simulation and secondary recovery programs.

REFERENCES

- Adams, J. E., 1965, Stratigraphic-tectonic development of Delaware Basin: American Association of Petroleum Geologists Bulletin, v. 49, pp. 2140-2148.
- Ali, M., 1997, Improved geological characterization of old hydrocarbon fields with sparse control points: a case study from the Sulimar Queen field, southeast New Mexico, Ph.D. Dissertation, New Mexico Institute of Mining and Technology, Socorro, NM, 1997.
- Ames, L. L., Jr., 1959, The genesis of carbonate apatites: Economic Geology, v. 54, pp. 829-841.
- Basan, P. B., 1978, Trace Fossils Concepts, Society of Economic Paleontologist and Mineralogist, short course No.5,. P. 142-143.
- Bjørkum, P.A., 1994, How important is pressure in causing dissolution of quartz in sandstones? (Abs.): American Association of Petroleum Geologists Annual Convention, Denver – Official Program, v. 3, p. 105.
- Bjørkum, P.A., and Walderhaug, O., Aese, N.E., 1993, A model for the effect of illitization on porosity and quartz cementation of sandstones: Journal of Sedimentary Petrology, v. 63, p. 1089-1091.
- Bloch, S., 1994, Secondary porosity in sandstones: Significance, origin, relationship to subaerial unconformities, and effect on predrill reservoir quality prediction. From Wilson M. D., Reservoir quality assessment and prediction in clastic rocks, 1994, SEPM short course 30, p. 137-162.
- Bloch, S., and McGowen, J. H., 1994, Influence of depositional environment on reservoir quality prediction. From Wilson M. D., Reservoir quality assessment and prediction in clastic rocks, 1994, Society of Economic Paleontologist and Mineralogist, short course 30, p. 41-57.
- Bloomer, R. R., 1977, Depositional environment of a reservoir sandstones in West-Central Texas: American Association of Petroleum Geologists Bulletin, v. 61, pp. 344-359.
- Boggs, S. Jr., 1995, Principles of Sedimentology and Stratigraphy, Second Edition, University of Oregon, Prentice-Hall, Inc
- Boles, and Franks, S.G., 1979, Clay diagenesis in Wilcox sandstones of southwest Texas: Implications of smectite diagenesis on sandstone cementation, Journal of Sedimentary Petrology, v. 49, p. 55-70.
- Boles, and Johnson, K.S., 1983, Influence of mica surfaces on pore water pH: Chemical Geology, v. 43, p. 303-317.

- Bozanich, R.G., 1979, The Bell Canyon and Cherry Canyon Formations, eastern Delaware basin, Texas: lithology, environments and mechanisms of deposition, in Guadalupian Delaware Mountain Group of west Texas and southeast New Mexico: Society of Economic Paleontologists and Mineralogists Permian Basin sec. Pub. 79-18, p 121-141.
- Byers, C. W., 1977, Biofacies patterns in euxinic basins: a general model: in Deep-water carbonate environments: Society of Economic Paleontologists and Mineralogists, Special Publication 25, p. 5-17.
- Cather, M., and Schechter, D.S., 1997, "Fracture Characterization for the Upper Spraberry Formation," in quarterly report issued date 12/17/1997: Schechter, D.S., 1997, "Advance reservoir characterization and evaluation of CO2 gravity drainage in the naturally fractured Spraberry reservoirs," Department of Energy, award No.: DE-FC22-95BC14942.
- Cheney, M.G. and Goss, L.F., 1952, Tectonics of Central Texas: American Association of Petroleum Geologists Bulletin, v. 36, pp. 2237-2265.
- Cherney, J., 1998, Investigation of Anisotropy from Spraberry Horizontal Core at In-situ Stress Conditions, New Mexico Tech and the Petroleum Recovery Research Center, Paper presented at the Naturally Fractured Reservoir Forum of October 27, 1998.
- Cordell, R. J., 1977, How oil migrates in clastic sediments: World Oil, v. 184, pp. 36-38.
- Crocker, M.E. and Donaldson, E.C., 1983, Comparison and analysis of reservoir rocks and related clays, Society of Petroleum Engineers, Society of Petroleum Engineers, paper 11073, Annual Technical Conference and Exhibition held in San Francisco, CA, October 5-8.
- Dutton, S. P., 1980, Petroleum source rock potential and thermal maturity, Palo Duro basin, Texas: University of Texas Bureau of Economic Geology, Geological Circulation, 80-10, 48 p.
- Eslinger, E., and Pevear, D., 1988, Clay Minerals for petroleum geologist and engineers: Society of Economic Paleontologist and Mineralogist, short course notes No. 22., Tulsa OK.
- Folk, R.L., 1989, Reconnaissance of Spraberry and Dean Thin Sections, unpublished manuscript by Robert L. Folk, University of Texas at Austin, Geological Science Department.

- Gautier, D.L., 1985, Interpretation of early diagenesis in ancient marine sediments, in Gautier, D.L., Kharaka, Y.K., and Surdam, R.C., eds., Relationship of organic matter and mineral diagenesis: Short Course Notes No. 17, Society of Economic Paleontologists and Mineralogists, p. 6-78.
- Guevara, E. H., 1988, Geological characterization of Permian submarine fan reservoirs of the Driver waterflood Unit, Spraberry Trend, Midland Basin, Texas; Bureau of Economic Geology, University of Texas at Austin; Report of Investigation No. 172.
- Guo, B., Schechter, D.S., 1997, "An analysis on Productivity of Spraberry Trend Wells," in "Advanced Reservoir Characterization and Evaluation of CO₂ Gravity Drainage in the Naturally Fractured Spraberry Trend Area," annual report, Contracts No. DEFC2295BC14942, U.S., Department of Energy.
- Handford, C. R., 1981, Deep-water facies of the Spraberry Formation (Permian), Reagan County, Texas; a core workshop (No. 2); Siemers, Tillman, and Williamson.
- Harrington, J.W., 1963, Opinion of structural mechanics of Central Basin Platform, West Texas; American Association of Petroleum Geologists Bulletin, v. 47, pp. 2023-2038.
- Heald, M.T., and Larese, R.E. 1974, Influence of coatings in quartz cementation: Journal of Sedimentary Petrology, v.44, p. 1269-1274.
- Heald, M.T., and Renton, J.J., 1966, Experimental study of sandstone cementation: Journal of Sedimentary Petrology, v. 36, p. 977-991.
- Heller, J.P., 1992, The PRRC Automatic Scanning Minipermeameter: Petroleum Recovery Research Center, report No. 92-20, New Mexico Institute of Mining and Technology, 14 pp.
- Hoffman, J., and Hower, J., 1979, Clay mineral assemblages as low grade metamorphic geothermometers: application to the thrust faulted disturbed belt of Montana, U.S.A., in P.A. Scholler and P.R. Schluger, eds., Aspects of diagenesis: Society of Economic Paleontologists and Mineralogists, Special Publication No. 26, p. 55-79.
- Horak, R.L., 1985, Tectonic and hydrocarbon maturation history in the Permian Basin, Oil and Gas Journal, May 27, p. 124.
- Houde, R. F., 1979, Sedimentology, diagenesis, and source bed geochemistry of the Spraberry sandstone, subsurface Midland Basin, west Texas, MS thesis, University of Texas at Dallas.

- Hower, J., 1981, Shale diagenesis, clays and the resource geologist, in Longstaffe, F.J., (ed.), short course handbook: Mineralogical Association of Canada, p. 199.
- Hower, J., Eslinger, E., Hower, M.E., and Perry, E.A., 1976, "Mechanism of Burial Metamorphism of Argillaceous Sediments: 1. Mineralogical and Chemical Evidence", Geological Society of America Bulletin, v.87, pp. 725-737.
- Hubbert, M., and Willis, D.G., 1955, Important fractured reservoirs in the United States: in proceedings of the fourth World Petroleum Congress, Rome, Section I, pp. 58-71.
- Hutcheon, I., and Abercrombie, H.J., 1990a, Carbon dioxide in clastic rocks and silicate hydrolysis: *Geology*, v. 18, p. 541-544.
- Jadgozinski, H., 1949, Eindimensionale Felordnung in Kristallen und ihr Einfluss auf die Rontgeninterferenzen. I. Berechnung des Fehlordnungsgrades aus der Rontgenintensitaten: *Acta Crystallography*, 2, 201-207.
- Jeary, D. R., 1978, Leonardian strata of northern Midland basin of west Texas (abs.): *American Association of Petroleum Geologists Bulletin*, v. 62, p.526.
- Katz, A., 1971, Zoned dolomite crystals: *Journal of Geology*, v. 79, pp. 38-51
- Krumbein, W. C., and Garrels, R. M., 1952, Origin and classification of chemical sediments in terms of pH and oxidation-reduction potentials: *Journal of Geology*, v. 60 pp. 1-33.
- Lorenz, J. C., Teufel, L. W., and Warpinski, N. R., 1991, Regional fractures 1: A mechanism for the formation of regional fractures at depth in flat-lying reservoirs. *American Association of Petroleum Geologists Bulletin*, V. 75, no. 11, p. 1714-1737.
- Lorenz, J. C., 1997, Non-Congruent Natural Fracture Sets in Adjacent Beds at Depth: Data From Horizontal Cores from the Spraberry Formation, Midland Basin, TX, presented at: American Association of Petroleum Geologists, Hedberg Research Conference, Reservoir Scale Deformation – Characterization and Prediction, June 22-28, 1997, Bryce, Utah.
- Lynch, F.L., 1986, Stoichiometry of the smectite-to-illite reaction, MSc Thesis, Dartmouth College.
- MacGowan, D.V., Surdam, R.C., and Ewing, R.E., 1990, The effect of carboxylic acid anions on the stability of framework mineral grains in petroleum reservoirs: *Society of Petroleum Engineers Formation Evaluation*, v.5, p. 161-166.

- Manheim, F., Rowe, G. T., and Jipa, D., 1975, Marine phosphorite formation off Peru: *Journal Sedimentary Petrology*, v. 45, pp. 243-251.
- McBride, E.F., 1989, Quartz cementation in sandstones: a review: *Earth Science Reviews*, 26, p. 69-112.
- Meshri, I.D., 1986, On the reactivation of carbonic and organic acids and generation of secondary porosity, in D.L. Gautier, ed., *Roles of organic matter in sediment diagenesis: Society of Economic Paleontologists and Mineralogists Special Publication No. 38*, p. 123-128.
- Miall, A.D., 1990, *Principles Of Sedimentary Basin Analysis*, 2nd edition. New York: Springer, 1990.
- Midland Map Company, 1993, Producing zone map. The Permian Basin, west Texas and southeast New Mexico. Midland, Texas.
- Moor, D.M. and Reynolds, R.C., 1989, *X-ray Diffraction And The Identification And Analysis Of Clay Minerals*: London, Oxford University Press.
- Mullis, A., 1992, A numerical model for porosity modification at a sandstone-mudstone boundary by quartz pressure solution and diffusive mass transfer: *Sedimentology*, v. 39, p. 233-239.
- Neasham, John W., 1977, The morphology of dispersed clay in sandstones reservoirs and its effect on sandstones shaliness, pore space and fluid flow properties, Society of Petroleum Engineers, Society of Petroleum Engineers, paper 6858, Annual Technical Conference and Exhibition held in Denver, CO, October 9-12, Shell Development Company
- Oelkers, E.H., Bjørkum P.A., and Murphy, W.M., 1992, The mechanism of porosity reduction, stylolite development and quartz cementation in North Sea sandstones, in N.K. Kharaka and A.S. Maest, eds., *Water-Rock Interaction, Vol II*: A.A. Balkema, Rotterdam, p. 1183-1186.
- Pittman, Larese and Heald, 1992, Clay Coats: Occurrence and relevance to preservation of porosity, in Houseknecht and Pittman, Eds., *Origin, Diagenesis, and Petrophysics of Clay Minerals in Sandstones: Society of Economic Paleontologists and Mineralogists, Special Publication No. 47*, p.241-255.
- Reservoirs Inc., 1996, Internal report: Core analysis, Parker & Parsley Development, L. P. Midland County, Texas
- Robin, M., and Rosenberg, E., 1995, Wettability studies at the pore level: a new approach by use of Cryo-SEM, Society of Petroleum Engineers, Formation Evaluation, March 1995, from the Institute Francais du Pétrole, and Omar Fassi-Fihri.

- Saleta, C.J., Banik, A.K., Cather, M.E., and Schechter, D.S., 1996, Application of Analytical Techniques to Evaluate the Heterogeneities of the Upper Spraberry Formation (Permian) and Its Influence on the Quality of the Reservoirs; poster presentation at the Permian Basin Oil & Gas Recovery Conference, Society of Petroleum Engineers, SPE 35225, Midland, Texas.
- Schechter, D.S., and Guo, B., 1998, An integrated investigation for design of a CO₂ pilot in Naturally fractured Spraberry Trend area, west Texas, Society of Petroleum Engineers, Inc., SPE 39881 paper presented at the International petroleum conference and exhibition held in Villahermosa, Mexico, 3-5 March, 1998.
- Schmitt, G. T., 1954, Genesis and depositional history of Spraberry Formation, Midland Basin: American Association of Petroleum Geologists Bulletin, v. 38, pp. 1957-1978.
- Silver, B. A., and Todd, R.G., 1969, Permian cyclic strata, northern Midland and Delaware Basins, West Texas and Southeastern New Mexico: American Association of Petroleum Geologists Bulletin, v. 53, pp. 2223-2251.
- Smith, J.T., and Ehrenberg, 1989, Correlation of carbon dioxide abundance with temperature in clastic hydrocarbon reservoirs: Relationship to inorganic chemical equilibrium: Marine and Petroleum Geology, v. 6, p. 129-135.
- Surdam, R.C., MacGowan, D.B., and Dunn, T.L., 1989, Diagenetic pathways of sandstone/shale systems: Contributions to Geology, University of Wyoming Press, Laramie, WY, p. 43-58.
- Surdam, R.C., Crossey, L.J., Hagen, E.S., and Haesler, H.P., 1989, Organic-inorganic interpretations and sandstone diagenesis: American Association of Petroleum Geologists Bulletin, v. 73, p. 1-23.
- Thomson, A., 1959, Pressure solution and porosity, in H.A. Irland, ed., Silica in Sediments: Society of Economic Paleontologists and Mineralogists, Special Publication 7, p. 92-111.
- Tyler, N. and Gholston, J. C., 1988, Heterogeneous deep-sea fan reservoirs, Shackelford and Preston waterflood units, Spraberry Trend, West Texas; Bureau of Economic Geology, University of Texas at Austin, Report of Investigation No. 171.
- Van der Plas, L., and Tobi, A.C. 1965, A chart for judging the reliability of point counting results: American Journal of Sciences, v. 263, p. 87-90.
- Walker, T. R., 1978, Deep-water sandstone facies and ancient submarine fans: Models for exploration of stratigraphic traps: American Association of Petroleum Geologists Bulletin, v. 62, pp. 932-966.

- Waldschmitt, W. A., 1952, Some microscopic characteristics: *The Petroleum Engineer*, v. 24, pp. B-54-B-58.
- Warn, F. G. and Sidwell, R., 1953, Petrology of the Spraberry Sands of West Texas: *Journal of Sedimentary Petrology*, v. 23, pp. 67-74.
- Wilson, M.D., Stanton, J.H., 1994, Diagenetic mechanisms of porosity and permeability reduction enhancement, in Wilson, M.D., *Reservoir quality assessment and prediction in clastic rocks*, Society of Sedimentary Geology, short course No. 30, p. 59.
- Wilson, M.D., 1994, Measurement of independent variables – hydrocarbon emplacement, clay content, textural measurements, in Wilson, M.D., *Reservoir quality assessment and prediction in clastic rocks*, Society of Sedimentary Geology, short course No. 30, p. 321.
- Winfrey, K.E., 1995, Post-Permian folding and fracturing of the Spraberry Formation within the Midland Basin, *West Texas Geological Society*, v. 35, number 3.
- Wright, F., 1962, Abo Reef: Prime west Texas target: *Oil & Gas Journal*, July 30 (1st part), v. 60, pp. 226-235 and August 6 (2nd part), v. 60, pp. 188-194.
- Yanfidra, 1998, A study of imbibition mechanisms in the naturally fractured Spraberry Trend area, Masters Thesis, New Mexico Institute of Mining and Technology, Socorro, NM.

APPENDIX

Petrographic data for the Upper Spraberry Formation

- Total Thin Section Point Count Analysis for Three Cored Wells

Petrophysic data for the Upper Spraberry formation

- Computer Controlled Scanning Air-Minipermeameter Data for Two Cored Wells
- Whole Core Analysis Data: Nitrogen and Helium Injection and Dean Stark Water Saturation for Two Cored Wells
- Mercury Injection Data for Two Cored Wells

Table 1 - POINT COUNT ANALYSIS - E.T O'DANIEL #37 CORED WELL - UPPER SPRABERRY FORMATION - 300 POINT COUNTED BY THIN SECTION		GRAIN COMPOSITION													MATRIX				CEMENT COMPOSITION				POROSITY							
SAMPLE LABEL & DEPTH (ft)	ROCK TYPE	TEXTURE		GRAIN COMPOSITION													MATRIX				CEMENT COMPOSITION				POROSITY					
		GRAIN SIZE (µm)	SORTING	MONOCRYSTALLINE QTZ	POLYCRYSTALLINE QTZ	CHERT	MUSCOVITE	PLAGIOCLASE	K-FELDSPAR	IRF	MRF	SRF	CARBONATE FRAGMENTS	ACCESSORY MINERALS	LAMINAR	DISPERSED	ORGANICS	DEPOSITIONAL CARBONATE	UNDIFFERENTIATED CLAY	QUARTZ OVERGROWTHS	CALCITE	DOLOMITE	PYRITE	PRIMARY	SECONDARY	MICRO	TOTAL POROSITY			
ET1/7050	F	40	W-MW	34.6	1.0	0.0	4.7	10.0	4.3	0.0	1.7	0.0	0.0	19.5	0.0	5.3	8.7	1.0	0.0	0.0	0.0	4.0	5.0	1.0	0.0	0.0	0.0	0.0		
ET2/7066	A	60	W	37.3	3.7	0.0	2.0	14.7	4.3	0.0	0.0	0.0	0.0	2.3	0.0	0.7	3.7	8.3	5.7	0.0	4.3	0.0	10.0	3.0	0.0	13.0				
ET3/7093.5	B	58	W-MW	29.6	1.0	0.0	3.7	13.3	8.7	0.7	0.0	0.0	0.0	7.3	1.7	2.0	5.3	4.3	6.3	0.0	4.0	2.0	4.0	1.0	1.7	0.0	5.7			
ET0/7131.8	B	62	W	37.0	0.0	Tr	2.0	17.3	3.7	0.0	1.3	1.0	0.0	1.3	0.7	1.3	2.0	4.0	11.0	5.0	0.0	3.7	3.0	2.7	3.0	0.0	5.7			
ET4/7149	F	54	W	41.3	2.3	0.0	3.0	13.7	1.3	0.7	0.0	0.0	0.0	3.3	0.0	0.7	3.3	4.0	4.7	1.0	4.0	3.0	1.3	0.0	1.0	2.0				
ET5/7195.4	E	52	W	44.3	0.0	0.0	1.0	7.3	3.0	0.0	1.0	0.3	2.3	1.7	2.0	0.0	4.3	4.7	0.0	1.3	0.0	1.7	2.0	0.0	0.0	0.0	0.0			
ET6/7206.9	C	60	W-MW	22.3	0.0	0.0	0.3	5.7	1.0	0.0	0.0	0.0	0.0	1.7	0.0	0.3	31.0	0.0	0.0	0.0	1.7	27.3	0.0	0.0	0.0	0.0	0.0	0.0		
ET7/7213.5	E	62	W-MW	33.3	3.3	0.3	4.0	6.3	1.7	0.7	0.0	2.0	0.3	35.3	0.0	5.7	1.7	0.0	0.0	0.0	2.3	2.0	0.3	0.0	0.0	0.0	0.0			
ET8/7221.9	B	62	MS	42.3	3.7	0.0	2.3	15.3	5.0	0.0	1.0	0.0	0.0	3.3	0.0	2.3	1.3	6.3	5.7	0.0	1.0	0.0	4.3	1.3	0.0	5.7				
ET9/7223	B	62	W	41.7	5.0	0.0	2.7	7.3	7.7	Tr	0.7	2.0	0.0	2.3	7.3	0.0	1.0	3.3	3.0	5.0	0.0	4.7	1.7	2.3	2.0	0.0	4.3			
ET10/7223.9	B	60	W	44.6	5.7	0.0	1.3	6.3	7.3	0.0	0.0	1.3	Tr	1.3	9.0	0.0	0.7	2.7	3.7	6.3	0.0	3.7	2.3	2.0	1.7	0.0	4.3			
ET11/7228.3	A	45	W	40.0	2.7	0.0	1.0	14.7	4.3	1.0	0.0	0.0	0.0	2.3	0.0	0.0	2.0	4.7	5.7	0.0	7.0	0.0	11.0	3.7	0.0	14.7				
ET12H2/7228.45	A	52	W	39.3	4.7	0.0	2.3	11.3	7.3	0.7	0.0	0.0	0.0	4.3	0.0	0.0	6.0	3.0	4.3	0.0	5.0	0.0	7.3	3.0	0.0	10.3				
ET12-1/7230.3	A	55	W	37.0	2.0	0.0	1.0	16.7	8.7	0.0	1.0	0.0	1.0	0.0	1.0	0.0	5.7	4.0	4.3	0.3	5.3	0.0	9.3	2.7	0.0	12.0				
ET13H4/7232	B	52	W	42.7	2.3	0.0	1.0	12.3	9.3	0.0	1.0	2.7	0.0	1.3	0.0	0.0	4.0	1.0	3.7	0.0	4.3	1.3	1.7	2.3	0.0	10.0				
ET14H5/7232.17	A	57	W	37.3	1.7	Tr	2.0	14.3	8.0	1.0	0.0	2.7	0.0	1.3	3.3	0.0	3.0	2.7	5.0	0.0	3.7	0.0	9.7	3.7	0.0	13.3				
ET15H6/7232.25	B	58	W	45.0	0.7	0.0	1.7	8.0	10.7	0.0	1.7	1.0	0.0	5.0	0.0	0.0	3.7	2.7	4.3	0.0	3.0	1.0	1.0	3.0	0.0	10.0				
ET16H7/7232.34	B	58	W	44.7	0.7	0.0	1.7	11.0	6.7	0.0	1.3	Tr	0.0	3.7	1.3	1.7	5.0	3.3	5.7	0.0	2.3	1.7	6.3	3.0	0.0	9.3				
ET17H8/7232.45	B	58	W	38.7	3.7	0.0	2.3	15.0	4.7	0.0	1.0	0.0	0.0	3.0	0.0	0.0	3.3	3.7	4.3	0.0	5.3	0.0	6.0	2.0	0.0	10.0				
ET18H9/7233	A	58	W	43.0	4.0	0.0	0.3	9.0	14.7	0.0	0.0	0.0	0.0	0.3	4.0	0.0	2.0	1.3	5.3	0.0	4.7	0.0	8.3	3.0	0.0	11.3				
ET19/7236.7	A	56	W-MW	36.0	3.0	Tr	1.0	12.3	6.0	2.0	4.0	0.0	0.0	0.0	2.0	0.0	5.7	3.0	4.0	0.0	4.7	2.0	9.3	4.0	1.0	14.3				
ET20/7237.6	B	58	W	47.0	5.0	0.0	0.7	9.7	11.7	0.0	0.0	0.0	Tr	1.3	3.3	0.0	Tr	3.7	5.7	4.0	0.0	4.0	0.0	4.0	0.0	0.0	4.0			
ET21-1/7238.7	B	40	W	33.3	1.0	0.0	2.7	10.0	4.3	1.7	1.0	0.0	0.0	1.0	1.0	2.0	5.3	3.7	7.0	3.3	0.0	4.7	4.0	0.3	0.0	6.7				

SAMPLE LABEL & DEPTH (ft)		TEXTURE		GRAIN COMPOSITION										MATRIX					CEMENT COMPOSITION					POROSITY				
		ROCK TYPE	GRAIN SIZE (µm)	SORTING	MONOCRYSTALLINE QTZ.	POLYCRYSTALLINE QTZ.	CHERT	MUSCOVITE	PLAGIOCLASE	K-FELDSPAR	IRF	MRF	SRF	CARBONATE FRAGMENTS	ACCESSORY MINERALS	LAMINAR	DISPERSED	ORGANICS	DEPOSITIONAL CARBONATE	UNDIFFERENTIATED CLAY	QUARTZ OVERGROWTHS	CALCITE	DOLOMITE	PYRITE	PRIMARY	SECONDARY	MICRO	TOTAL POROSITY
Plog5 / 7068.50	B	45	W	40.7	1.7	0.0	1.7	5.0	7.0	0.0	0.0	0.0	0.0	1.3	6.3	0.0	2.7	0.3	12.7	3.7	0.0	2.3	3.0	5.7	0.3	0.0	5.7	
SPX5 / 7069.00	F	46	MW	37.7	1.0	Tr	2.0	11.3	5.3	0.0	0.7	0.7	0.0	1.0	10.3	8.0	2.3	2.0	7.3	4.0	0.0	2.3	2.3	1.7	0.0	0.0	1.7	
Plog6 / 7069.50	A	56	W	45.3	0.0	0.0	0.7	13.3	4.0	0.7	1.3	Tr	0.0	1.3	8.7	0.0	1.3	4.0	5.3	6.3	0.0	3.7	0.7	4.3	3.0	0.0	7.2	
SPX4 / 7070.50	F	58	W	42.7	4.0	0.0	1.3	7.3	11.7	0.3	0.7	0.0	0.0	0.7	14.3	0.0	0.7	2.3	5.7	2.7	0.0	1.7	0.0	4.0	0.0	0.0	4.0	
Plog10 / 7073.50	E	46	W	23.7	0.0	0.0	4.3	4.0	2.7	0.0	0.0	0.0	0.0	0.0	44.0	2.7	8.7	1.3	4.3	0.0	0.0	0.7	3.7	0.0	0.0	0.0	0.0	
SPX3 / 7076.50	C	50	MW	19.7	0.0	Tr	1.7	3.3	1.3	0.0	0.0	0.0	0.0	0.0	2.7	0.0	0.0	38.3	0.0	0.0	3.3	25.3	0.7	0.0	0.0	0.0	0.0	
SPX6 / 7080.00	F	56	W	35.7	2.3	0.0	5.0	12.7	6.0	0.0	0.0	Tr	0.0	0.0	15.3	1.0	4.7	2.7	5.3	2.0	0.0	1.7	3.7	2.0	0.0	0.0	2.0	
SPX7 / 7081.50	E	28	MW	24.0	0.0	0.0	5.3	3.0	0.7	0.0	0.3	0.0	0.0	0.0	3.7	25.3	1.0	8.0	1.3	20.7	0.0	0.0	0.0	6.7	0.0	0.0	0.0	
SPX2 / 7083.30	B	50	MW	40.0	3.0	0.0	1.0	11.0	4.3	0.0	1.3	0.0	1.0	0.0	5.3	1.3	0.0	7.7	2.7	3.7	0.0	6.7	1.7	8.3	2.7	1.3	12.3	
Plog21 / 7084.50	A	62	W	40.7	1.3	0.3	2.0	13.7	3.7	0.0	0.0	0.0	0.0	2.3	0.0	0.0	Tr	2.0	4.3	5.3	0.0	7.3	0.0	12.3	4.7	0.0	17.0	
SPX6 / 7085.00	A	62	W	39.7	4.3	0.0	0.0	8.7	5.0	1.3	0.0	0.0	1.0	0.0	0.0	3.0	0.0	5.3	3.7	6.0	0.0	3.7	1.7	12.7	5.3	0.0	15.0	
SPX9 / 7087.00	A	64	VW	42.0	1.0	0.0	0.7	7.3	11.7	1.7	0.0	0.0	0.0	0.0	0.0	4.3	0.0	4.0	2.7	5.7	0.0	2.7	0.0	10.7	5.7	0.0	16.3	
Plog22 / 7087.50	A	64	W	41.3	2.7	0.3	14.3	5.7	14.3	3.7	1.3	0.0	0.0	0.0	0.0	0.0	0.0	3.3	4.0	7.0	0.0	2.7	0.7	13.0	3.3	0.0	16.3	
SPX10 / 7088.00	E	32	MW	36.3	0.0	0.0	7.7	1.3	1.3	0.3	0.0	0.3	0.0	1.0	29.3	0.7	5.3	0.0	14.3	0.0	0.0	0.0	2.0	0.0	0.0	0.0	0.0	
Plog23 / 7088.50	D	56	MW	27.3	0.0	0.0	0.0	9.0	3.7	0.3	0.7	0.0	0.0	0.0	4.3	3.3	2.7	2.5	0.0	0.0	0.0	13.7	3.0	4.3	3.0	0.0	6.3	
SPX11 / 7089.20	D	56	MW	34.0	1.7	0.0	2.3	6.3	3.0	0.0	0.3	0.0	1.0	0.0	2.0	1.3	1.3	14.3	3.0	4.7	3.0	15.3	0.0	3.3	4.0	0.0	7.3	
SPX12 / 7090.00	D	56	MW	39.3	2.3	0.0	1.7	5.0	3.0	0.3	0.0	0.3	0.0	0.0	1.0	1.7	0.0	15.3	1.0	2.3	1.7	16.0	0.0	3.7	2.3	0.0	6.0	
Plog25 / 7090.50	D	58	MW	37.0	1.0	0.0	0.0	6.7	3.3	0.0	0.0	0.0	0.0	0.7	0.0	1.7	1.3	0.0	19.0	0.0	4.0	2.3	18.3	0.0	2.7	2.0	0.0	4.7
SPX13 / 7091.00	A	65	W	38.3	6.0	0.0	1.7	10.3	6.3	1.0	0.0	0.0	0.0	1.3	0.0	2.7	0.0	3.3	4.3	6.7	0.0	4.7	0.0	9.3	4.0	0.0	13.3	

SPX14 / 7092.67	A	65	W	44.7	2.0	0.0	2.7	6.3	9.0	0.0	Tr	0.0	0.0	0.0	0.0	0.0	2.0	0.0	4.3	2.0	4.3	0.0	3.0	0.0	13.3	5.3	0.0	18.7	
SPX15 / 7093.76	E	38	MW	21.3	0.0	0.0	6.3	2.7	2.0	0.0	0.0	0.0	0.0	0.0	0.0	0.0	35.3	2.3	3.3	0.0	16.3	0.0	0.0	0.0	0.0	0.0	0.0	0.3	0.3
SPX16 / 7095.00	F	46	MW	40.0	0.0	0.0	5.3	13.3	4.3	0.7	0.3	0.0	0.0	0.0	0.0	16.0	5.7	1.3	2.3	2.7	2.0	0.0	2.7	0.0	2.7	0.0	0.7	3.3	3.3
SPX17 / 7097.25	E	54	MW	37.7	2.7	0.0	6.7	12.7	7.7	0.0	0.0	0.0	0.0	0.0	0.0	0.0	3.0	0.0	2.0	5.7	3.7	0.0	5.3	0.0	5.7	3.3	0.0	13.0	13.0
SPX17 / 7099.80	B	60	W	42.3	1.7	0.0	2.0	11.3	5.0	0.0	1.0	0.0	0.7	0.0	0.0	6.7	0.0	1.3	2.0	6.3	5.0	0.0	2.7	1.0	6.3	4.7	0.0	11.0	11.0
PLOG35 / 7100.50	A	56	MW	46.0	1.0	1.0	6.7	13.0	6.3	0.0	0.0	0.0	0.0	1.0	0.0	6.0	3.3	0.0	2.7	5.3	4.3	0.0	2.7	0.0	6.0	5.7	0.0	9.3	9.3
PLOG36 / 7101.50	F	58	MW	38.7	0.0	0.0	2.0	11.3	6.7	0.0	0.0	0.0	0.0	0.0	0.0	17.0	3.3	4.7	2.7	9.3	0.0	0.0	3.3	0.0	1.0	0.0	Tr	1.0	1.0
SPX26 / 7102.67	E	36	MW	35.0	3.3	0.0	3.3	13.7	5.0	0.0	0.7	0.0	0.0	0.0	0.0	5.0	6.0	5.0	3.3	6.3	2.7	0.0	2.3	4.0	4.7	5.0	0.0	2.7	2.7
SPX27 / 7104.00	C	50	MW	23.3	0.0	0.0	2.0	4.0	2.7	0.7	0.3	0.0	0.0	0.0	0.0	1.3	2.7	8.7	2.50	4.3	0.0	0.0	21.3	3.7	0.0	0.0	0.0	0.0	0.0
SPX28 / 7105.76	F	56	MW	42.3	0.0	0.0	3.3	12.7	4.7	0.0	0.0	0.0	0.0	0.0	0.0	4.3	1.7	2.3	3.0	3.7	2.0	0.0	4.3	0.0	3.3	0.7	0.0	4.0	4.0
PLOG42 / 7107.50	B	48	MW	38.0	1.0	0.0	3.0	10.3	6.3	0.0	0.0	0.0	0.0	0.0	0.0	2.7	1.7	2.7	4.3	9.3	3.3	0.0	3.3	1.0	5.7	4.3	0.0	10.0	10.0
SPX25 / 7107.76	E	53	MW	39.7	2.7	1.7	1.7	14.7	3.3	0.0	0.0	1.0	0.0	0.0	0.0	0.0	0.0	3.7	2.3	3.7	3.0	0.0	3.0	3.0	7.0	0.0	1.3	6.3	6.3
PLOG44 / 7109.5	B	50	M	38.7	1.7	0.0	4.7	11.7	5.7	0.0	0.7	0.0	1.0	3.7	5.7	2.0	2.0	6.0	6.0	2.3	2.7	0.0	3.7	1.7	2.7	2.0	1.7	6.3	6.3
SPX30 / 7110.46	F	56	MW	36.7	1.3	0.0	2.0	16.3	4.7	0.3	0.0	0.0	Tr	0.0	7.3	4.3	3.7	4.7	2.7	3.3	0.0	3.7	0.0	4.7	2.3	0.0	7.0	7.0	
PLOG45 / 7110.80	E	44	MW	21.0	0.0	0.0	7.3	4.3	3.7	0.0	0.7	0.3	0.0	0.0	0.0	30.3	3.3	9.7	2.0	15.0	0.0	0.0	1.7	0.0	0.0	0.0	0.7	0.7	0.7
PLOG46 / 7111.56	E	44	MW	28.3	0.0	0.0	6.7	6.3	5.3	0.0	0.0	0.0	0.0	0.0	0.0	25.7	2.3	7.7	2.3	16.3	0.0	0.0	1.0	0.0	0.0	0.0	1.0	1.0	1.0

Cont. Table 2

SAMPLE LABEL & DEPTH (ft)		Table 3 - POINT COUNT ANALYSIS - A. JUDKINS #5 - CORED WELL - UPPER SPRABERRY FORMATION - 300 POINT COUNTED BY THIN SECTION																											
		TEXTURE			GRAIN COMPOSITION							MATRIX			CEMENT COMPOSITION			POROSITY											
PETROGRAPHIC CATEGORY		GRAIN SIZE (µm)	SORTING	MONOCRYSTALLINE QTZ.	POLYCRYSTALLINE QTZ.	CHERT	MUSCOVITE	PLAGIOCLASE	K-FELDSPAR	IRF	MRF	SRF	CARBONATE FRAGMENTS	ACCESSORY MINERALS	LAMINAR	DISPERSED	ORGANICS	DEPOSITIONAL CARBONATE	UNDIFFERENTIATED CLAY	QUARTZ OVERGROWTHS	CALCITE	DOLOMITE	PYRITE	PRIMARY	SECONDARY	MICRO	TOTAL POROSITY		
J15b / 7035.0	C	57	W-MW	33.7	0.0	0.3	0.7	5.3	2.0	0.3	0.7	0.0	0.0	0.0	3.3	0.0	26.3	0.0	0.0	0.0	3.3	3.3	0.0	0.0	0.0	0.0	0.0	1.0	0.0
J14a / 7035.0	B	66	W-MW	40.0	3.3	1.3	1.0	10.7	4.3	0.0	1.7	Tr	0.0	2.0	3.3	0.0	1.7	4.0	2.3	4.7	0.0	8.7	1.3	6.7	3.0	0.0	0.0	0.0	9.7
J15a / 7035.0	D	66	W-MW	37.3	4.7	0.0	2.0	6.3	3.0	0.0	0.3	0.0	1.0	0.0	2.0	3.3	1.3	9.3	3.0	4.7	3.0	14.7	0.0	2.7	3.3	0.0	0.0	0.0	6.0
J15bg / 7038.5	D	60	W-MW	34.3	2.0	0.0	1.0	5.7	3.7	0.0	0.0	0.0	0.7	0.0	1.7	0.0	2.3	19.0	2.7	3.0	2.3	18.3	0.0	2.0	1.3	Tr	Tr	3.3	
J16a / 7039.0	A	54	W	39.7	4.7	Tr	0.7	9.0	10.3	0.0	0.7	0.0	0.0	0.3	2.0	0.0	1.7	3.3	2.7	5.3	0.0	4.7	0.7	10.3	4.0	0.0	0.0	4.3	
J17a / 7041.0	B	66	W	43.3	3.0	0.0	0.3	12.0	6.0	0.0	0.0	1.3	0.0	0.0	1.3	1.3	0.0	5.7	0.7	7.0	0.0	7.7	1.7	6.3	2.3	0.0	0.0	8.7	
J18a / 7042.0	A	56	W	44.0	1.3	1.7	0.3	14.0	4.3	1.0	0.3	0.0	0.3	2.3	0.0	0.0	0.0	1.7	4.3	5.3	0.0	7.0	0.0	7.3	4.0	0.0	0.0	1.3	
J19a / 7045.0	B	58	W	42.0	3.0	0.0	1.0	11.0	5.3	0.0	1.3	0.0	0.0	0.0	3.3	1.3	0.0	7.7	2.7	3.7	0.0	6.7	1.7	5.7	3.7	0.0	0.0	9.3	
J21 / 7051	F	58	W-MW	43.3	0.0	0.3	0.7	13.3	4.0	0.7	1.3	0.0	1.3	1.3	5.3	0.0	3.0	4.0	3.3	6.3	0.0	3.7	0.7	4.0	4.7	0.0	0.0	9.0	
J24 / 7059.5	B	56	W	37.7	1.0	0.0	3.0	10.3	6.3	0.0	0.0	0.3	0.0	3.0	4.7	1.7	3.0	4.3	5.3	4.3	0.0	5.3	2.3	4.3	3.0	0.0	0.0	7.3	
J26b / 7063.5	F	58	W	40.0	3.0	0.0	1.0	11.0	4.3	0.0	0.0	1.0	0.0	0.0	5.0	3.2	2.7	6.0	4.7	4.7	0.0	5.3	2.7	3.3	3.0	0.0	0.0	4.3	
J28B / 7066.5	E	25	MW	28.3	0.0	0.0	6.7	6.0	5.3	0.0	0.0	0.0	0.0	0.0	25.7	2.3	7.7	2.3	10.3	0.0	0.0	1.0	3.7	0.0	0.0	0.0	0.7	0.7	
J34 / 7191.5	F	54	MW	35.7	0.3	0.0	2.0	8.0	6.7	0.0	0.0	1.0	0.0	0.0	17.0	3.3	4.7	2.7	9.3	0.0	0.0	3.3	3.3	1.0	0.0	1.0	1.0		
J35b / 7193.0	B	66	MW	41.3	1.0	0.0	2.7	9.7	7.0	1.0	Tr	0.0	0.0	2.0	5.0	0.0	3.3	3.7	3.7	5.0	0.0	5.7	1.3	3.0	4.7	0.0	0.0	7.7	
J36 / 7195.0	A	56	W	42.7	1.3	1.0	2.0	12.0	4.3	0.0	0.0	0.0	0.3	2.3	3.3	0.0	1.3	2.0	6.0	5.3	0.0	7.3	0.0	9.3	5.7	0.0	0.0	15.0	
J37 / 7197.0	A	66	W	39.7	2.7	0.0	2.0	13.7	4.7	0.0	0.0	0.0	0.0	2.3	2.3	Tr	2.3	2.0	1.0	4.7	0.0	6.0	0.0	9.0	7.7	0.0	0.0	16.7	
J50 / 7199.0	A	56	W	40.3	1.3	0.3	1.7	9.3	6.0	0.0	2.0	0.0	0.0	3.0	3.3	0.0	2.0	4.7	3.7	3.0	0.0	5.0	1.0	7.3	6.3	0.0	0.0	3.7	

**DATA FROM COMPUTER - CONTROLLED
SCANNING AIR MINIPERMEAMETER (CCSAM)
TABLE 4 - CORED WELL: E.T. O'Daniel #37**

Depth (ft)	Kavg	Depth (ft)	Kavg	Depth (ft)	Kavg	Depth (ft)	Kavg
7195,08	0,01	7220,62	0,001	7227,6	0,04	7237,3	0,275
7195,28	0,01	7220,83	0,001	7227,7	0,06	7239	0,01
7195,5	0,02	7220,92	0,0055	7227,8	0,08	7239,1	0,01
7206,17	0,001	7221,08	0,05	7227,9	0,195	7239,2	0,01
7206,5	0,01	7221,17	0,05	7228	0,14	7239,3	0,015
7206,75	0,04	7221,25	0,065	7228,4	1,38	7239,4	0,02
7206,92	0,01	7221,33	0,08	7228,5	0,485	7239,5	0,02
7207,12	0,01	7221,42	0,04	7228,7	1,415	7239,6	0,02
7207,42	0,01	7221,5	0,16	7228,8	1,235	7239,7	0,02
7207,58	0,01	7221,58	0,16	7228,9	1,605	7239,8	0,03
7207,83	0,01	7221,67	0,16	7229,1	1,565	7239,9	0,005
7208,12	0,01	7221,75	0,16	7229,2	1,67	7239,95	0,04
7208,33	0,01	7222,08	0,15	7229,3	1,81	7240,05	0,265
7208,5	0,01	7222,17	0,18	7229,4	1,735	7240,15	0,4
7208,71	0,01	7222,25	0,09	7229,5	1,75	7240,2	0,045
7208,83	0,01	7222,33	0,145	7229,6	1,79	7240,4	0,05
7208,92	0,001	7222,42	0,135	7229,7	1,935	7240,6	0,05
7209	0,001	7222,5	0,13	7229,8	1,84	7240,7	0,03
7209,5	0,001	7222,58	0,13	7229,85	1,88	7241,3	0,01
7210	0,001	7222,67	0,11	7229,9	1,8	7241,7	0,12
7210,5	0,001	7222,75	0,135	7229,95	2,03	7242,1	0,235
7211	0,001	7224	0,11	7230	2,15	7242,6	0,005
7212	0,001	7224,08	0,115	7230,25	1,765	7243,8	0,01
7212,5	0,001	7224,17	0,11	7230,2	1,6	7243,93	0,04
7213,08	0,03	7224,25	0,02	7230,3	1,43	7243,95	0,03
7213,33	0,04	7224,33	0,03	7230,4	1,55	7244	0,455
7213,58	0,03	7224,42	0,03	7230,5	1,585	7244,1	0,37
7213,83	0,04	7224,5	0,01	7230,6	1,54	7244,2	0,035
7214,08	0,06	7224,58	0,09	7230,7	1,42	7244,3	0,035
7214,25	0,01	7224,67	0,01	7230,75	1,44	7244,4	0,02
7214,42	0,01	7224,75	0,01	7230,8	1,38	7244,5	0,28
7214,58	0,07	7224,83	0,01	7230,9	1,375	7244,6	0,045
7214,75	0,001	7225,12	0,01	7231	1,49	7244,7	0,025
7214,92	0,06	7225,25	0,01	7231,08	1,325	7244,8	0,02
7215,33	0,001	7225,67	0,01	7231,17	1,21	7244,9	0,04
7215,67	0,001	7225,7	0,02	7231,25	1,25	7245	0,07
7216,33	0,001	7226,08	0,01	7231,38	1,24	7245,05	0,065
7216,67	0,001	7226,17	0,07	7231,5	1,15	7245,1	0,065
7217,21	0,001	7226,25	0,01	7231,6	0,885	7245,15	0,05
7217,71	0,001	7226,5	0,06	7231,7	0,885	7245,2	0,1
7218,17	0,001	7226,55	0,15	7231,8	1,22	7245,25	0,09
7218,38	0,001	7226,6	0,08	7231,9	1,065	7245,3	0,155
7218,79	0,001	7226,7	0,04	7232,2	0,855	7245,35	0,025
7219,2	0,001	7226,8	0,04	7232,4	0,715	7245,4	0,025

7219,28	0,001	7226,9	0,305	7236,2	0,78	7245,45	0,025
7219,67	0,001	7226,95	0,05	7236,4	0,73	7245,5	0,1
7219,75	0,001	7227,1	0,02	7236,6	0,695	7245,55	0,04
7219,83	0,001	7227,2	0,02	7236,8	0,575	7245,6	0,04
7219,92	0,001	7227,3	0,035	7237	0,033	7245,65	0,015
7220,17	0,001	7227,4	0,035	7237,1	0,265	7246,1	0,135
7220,38	0,001	7227,5	0,05	7237,2	0,35	7246,2	0,13

CONTINUATION OF TABLE 4 - E.T. O'Daniel 37

**DATA FROM COMPUTER-CONTROLLED
SCANNING AIR MINIPERMEAMETER (CCSAM)
TABLE 5 - CORED WELL: Shackelford #138A**

Depth (ft)	Kavg	Depth (ft)	Kavg	Depth (ft)	Kavg	Depth (ft)	Kavg
7067,085417	0,025	7084,50792	0,595	7092,12755	0,53	7108,98458	0,315
7067,222083	0,165	7084,59042	0,585	7092,21042	0,525	7109,11125	0,335
7067,348333	0,18	7084,66542	0,485	7092,70542	0,465	7109,27292	0,275
7067,474167	0,19	7084,74875	0,485	7092,78792	0,455	7109,44833	0,38
7067,594167	0,13	7084,85458	0,755	7092,86208	0,345	7109,60917	0,31
7067,656667	0,13	7084,92792	0,635	7092,95167	0,42	7109,68458	0,215
7067,80375	0,145	7084,93833	0,26	7093,00458	0,055	7109,85458	0,255
7067,972083	0,165	7085,02792	0,335	7093,09042	0,085	7110,01917	0,23
7068,135833	0,13	7085,12625	0,515	7095,0312	0,12	7110,195	0,34
7068,891667	0,2	7087,28917	0,97	7097,05797	0,23	7110,36125	0,335
7068,9925	0,41	7087,37917	1,05	7097,31579	0,1	7110,51792	0,215
7069,0575	0,19	7087,485	1,32	7097,4565	0,13	7110,92	0,04
7069,123333	0,105	7087,56875	1,325	7097,85233	0,2	7111,09125	0,095
7069,474333	0,231	7087,96042	0,025	7098,51567	0,35		
7070,102567	0,452	7088,04333	0,02	7098,75133	0,2		
7070,401067	0,291	7088,17	0,54	7099,201	0,092		
7071,231033	0,13	7088,23	0,26	7099,631	0,057		
7075,236333	0,053	7088,39167	1,2	7100,102	0,14		
7078,932667	0,075	7088,88333	0,1	7100,85	0,39		
7080,386333	0,254	7088,97667	0,22	7102,003	0,033		
7080,922667	0,0922	7089,0475	0,07	7103,34	0,15		
7081,087917	0,055	7089,13167	0,08	7104,1	0,0423		
7081,174167	0,09	7089,21333	0,06	7106,39083	0,19		
7081,254583	0,055	7089,30083	0,11	7106,48042	0,091		
7081,339167	0,07	7089,38417	0,11	7106,56917	0,33		
7081,83875	0,065	7089,42333	0,08	7106,64708	0,265		
7081,927083	0,125	7089,50792	0,095	7106,73375	0,305		
7082,095833	0,65	7089,59208	0,105	7106,82333	0,38		
7082,148333	0,28	7089,67542	0,105	7106,89958	0,295		
7082,244167	0,43	7089,75875	0,105	7106,98708	0,345		
7082,347083	0,665	7089,84333	0,12	7107,0675	0,31		
7082,429583	0,655	7089,92583	0,11	7107,14792	0,275		
7082,51375	0,665	7090,00792	0,095	7107,22625	0,215		
7082,598333	0,68	7090,09125	0,095	7107,31208	0,245		
7082,683333	0,7	7090,58	0,46	7107,39625	0,255		
7082,77625	0,815	7090,65417	0,35	7107,47625	0,215		
7082,862083	0,845	7090,74208	0,405	7107,56083	0,23		
7082,94875	0,885	7090,81958	0,335	7107,6475	0,27		
7083,114583	0,875	7090,915	0,48	7107,73375	0,305		
7083,193333	0,82	7090,99292	0,415	7107,81083	0,23		
7083,2775	0,83	7091,08292	0,495	7107,89667	0,26		
7083,557083	0,685	7091,16583	0,49	7108,06083	0,23		

7083,644583	0,735	7091,24958	0,495	7108,14875	0,285
7083,730417	0,765	7091,40458	0,355	7108,22958	0,255
7083,8175	0,81	7091,49208	0,405	7108,31458	0,275
7083,93	1,16	7091,57167	0,36	7108,39417	0,23
7084,094167	0,63	7091,70708	0,485	7108,47875	0,245
7084,160417	0,425	7091,77917	0,35	7108,56292	0,255
7084,250417	0,505	7091,86833	0,42	7108,64333	0,22
7084,322917	0,375	7091,95625	0,475	7108,775	0,3
7084,401667	0,32	7092,04546	0,48	7108,93667	0,24

CONTINUATION OF TABLE 5 - SHACKELFORD 138

TOTAL RESULTS FROM WHOLE CORE ANALYSIS

Table 6 - CORED WELL: E.T. O'DANIEL 37

Depth ft.	Kmax MD	K90 MD	Kvert MD	Porosity (%)	Grain Density (g/cc)	Sw (%)
7081,5				0,094	2,69	42,6
7082,5				0,111	2,67	32,3
7083,5				0,109	2,67	34,5
7084,5				0,11	2,69	43,6
7085,5				0,107	2,67	38,1
7086,5				0,109	2,67	43,5
7087,5				0,108	2,67	36,9
7088,5				0,115	2,66	29,9
7089,5				0,064	2,74	42,3
7090,5				0,05	2,73	50,9
7092,5	0,07	0,06	0,03	0,103	2,68	40,4
7093,5	0,05	0,05	0,01	0,103	2,67	30,3
7094,5				0,075	2,7	52
7096,5				0,091	2,69	58,8
7097,5				0,095	2,68	59,8
7098,5				0,099	2,67	54,4
7099,5	0,03	0,03	0,01	0,096	2,66	45,2
7100,5				0,092	2,66	50,3
7101,5				0,052	2,61	89,8
7102,5				0,067	2,66	67,3
7103,5	0,02	0,02	0,01	0,075	2,64	54,8
7104,5	0,04	0,03	0,73	0,07	2,64	57,9
7105,5	0,01	0,01	0,01	0,053	2,61	73
7106,5				0,043	2,58	94,3
7107,5				0,028	2,58	90,8
7109,5				0,035	2,58	85,5
7115,5				0,084	2,66	31,3
7116,5				0,054	2,64	84,6
7117,5				0,087	2,67	54,4
7118,5				0,099	2,66	47,7
7119,5				0,098	2,66	39,6
7120,5				0,068	2,66	45,4
7121,5				0,092	2,66	44,4
7122,5				0,092	2,66	54,8
7123,5				0,102	2,67	49,8
7124,5				0,092	2,66	54

Table 6 cont. - CORED WELL: E.T. O'DANIEL 37

Depth ft.	Kmax MD	K90 MD	Kvert MD	Porosity (%)	Grain Density (g/cc)	Sw (%)
7125,5				0,084	2,66	57,3
7126,5				0,059	2,61	67,1
7127,5				0,055	2,6	47,7
7128,5				0,057	2,62	64,2
7133,5	0,02	0,02	0,01	0,013	2,7	61,8
7134,5	0,02	0,02	0,01	0,012	2,72	55,9
7141,5	0,06	0,05	0,01	0,093	2,67	53,8
7142,5	0,1	0,08	0,06	0,078	2,67	60,7
7143,5	0,02	0,02	0,01	0,088	2,67	52,9
7144,5	0,02	0,02	0,01	0,012	2,74	96,4
7146,5	0,02	0,02	0,01	0,057	2,63	69,9
7147,5				0,064	2,63	60,1
7148,5				0,053	2,61	68,7
7149,5	0,55	0,51	0,01	0,07	2,65	57,1
7150,5	0,07	0,05	0,01	0,045	2,62	73,8
7151,5	0,03	0,02	0,01	0,077	2,67	56
7152,5	0,19	0,02	0,01	0,053	2,62	73,6
7153,5	0,02	0,02	0,01	0,059	2,61	59,2
7154,5	0,01	0,01	0,01	0,045	2,62	47,3
7155,5	3,17	0,19	0,01	0,031	2,57	80,5
7156,5	0,11	0,09	0,01	0,023	2,55	87,3
7157,5	0,09	0,04	0,01	0,015	2,53	91,9
7158,5	0,08	0,03	0,01	0,026	2,54	90
7159,5	0,73	0,39	0,01	0,016	2,52	97,7
7160,5				0,012	2,5	96,6
7161,5	1,39	1,28	0,01	0,041	2,59	89,1
7162,5	0,06	0,05	0,01	0,026	2,56	89
7163,5	0,17	0,06	0,01	0,014	2,52	91,9
7164,5	0,06	0,02	0,01	0,012	2,75	88,9
7165,5				0,022	2,53	89,4
7166,5	1,12	0,88	0,01	0,025	2,57	88,4
7167,5	0,01	0,01	0,01	0,043	2,59	84,2
7170,5	0,01	0,01	0,01	0,071	2,64	52,6
7171,5				0,054	2,61	69,3
7172,5				0,024	2,55	80,4
7173,5	0,17	0,13	0,01	0,024	2,56	77,8

Table 6 cont. - CORED WELL: E.T. O'DANIEL 37

Depth ft.	Kmax	K90 MD	Kvert	Porosity (%)	Grain Density (g/cc)	Sw (%)
7175,5	0,01	0,01	0,01	0,012	2,71	74,8
7176,5	0,02	0,01	0,01	0,005	2,67	94,4
7180,5	8,17	7,48	0,01	0,05	2,62	66,3
7182,5	0,12	0,05	0,01	0,073	2,63	53,9
7185,5	8,98	1,97	0,01	0,045	2,62	82,4
7187,5	0,24	0,1	0,01	0,019	2,53	94,8
7188,5	0,03	0,03	0,01	0,026	2,57	90,9
7189,5	0,01	0,01	0,01	0,048	2,61	88,3
7191,5				0,019	2,56	84,4
7192,5				0,022	2,55	93
7193,5				0,018	2,73	79,9
7194,5				0,034	2,6	58,5
7195,5	0,34	0,09	0,05	0,044	2,61	38,8
7196,5	0,12	0,11	0,02	0,045	2,62	58,4
7197,5	0,11	0,09	0,04	0,046	2,61	49,5
7198,5	0,12	0,1	0,02	0,051	2,6	43,9
7200,5				0,02	2,56	98,4
7201,5				0,016	2,55	94,5
7202,5				0,02	2,56	93,4
7204,5			0,01	0,023	2,57	99,6
7206,5	0,19	0,11	0,01	0,013	2,71	86,4
7207,5	0,09	0,07	0,02	0,013	2,71	81
7208,5	0,12	0,09	3,15	0,023	2,64	35,3
7209,5				0,016	2,51	94
7210,5				0,022	2,54	94
7212,5			0,04	0,054	2,62	86,6
7213,5	0,08	0,07	0,04	0,065	2,63	67,2
7214,5	0,11	0,1	0,04	0,067	2,64	66,6
7215,5	3,37	1,16	0,02	0,05	2,63	92
7216,5	0,11	0,1	0,02	0,061	2,66	85,2
7217,5	0,16	0,1	0,02	0,079	2,67	72,6
7218,5	0,1	0,1	0,05	0,089	2,68	69,2
7219,5	0,12	0,12	0,02	0,085	2,69	61,6
7220,5	0,11	0,08	0,04	0,018	2,73	79,9
7222,5	0,24	0,21	0,18	0,111	2,66	29,7
7223,5	0,28	0,28	0,21	0,117	2,65	26

Table 6 cont. - CORED WELL: E.T. O'DANIEL 37

Depth ft.	Kmax	K90 MD	Kvert	Porosity (%)	Grain Density (g/cc)	Sw (%)
7224,5	0,17	0,16	0,04	0,092	2,67	38,6
7225,5	0,1	0,08	0,03	0,057	2,68	87,8
7226,5	1,81	0,13	0,18	0,063	2,74	68,1
7230,5	1,63	1,48	1,13	0,134	2,65	19,7
7231,5	1,31	1,3	1,19	0,136	2,65	33,5
7232,5	1,14	1,13	0,72	0,133	2,65	25,2
7233,5	0,98	0,98	0,78	0,129	2,65	23,6
7236,5	0,67	0,66	0,47	0,123	2,65	21,8
7238,5	0,12	0,1	0,07	0,092	2,69	42,7
7239,5	0,16	0,15	0,32	0,11	2,67	39,9
7240,5	0,21	0,19	0,08	0,115	2,68	50,4
7241,5	0,84	0,61	2,53	0,075	2,68	71,4
7244,5				0,023	2,52	88,2
7245,5				0,106	2,66	37,7

SHACKELFORD 138A
TOTAL RESULTS FROM WHOLE CORE ANALYSIS
Table 7 - CORED WELL: SHACKELFORD 138A

Depth ft.	Kmax MD	K90 MD	Kvert MD	Porosity (%)	Grain Density (g/cc)	Sw (%)
7064,5	0,02	0,02	0,01	0,03	2,62	81,2
7065,5	0,03	0,02	0,01	0,01	2,72	95,6
7066,5	0,02	0,02	0,01	0,004	2,76	72,5
7067,5	0,01	0,01	0,02	0,101	2,67	46,4
7068,5	0,18		0,4	0,079	2,67	42,5
7069,5	0,12		0,06	0,136	2,67	63,4
7070,5	0,03	0,03	0,02	0,063	2,63	74,9
7071,5	0,04	0,04	0,02	0,068	2,64	77,8
7072,5	0,03	0,02	0,01	0,031	2,6	83,4
7073,5			0,02	0,047	2,64	75,8
7074,5	0,07	0,03	0,01	0,02	2,59	84,8
7075,5	0,02	0,02	0,01	0,026	2,57	94,7
7076,5	0,01	0,01	0,01	0,004	2,74	70,9
7077,5	0,02	0,02	0,04	0,104	2,66	48,1
7078,5	0,11	0,03	0,06	0,1	2,64	45,5
7079,5	0,02	0,02	0,01	0,051	2,64	52,3
7080,5	0,03	0,02	0,02	0,046	2,64	79,5
7081,5	0,02	0,02	0,01	0,069	2,68	48
7082,5	0,43	0,42	0,2	0,115	2,64	28,2
7083,5	0,49	0,49	0,76	0,109	2,64	25,1
7084,5	0,33		0,48	0,115	2,66	32,5
7087,5	1,97			0,137	2,64	43,1
7088,5	0,26		0,09	0,087	2,68	30,7
7089,5	0,06	0,04	0,07	0,071	2,72	29,5
7090,5	0,2		0,1	0,1	2,66	26,6
7091,5	0,32	0,31	0,23	0,108	2,64	30
7092,5	0,29	0,27	0,23	0,119	2,64	29
7093,5	0,02	0,02	0,01	0,066	2,67	66,9
7094,5	0,03	0,03	0,01	0,099	2,68	70,1
7095,5	0,04	0,04	0,01	0,095	2,67	68,5
7096,5	0,02	0,02	0,01	0,089	2,66	66,6
7097,5	0,1	0,1	0,05	0,113	2,67	36,1
7098,5	0,16	0,04	0,04	0,109	2,67	48,3
7099,5	0,07	0,07	0,02	0,111	2,67	57
7100,5	0,11		0,07	0,112	2,67	54,5
7101,5	0,12		0,04	0,062	2,63	68,2

Table 7 cont. - CORED WELL: SHACKELFORD 138A

Depth ft.	Kmax MD	K90 MD	Kvert MD	Porosity (%)	Grain Density (g/cc)	Sw (%)
7102,5	0,06	0,06	0,04	0,102	2,66	52,6
7103,5	0,03	0,03	0,02	0,105	2,69	44,1
7104,5	0,03	0,02	0,01	0,04	2,72	78,2
7105,5	0,04	0,03	0,02	0,105	2,66	63,1
7106,5	0,02	0,02	0,01	0,094	2,64	44,2
7107,5	0,09		0,06	0,102	2,66	62,9
7108,5		0,04		0,096	2,65	52,5
7109,5	0,11		0,13	0,11	2,67	62,2
7110,5	0,02		0,02	0,121	2,68	60,8
7111,5	0,03		0,01	0,046	2,66	70,3
7112,5	0,02		0,02	0,061	2,67	88,9
7113,5	0,05		0,02	0,045	2,61	84,1
7114,5	0,08		0,04	0,04	2,6	93,8
7115,5	0,02	0,02	0,01	0,038	2,56	73,3
7116,5	0,05		0,03	0,051	2,58	88,4
7117,5	0,05		0,06	0,077	2,62	78,1
7118,5	0,03		0,03	0,039	2,55	88,7
7119,5	0,06		0,02	0,035	2,6	88,1
7120,5	0,02	0,01	0,01	0,04	2,61	86,8
7121,5	0,01	0,01	0,01	0,03	2,57	92,7
7122,5	0,06	0,01	0,01	0,025	2,59	84,7

Whole Core Analysis Results with Thin Section Control

Table 8

PERMEABILITY (MD)-Nitrogen						
	A	B	C	D	E	F
Average	0,64208	0,11759	0,04833	0,18071	0,05667	0,03397
Max	1,97	0,29	0,10333	0,70667	0,16	0,08
Min	0,09	0,02	0,01	0,02	0,02	0,01

POROSITY (%) - Helium						
	A	B	C	D	E	F
Average	11,9952	9,95128	1,04545	8,00357	3,75806	7,24419
Maximum	13,7	12,1	1,8	10	6,3	9,9
Minimum	10,7	7,7	0,4	4	1,2	4,6
Median	11,5	10	1,2	8,6	3,95	7

WATER SATURATION (Sw)-Dean Stark						
	A	B	C	D	E	F
Average	0,35474	0,44411	0,792	0,5997	0,7533	0,61317
Maximum	0,634	0,631	0,889	0,878	0,927	0,781
Minimum	0,197	0,203	0,709	0,266	0,388	0,403
Median	0,325	0,442	0,7955	0,5965	0,8	0,601

Letters from A to B represent the six small-scale flow units described in chapters 5 and 6

Table 9 - Petrophysical data using helium, nitrogen and mercury injection

Core	Depth ft	SSFU	Porosity (%) (helium)	Permeability (nitrogen) md	Pore Throat (µm)*	Modal Radius (psia)*	Pc (psia)*	Pt (psia)*	Pore Throat Distribution
F.T. Odaniel 37	7058,0	A	8,9	0,156	0,35	201	161		Normal-Skewed
	7066,0	A	12,0	0,245	0,35	201	161		Normal -Skewed
	7228,3	A	11,5	0,609	0,66	111	75,5		Normal -Skewed
	7236,7	A	11,0	0,407	0,66	111	75,5		Normal -Skewed
	7093,5	B	9,6	0,035	0,13-0,11	802	602		Normal -Skewed
	7131,8	B	9,1	0,035	0,13-0,11	802	602		Normal -Skewed
	7040,0	C	0,7	0,006	0,0035	5,984	4,980		Uniform distribution
	7206,9	C	0,7	0,019	0,0035	14,944	11,943		Polymodal distribution
	7113,0	D	4,7	0,009	0,045	1,196	987		Normal -Skewed
	7050,0	F	5,9	0,014	0,07	1,600	1,400		Uniform Distribution
	7174,9	F	6,1	0,013	0,06	1,601	1,401		Normal
	7195,4	F	5,3	0,022	0,0045	4,496	3,989		Normal
	7213,5	F	6,0	0,036	0,015-0,006	3492	2993		Polymodal distribution
	Shackelford 138-A	7083,4	A	10,7	0,392	0,66	161	111	
7087,4		A	13,1	1,110	0,66	111	74,8		Normal-Skewed
7091,5		A	10,3	0,193	0,35	201	161		Normal-Skewed
7068,5		B	7,6	0,002	0,13	801	600		Normal-Skewed
7078,2		B	9,1	0,064	0,27	401	300		Normal-Skewed
7097,4		B	10,1	0,060	0,18	401	301		Normal-Skewed
7102,6		B	10,3	0,046	0,13	601	401		Normal
7109,5		B	10,6	0,044	0,13	601	401		Normal-Skewed
7117,5		F	8,5	0,025	0,05	2,000	1,500		Uniform distribution

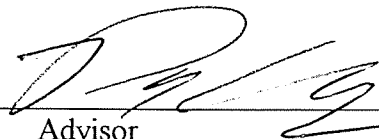
Pc = capillary pressure after first stage of pore throat has been filled with mercury

Pt = threshold pressure, first reading when fluid start penetrating the pore system

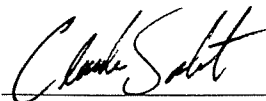
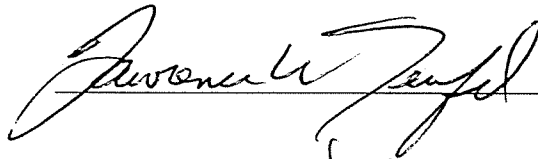
Pt is always a lower reading than Pc

* from mercury injection

This thesis is accepted on behalf of the faculty
of the institute by the following committee:



Advisor

 15 March 99 18 MARCH 1999

Date